ABSTRACT

XU, SIQI. Electro-Mechanical-Thermal Modeling of Carbon Nanotube-Polymer Composites. (Under the direction of Professor Mohammed A. Zikry).

The focus of this research has been to develop a validated computational framework to investigate the electro-mechanical-thermal behavior of carbon nanotube (CNT)-polymer composites. The computational framework included the development of both a new percolation approach and an electro-mechanical-thermal finite-element (FE) approach. The percolation approach addressed current shortcomings and inconsistencies of classical percolation theory, and it was used to predict the electrical conductivity of CNT-epoxy composite based on variations in tunneling resistances, aspect ratios, CNT volume fractions and distributions. This approach is based on an electrical network model and a junction-identifying search algorithm. For the search algorithm, the distances between all the generated CNTs were computed, and if the distance between two CNTs was smaller than a pre-determined maximum distance, the two CNTs were assumed to be in contact, and a junction can then be identified. The tunnel resistances at each junction and the overall electrical resistance of 3D CNT-polymer networks were then obtained. The predicted conductivity behavior was used to predict different percolation thresholds and the critical exponents for different CNT arrangements within an epoxy matrix, and this approach was validated with experimental observations and measurements.

The FE modeling method was then developed to investigate how the electro-mechanical-thermal behavior of CNT reinforced polymer composites is affected by electron tunneling distances, volume fraction, and physically realistic tube aspect ratios. A specialized Maxwell FE formulation with a Fermi-based tunneling resistance was then used to obtain

current density evolution for different CNT-polymer dispersions and tunneling distances. Analyses based on coupled thermo-electrical and electro-mechanical FE approaches were used to investigate how temperatures, conductivities, stresses, and strains were affected by variations in tunneling distances and electro-thermo-mechanical loading conditions. In the coupled thermo-electrical analyses, the Maxwell equations were coupled to the heat conduction equations through Seebeck coefficients. The current flow, total current density, thermal distributions, and Joule heating were determined for different CNTs arrangements and tunnel distances. The analyses has indicated that tunneling has a dominant role in the overall electrical conductivity and thermal behavior of the composite. There was no clear correlation with tunneling distance, however, since the behavior is dominated by CNT orientation and distribution. This further underscores how the behavior of randomly distributed functionalized CNTs in an epoxy matrix with varying tunneling distances can be difficult to predict, since the physical scales range from tunnel lengths of a few nanometers to CNTs with lengths of hundreds of nanometers.

The coupled electro-mechanical FE approach was developed to investigate the piezoresistive response of the polymer composite. Gauge factors (GFs) and resistance variations of CNT-polymer composite systems were obtained by coupling Maxwell equations to mechanical loads and deformations through initial piezoresistive coefficients of the CNTs, the epoxy, and the tunnel regions, for different arrangements, percolated paths, tunnel distances, and loading conditions. The influences of loading conditions, such as tension, compression, and bending on the piezoresistivity of CNT polymer composites were investigated. A scaling relation between GFs and applied strains was obtained to understand how variations in loading and CNT arrangements affect sensing capabilities. These variations in GFs were then used to understand how the coupled strains, stresses and current densities vary for aligned and percolated paths for the different loading conditions, CNT arrangements, and tunnel distances. For the percolated path under tensile loading conditions, elastic strains as high as 16% and electrical conductivities that were four orders in magnitude greater than the initial matrix conductivity were obtained. Results for the three loading conditions clearly demonstrate that electrical conductivity and sensing capabilities can be optimized as a function of percolation, tunneling distance, orientation, and loading conditions for piezoresistive applications with large elastic strains and conductivities.

Electro-Mechanical-Thermal Modeling of Carbon Nanotube-Polymer Composites

by
Siqi Xu

A dissertation submitted to the Graduate Faculty of
North Carolina State University
in partial fulfillment of the
requirements for the degree of
Doctor of Philosophy

Mechanical Engineering

Raleigh, North Carolina

2012

APPROVED BY:

Professor Mohammed A. Zikry
Committee Chair

Professor Kara Peters

Professor Jeffrey Eischen

Professor Donald Brenner

Professor Philip Bradford

DEDICATION

For my parents,

Their endless love, support and encouragement made this possible.

BIOGRAPHY

Siqi Xu was born and raised in Huai'an, Jiangsu, China. She attended Xi'an Jiaotong University, China for undergraduate studies in nuclear engineering. She received a Bachelor of Science Degree in Nuclear Engineering in the summer of 2006. After graduation, she joined the Department of Nuclear Engineering at North Carolina State University (NCSU) and earned a Master of Science in Nuclear Engineering degree in the spring of 2008. In the summer of 2008, she continued her studies in Ph. D program in Mechanical Engineering at NCSU under advisor Professor Mohammed A. Zikry. Her research area mainly focuses on finite element modeling and analyses of polymer nanocomposites.

ACKNOWLEDGMENTS

This dissertation would not have been possible without the help and support of a great number of people. First of all, I would like to express my deepest appreciation to Dr. Mohammed A. Zikry, who has been my advisor, mentor and a source of support throughout my years of Ph. D study. Without his patience, encouragement and advisory, the dissertation would be impossible. His insightful suggestion and inspiration not only helped me in my current research, but will also enlighten my future career path. Perhaps the individual to whom I am most indebted is Dr. Zikry. Thank you sincerely.

I would also like to offer my special thanks to my committee members, Dr. Jeffrey Eischen, Dr. Kara Peters, Dr. Donald Brenner and Dr. Philip Bradford for their willingness to be my committee members and their time to provide beneficial suggestions and comments.

Support from National Science Foundation (NSF) and Air Force Office of Scientific Research (AFOSR) grant #FA9550-08-1-0017 is gratefully acknowledged.

I would also like to express my sincere thanks to my coworkers in the Computational and Experimental Mechanics of Materials Lab. Dr.James Pearson, Dr. Khalil Khodary, Dr. Tarek Hatem, Dr. Pratheek Shanthraj, Dr. William Lee, Prasenjit Khanikar, Letisha Mclaughlin, Qifeng Wu, Shoayb Ziaei, Darrell LaBarbera, Judy Brown and Bingxiao Zhao. Their many helpful lab discussions have contributed to this work and the friendship is memorable.

I would especially like to thank Dr. Omid Rezvanian for his many insightful discussions and guidance. Without his help, this work would have been impossible.

And to my parents, my partner, and my dear friends, thank you for giving me all the love and support I needed to accomplish what I have so far.

There are numerous colleagues and cast too numerous to list here who also deserve recognition for their advice and assistance throughout the years. In lieu of a formal listing , Thank you so much!

TABLE OF CONTENTS

LIST OF TABLES

LIST OF FIGURES

CHAPTER 1

INTRODUCTION

1.1 Properties of Carbon Nanotubes

Carbon nanotubes (CNTs) have stimulated strong interest, since they were first investigated by Iijima (1991). CNTs are allotropes of a carbon, and they are generally categorized either as single-walled carbon nanotubes (SWNTs) or as multi-walled carbon nanotubes (MWNTs). Conceptually, a SWNT can be formed by rolling a graphene sheet into a cylinder, and a MWNT is composed of these concentric graphene cylinders. There are three types of CNTs structures: zigzag, chiral, and armchair, as shown in Figure 1.1 (Saito, R., Dresselhaus, G., Dresselhaus, 1998). These are formed based on the coordination of carbon atoms in the crystal structure. The coordinate system used to define individual SWNT is indicated in Figure 1.2, where a_1, a_2 are the basis vectors. A chiral vector is defined as

$$C_h = na_1 + ma_2 , \qquad (1.1)$$

where (n, m) is a pair of positive integers. The chiral vector C_h is perpendicular to the axis of the tube, and the magnitude, $|C_h|$, is the circumference of the tube. The diameter of tube can be expressed in terms of (n, m) and $|C_h|$ as

$$d = \frac{|C_h|}{\pi} = \frac{\sqrt{3}a_{c-c}}{\pi}\sqrt{n^2 + m^2 + nm} , \qquad (1.2)$$

where a_{c-c} (=1.421Å) is the carbon-carbon distance in a graphene sheet.

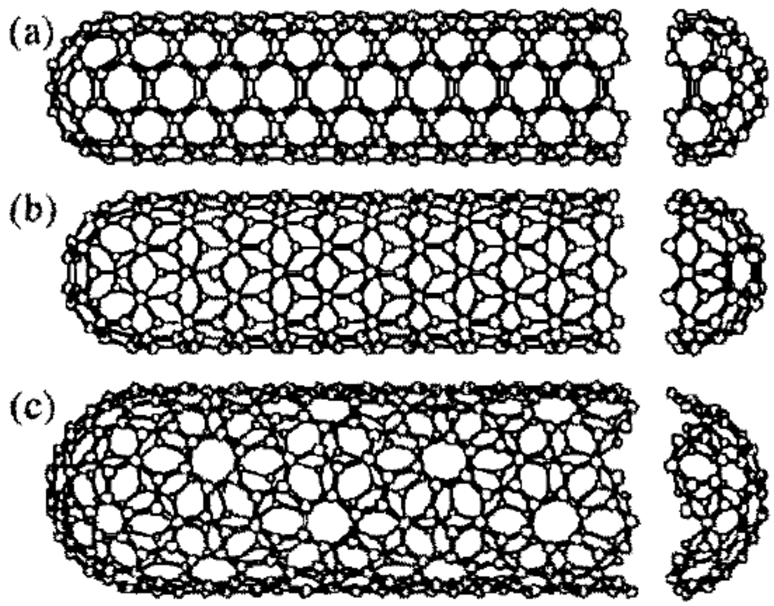

Figure 1.1 Classification of carbon nanotubes: (a) armchair, (b) zigzag, and (c) chiral nanotubes.

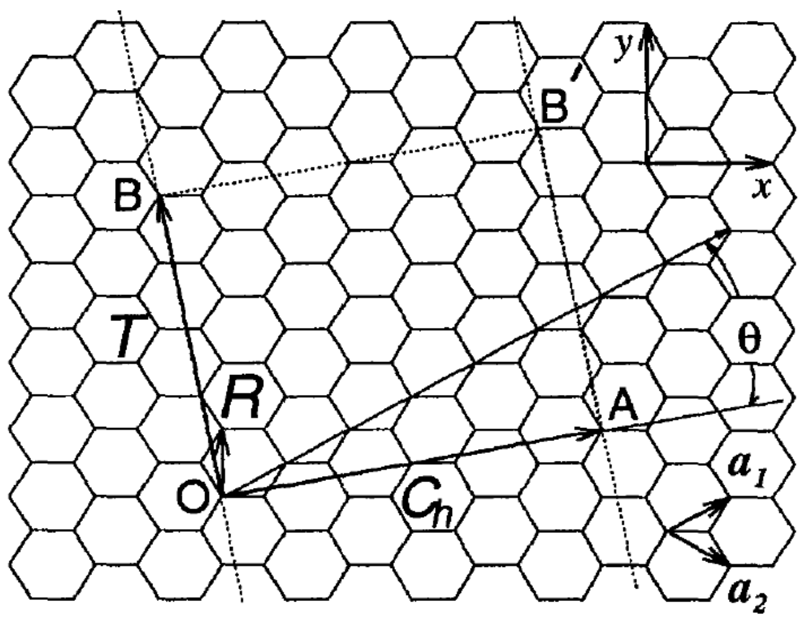

Figure 1.2 Chiral vector of a single-walled carbon nanotube.

The chirality (Figure 1.2) of the CNT describes the structure of the graphene sheet, which in turns strongly affects the electrical and thermal properties of CNTs. CNTs can be either be metallic or semi-conducting depending on chirality. CNT properties are highly structural and size dependent due to atomic arrangement (chirality), nanotube diameter and length, and morphology, or nanostructure (Li et al., 2008b).

Due to their high sensitivity, superior electrical conductivity, high thermal conductivity, and large aspect ratio, CNTs have the potential to be used in many new technological applications in areas related to quantum mechanical, micro-electronic, structural and mechanical, and piezoresistive sensing applications.

1.2 Overview of CNT-Polymer Composites

In recent years, CNT-reinforced polymer composites have been an area of intense applied and basic research. The introduction of CNTs into conventional fiber-reinforced polymer composites can significantly improve composite performance by increasing strength and reducing weight. Much attention has been paid to the fabrication of nanocomposites with use of various CNTs in polymer materials to improve their structural and electrical properties. In the area of high strength and stiffness materials, extensive research has been undertaken in areas related to randomly oriented, discontinuous CNT composite (see, for example, Ding et al. 2003; Jonghwan Suhr et al. 2005; E T Thostenson et al. 2002; Veedu et al. 2006), and there has also investigations on continuous CNT reinforced polymer composites (Ci et al., 2008a). In this section, the literature review will be focused on CNT-polymer composites as electrically conductive materials.

The first realized major commercial application of MMWNTs is their use as electrically conducting components in polymer composites (Baughman et al., 2002). To harness the exceptional electrical properties of CNTs and their high compatibility with polymer matrices, polymers reinforced with CNTs have been studied for the potential in numerous electronic device applications, such as organic field emitting displays, photovoltaic cells, highly sensitive strain sensors, and electromagnetic interference materials (Alamusi et al., 2011).

Generally, strain sensors utilizing CNTs can be employed practically through two main approaches. On the one hand, CNTs are Raman active, and can be blended with a polymer to make a strain sensor, provided a relationship between mechanical strain and Raman spectrum shift can be calibrated and obtained (Frogley et al., 2002; Halary et al., 2004). Alternatively, macro-scale resistance-type strain sensors, e.g., with dimensions of mms, have been increasingly used to measure static and low-frequency dynamic strains on the surfaces of a structure (Alamusi et al., 2011). To this end, two types of strain sensors have been developed, i.e., SWNT buckypaper sensors (Li et al., 2004; Dharap et al., 2004; Kang et al., 2006) and sensors made from various CNT-polymer composites (Ramaratnam, 2006; Zhang et al., 2006; Park et al., 2008; Hu et al., 2008a; Karube and Fukunaga, 2011; Hsu et al., 2011). Except for a piezoelectric device proposed by Ramaratnam (2006), in which a piezoelectric-type strain sensor was fabricated, most studies have focused on the development of piezoresistive sensors (Alamusi et al., 2011).

A commons feature of piezoresistive CNT-polymer systems, which is of the most interest, is that compared to conventional strain sensors, e.g. strain gauges, higher sensitivity has been observed in these novel sensors, at least at a macro-scale (Kang et al., 2006; Hu et al., 2008a, 2010; Yasuoka et al., 2010; Karube and Fukunaga, 2011).

The use of thin films of randomly oriented CNTs, as sensors, has been investigated and the resistance changes were measured using a four-point probe (see, for example, Dharap et al. 2004). MWNT-reinforced composites utilized as strain sensors have also been used by Zhang et al. (Zhang et al., 2006). The sensitivity of their nanocomposite electrical conductivity to applied strain was reported to be 3.5 times higher than for a traditional strain gauge, which indicates the potential for self-diagnostics and real-time health monitoring. Piezoresistivity behavior of CNTs has also been demonstrated by Kang et al. (Kang et al., 2006) where SWNT/polymer composite films were used for strain sensing for static and dynamic behavior. These piezoresistive properties underscore the potential of CNT-polymer composites as high gauge factor (GF) low-voltage strain gauges.

1.3 Percolation Theory

The electrical conductivity behavior of a polymer composite comprised of the insulating polymers and conducting fillers has been commonly empirically described by percolation theory. In classical percolation theory, there is a sharp increase in conductivity, σ, once a critical volume fraction, p_c, of the conductive phase is reached (Stauffer and Aharony, 1994). When the threshold, pc, is attained, the conductivity of the composite can be described by the power law

$$\sigma = \sigma_0 \bullet (p - p_c)^t , \qquad (1.3)$$

where σ is the electrical conductivity of the composite, σ_0, the scaling factor, is a proportionality constant related to the intrinsic conductivity of the filler, p, is the volume fraction of the filler, p_c is the percolation threshold, and t is the critical exponent. The universal values of t that have been commonly used are approximately 1.3 for two-dimensional systems and approximately 2 for three dimensional systems (Kirkpatrick, 1973; Balberg and Binenbaum, 1983). However, for CNT-polymer composites, the broad range of t values fitted from experimental measurements, as well as the differences for values obtained by different simulations clearly indicates that the critical exponent is not universal. Bauhofer and Kovacs (2009) have indicated that values of the critical exponent, t, obtained from experiments for three-dimensional percolating systems range from below 2 to 10 for CNTs, and for MWNTs, values of t were generally between 1.3 and 4. Other experimental and theoretical studies have also shown that the percolation threshold is dependent on the morphology of conductive fillers, such as the sizes, the shapes, and the aspect ratio of the fillers (Heo et al., 2006; Celzard et al., 1996; Kirkpatrick, 1973; Balberg and Binenbaum, 1983).

Furthermore, it has also been noted that geometrical percolation theory cannot fully explain the electrical conductive behavior of CNT-filled polymer composite (McLachlan et al., 2005; Kovacs et al., 2007), where the fillers are not necessarily in perfect contact, and that the electrical connectedness is established through quantum tunneling between the conducting fillers (Ambrosetti et al., 2010), while in the classical geometrical percolation theory, the conducting fillers are either connected or disconnected (Stauffer and Aharony 1994).

However, classical percolation behavior (Eqn. (1.3)), has been applied to almost all the measured conductivities to relate behavior dependencies on the volume fraction of the conductive filler (Stauffer and Aharony 1994). From previously published experimental results, it was found that the electrical behavior of nanocomposites using CNTs as conductive filler particles in polymer matrices, (see, for example, Bauhofer and Kovacs 2009; Hu, Masuda, et al. 2008; Kilbride et al. 2002; Kymakis and Amaratunga 2006; Martin et al. 2004; Sandler et al. 2003) follows the similar percolation phenomenon to that stated above for traditional conductive filler particles. This fundamental incompatibility has been discussed (Ambrosetti et al., 2010; Balberg, 2009), and, therefore, a better understanding of the electrical conductivity and related quantum tunneling effects in CNT-polymer composite is needed.

Furthermore, in 3D CNT networks in polymer composites, current leakage through tunneling can play a dominant role in the overall electrical conductivity of the composites. Tunneling resistance can vary significantly as a function of junction configuration and the electrical properties of nanotubes and the polymer matrix (Yu et al., 2010). Most analytical investigations have used constant values for tunnel resistance (Yu et al., 2010; Eken et al., 2011). Analytical studies (Berhan and Sastry, 2007) and numerical studies (Natsuki et al., 2005) have indicated that tunneling length has a significant effect on the percolation threshold. These investigations showed that the percolation threshold decreases as the tunneling increases, and this effect is more pronounced at low aspect ratios (Eken et al., 2011).

1.4 Computational Approaches

Recent experimental, theoretical and numerical studies have been used to uncover the dominant mechanism of CNT strain sensors and CNT polymer composites to understand and predict key factors for improving sensor sensitivities and composite behavior.

Molecular dynamic (MD) simulations have provided insights on how the molecular carbon structure can affect behavior, but cannot be used for physically representative aspect ratios and temporal scales (Prylutskyy et al., 2000). Finite element (FE) approaches have mainly focused on the mechanical behaviors of CNT polymer composites (Liu and Chen, 2003; Tserpes et al., 2008; Ashrafi and Hubert, 2006). Recent computational efforts have been reported, such as computational two-dimensional (2D) micromechanics models based on finite element analysis to study the effective macroscale piezoresistance of CNT-polymer composites ((Ren and Seidel, 2012), in which the electrical tunneling effects between adjacent are not account. Since Simmons (1963) derived an analytical approach to evaluate the quantum tunneling current between electrodes separated by an insulating film, there have been attempts made to understand and take into account of the effects of electron tunneling upon the electrical conductivity of CNT polymer nanocomposites. Monte Carlo simulations have been used to investigate the tunneling effects on the electrical conductivity of the bulk CNT composites. A number of studies have simulated the electrical conductivity and piezoresistivity behaviors of CNT polymer composites have used 3D resistor network percolation threshold methods (Dalmas et al., 2006; Hu et al., 2008a; Alamusi et al., 2011; Hu et al., 2010).

1.5 General Research Objectives

Fundamental understandings and accurate predictions of electrical conductivity and piezoresistivity behavior in CNT-polymer composite are still lacking, largely due to the complex electrical conduction mechanisms of CNT-polymer composites that span length scales from the nano to the micro. Coupling electrical to thermo-mechanical behavior is also difficult due to accurately ascertaing Seebeck coefficients for thermal coupling and GFs for coupling of piezoresistive behavior.

In modeling, most percolation investigations have used constant values for tunnel resistance (Yu et al., 2010; Eken et al., 2011). Another shortcoming of these approaches is that the CNTs are represented as line segments, which is different than the actual three dimensional CNT morphology, and this 3D morphology can obviously have significant effects on CNT conductivity (Li et al., 2008a; Cebeci et al., 2009; Liu and Chen, 2003; Chang et al., 2009).

In terms of processing, the critical challenge is uniformly dispersing the nanotubes, achieving nanotube-matrix adhesion that provides effective stress transfer, and avoiding intratube sliding between concentric tubes within MWNTs and intrabundle sliding within SWNT ropes ((Baughman et al., 2002). This further complicates most modeling approaches, since well dispersed CNTs provide an electrical network within the insulating matrix. One of the key issues of the structural and electrical properties is the optimal dispersion of the nano-scale fillers in the polymer matrices (Grammatikos et al., 2011).

Hence, while there is ample experimental evidence demonstrating the piezoresistive response nanocomposites, the mechanisms governing their electrical conductivity and piezoresistivity are not well understood. To accurately model and design piezoresistive nanocomposite strain sensors with tailored and desired sensitivities, it is necessary to develop predictive capabilities to understand the underlying mechanisms at scales spanning the nano to the micro.

The goals of this research are to obtain a better understanding of how conductivity in different CNT arrangements can be affected by tunneling that is critical to better controlling potential sensing capabilities, to develop a validated finite element methodology based on a new percolation method as a function of variations in tunneling resistance, aspect ratios, CNT volume fractions and distributions, to investigate how coupled temperatures, stresses, and conductivities are affected by variations in tunneling distances. This will provide for a predictive framework of electrical conductivity and piezoresistivity behavior of CNT-epoxy composites under different electrical, electro-thermal and electro-thermo-mechanical loading conditions.

This dissertation is outlined as follows: Chapter 2 presents the computational approach, including the 3D CNT network model and the percolation results generated from this model. Chapter 3 contains the finite models, based on the percolation results covered in Chapter 2. Chapter 4 presents the results of an investigation into the piezoresistivity behavior of CNT-polymer composite models, using finite element analyses. Chapter 5 concludes the dissertation with recommendations for future research.

CHAPTER 2

THE VIABILITY AND LIMITS OF A PERCOLATION THEORY IN MODELING THE ELECTRICAL BEHAVIOR OF A CARBON NANOTUBE POLYMER COMPOSITES

2.1 Introduction

In this chapter, to address the shortcomings of classical percolation theory and inconsistencies described in Chapter 1, a modeling approach was proposed to predict the electrical conductivity of CNT-epoxy composite based on variations in tunneling resistance, aspect ratios, CNT volume fractions and distributions. The approach is based on an electrical network model and a junction-identifying search algorithm. The tunnel resistance at each junction and the overall electrical resistance of the 3D CNT-polymer network were then obtained. The predicted conductivity behavior was used to obtain different percolation thresholds and the critical exponents for different CNT arrangements within an epoxy matrix, to understand the limitations of classical percolation theory.

2.2 Computational Approach

The scanning electron microscopy (SEM) images in Figure 2.1 demonstrate the random dispersion of CNTs in a polymer with a 2.0-wt% weight fraction of MWNTs (Hu et al., 2008).

To model experimentally observed randomly dispersed CNT-epoxy network, we generated a 3D unit cell network model by using an algorithm based on a random arrangement of CNTs. The CNTs were randomly distributed into this 3D unit cell by setting the coordinates of their two ends as described in our recent study (Li et al., 2007) . A search

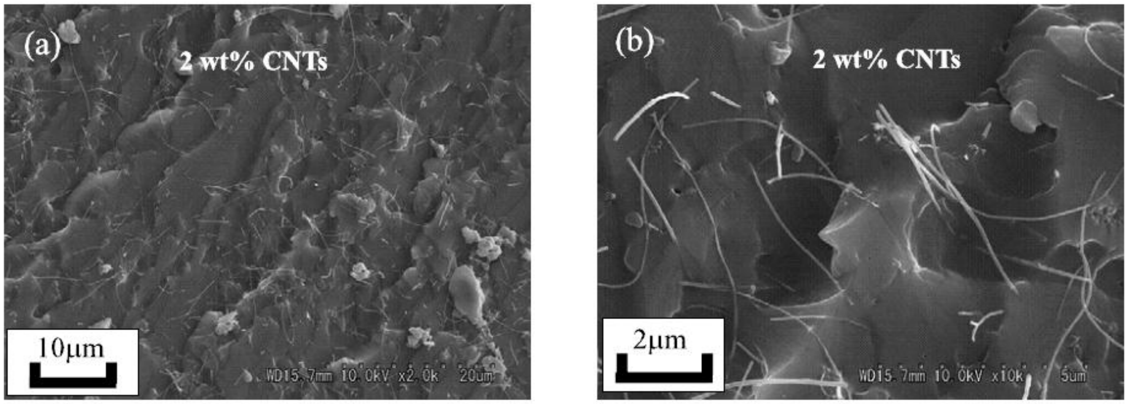

Figure 2.1 CNT distributions in an experimental sample (a) SEM image at low magnification (2000×), and (b) SEM image at high magnification (10000×).

algorithm based on junction identification was then used to obtain different conductive paths in CNT networks. This algorithm can be used to identify non-contacting CNTs, for which the separation distance is such that electrons can tunnel through the polymer matrix, and form a quantum conductive junction. The dominant role of tunneling in the conductivity and percolation threshold of CNT composites has been previously shown by several studies (Hu et al., 2008c, 2008a; Berhan and Sastry, 2007; Yu et al., 2010; Simmons, 1963; Kilbride et al., 2002). To model tunneling, in our proposed search algorithm, the distances between all the generated CNTs are computed, and if the distance between two CNTs at any point is found to be smaller than a pre-determined maximum distance, the two CNTs are assumed to be in contact, and a junction can then be identified. A cut-off distance from the free surfaces was also set to identify the initial and terminal points of each path. Figure 2.2 (Salvato et al., 2012) is an example of a tunneling junction between two SWNT bundles.

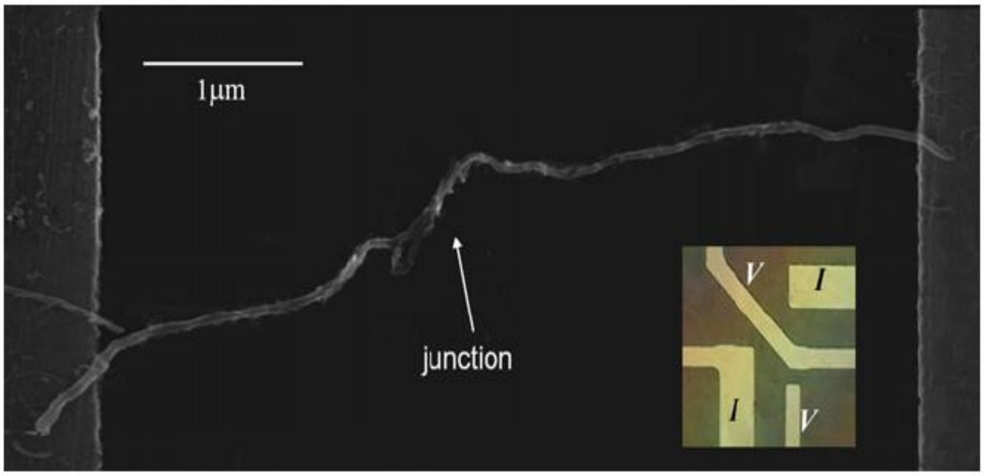

Figure 2.2 SEM image showing a two bundles chain with the arrow indicating the position of the junction; inset: schematic of the four leads configuration

In this dissertation, the electron tunneling is defined as the passage of electrons through a potential barrier which they would not be able to cross according to classical mechanics, such as a thin insulating barrier between two electrodes, and the tunneling resistance that we used in our approach is estimated by Simmons' formula (Simmons, 1963) as

$$J = (6.2\times10^{10} / \Delta s^2)\{\varphi_I \exp(-1.025\Delta s \varphi_I^{\frac{1}{2}})\} - (\varphi_I + V)\exp[-1.025\Delta s(\varphi_I + V)^{\frac{1}{2}}]\}, \quad (2.1a)$$

$$\varphi_I = \varphi_0 - (V/2s)(s_1 + s_2) - 5.75 / K(s_2 - s_1)]]\ln[s_2(s - s_1)/s_1(s - s_2)], \quad (2.1b)$$

$$s_2 = 6/K\varphi_0, \quad s_2 = s[1 - 46/(3\varphi_0 Ks + 20 - 2VKs)] + 6/K\varphi_0, \quad \Delta s = s_2 - s_1, \quad (2.1c)$$

$$R_{tunnel} = \frac{V}{A\cdot J}, \quad (2.1d)$$

where J is the tunneling current density, V is the electrical potential difference, s_1, s_2 are the limits of barrier at Fermi level, s is the thickness of the insulating barrier, A is the cross sectional area of the tunnel, and φ_0 is the barrier height, which for epoxy is 0.5-2.5 eV and

1.5 eV was used in this work (Yu et al., 2010). In this equation, s is the junction distance in the simulated CNT network. Once a junction is identified, the value of s is calculated and updated in Eqn. (2.1) to generate tunneling resistance at each junction along a conductive path.

The tunneling resistance and intrinsic resistance of CNTs were calculated based on junction configuration, rather than using a constant value for the tunneling resistance. Since the CNT network is randomly generated, the tunneling resistance and CNT resistance between junctions were varied for each simulation. Assuming the CNTs are straight solid tubes and the identified conductive paths are in a parallel configuration, the overall resistance of the composite unit cell could then be obtained. The conductivities of the CNT-epoxy composite were then generated as a function of tunneling resistance at junctions, CNT aspect ratios and volume fractions.

2.3 Results and Discussion

The randomly oriented CNT network, the junction-identification based search algorithm and the incorporated tunneling resistance calculation were used to investigate the electrical conductivity and percolation-tunneling behavior of CNT-epoxy composite. Percolation theory is generally used to determine whether clusters or fillers (in this case, CNTs) in a unit cell attained a conductive path, which is characterized by a sharp increase in conductivity at a critical threshold value of p_c. Based on this, a power law or a scaling relation can be obtained to relate conductivity to this critical threshold.

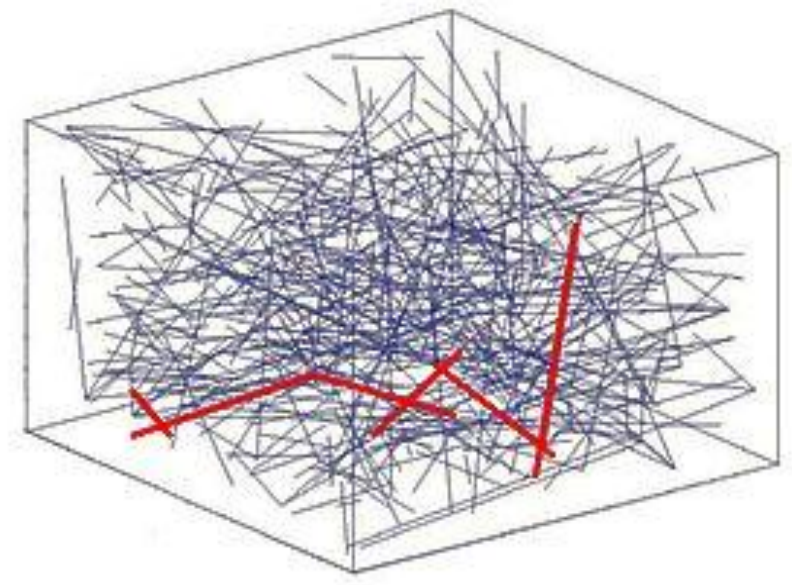

Figure 2.3 A 3D unit cell of a polymer composite with a random CNT network. The intersecting red line segments indicate an electrically conductive path based on the percolation analysis.

An example of generated unit cell of such randomly distributed CNTs is shown as Figure 2.3. The tunneling length, d, is defined as the cut-off distance beyond which the tunneling effect has a negligible contribution to the conduction. A common value used for cut-off distance is approximately 1.8 nm in previous studies (Hu et al., 2008c). We investigated different tunneling lengths of 1.5 nm, 1.8 nm, and 3 nm, and CNT aspect ratios of 100, 200, and 500. An average value of 10^6 S/m for CNT conductivity was used, and the volume fraction of CNTs was varied from 0.1% to 5.5%.

2.3.1 Electrical conductivity of CNT-epoxy composites

The electrical conductivity is shown in Figure 2.4 as a function of CNT volume fraction. The results are for a tunneling length of 1.8 nm for CNTs with an aspect ratio 100.

As these results show, there is an abrupt increase in the electrical conductivity at approximately a volume fraction of 0.15%. This can indicate the formation of a percolating path through the CNT-epoxy system. The critical volume fraction, p_c, and the critical exponent, t, were obtained by plotting a log of the specific conductivity σ as a function of the log of ($p - p_c$) and incrementally varying p_c until the best linear fit was obtained. This linear regression fit is shown in the inset of Figure 2.4. Based on Eqn. (1.3), the linear fit results in a value of 3.07 for the critical exponent t, and a percolation threshold p_c of 0.15%.

The results in Figure 2.4 correspond and are consistent with classical percolation theory. An abrupt increase in the electrical conductivity occurred at a volume fraction of approximately 0.15%, indicating the formation of a percolating path through the CNT-epoxy system. Recent experiments on MWCNT-epoxy composites have achieved percolation threshold values of between 0.05 -1 % by weight and critical exponents varying from 1.3 to 3 (Safadi et al., 2002; Dufresne et al., 2002; Yu et al., 2006; Gao et al., 2010) for MWCNTs, with a volume fraction of 1 %. Hence, these results are in good agreement with these percolation values. The specific conductivity increases from 10^{-12} S/m to 10^{-5} S/m at the critical volume fraction, and eventually reaches a saturation value of 300 S/m at approximately a volume fraction of 5 % (Figure 2.4). These results are consistent with experimental results that indicate that the conductivity of CNT-epoxy composites is in the range of 10^{-5}-10^{2} S/m corresponding to a volume fraction range from 0.04% to 4% (Bryning et al. 2005; Gao et al. 2010; Gojny et al. 2006; Yu et al. 2006).

The obtained fitting constant, scaling factor σ_0 in Eqn. (1.3), is approximately 10^6 S/m. Based on percolation theory, this constant is on the order of the conductivity of the filler, which is consistent with classical percolation theory.

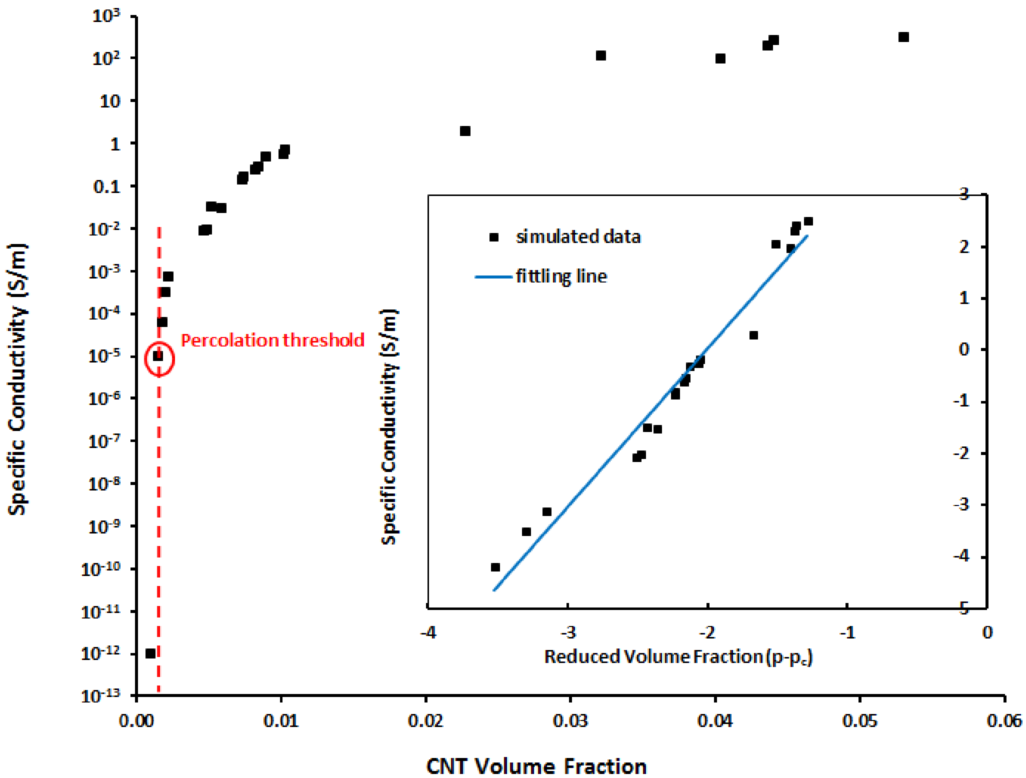

Figure 2.4 Electrical conductivity as a function of CNT volume fraction. CNTs used in the simulation have an aspect ratio of 100 and a tunneling length of 1.8 nm. The inset shows the log-log plot of the conductivity of the composite as a function of (p - p_c) with a linear fit.

2.3.2 Nanotube aspect ratio effects

Based on excluded volume theory (Celzard et al., 1996), the percolation threshold should decrease, as the aspect ratio of randomly oriented fibers increases. Experiments (Hu et al., 2008a) have, however, shown an increase in percolation threshold as a result of increase in aspect ratio, and therefore we wanted to investigate the effects of aspect ratio on the percolation threshold.

Using a tunnel cut-off distance of 1.8 nm and aspect ratios of 200 and 500, electrical conductivities were obtained (Figure 2.5-Figure 2.6). Each inset is a linear regression fit which results in different values of the critical exponent t. In comparison with the case of the CNTs with an aspect ratio of 100, the CNTs with an aspect ratio 200 have a percolation threshold that decreases from 0.15% to 0.10%, and the critical exponent decreases from 3.07 to 1.71.

For the CNTs with an aspect ratio 500, there is a pronounced effect on the percolation threshold which is 0.013%, and the critical exponent is 1.44. These values are significantly different than those for CNTs with an aspect ratio of 100, where the percolation threshold is 0.15% and the critical exponent is 3.07.

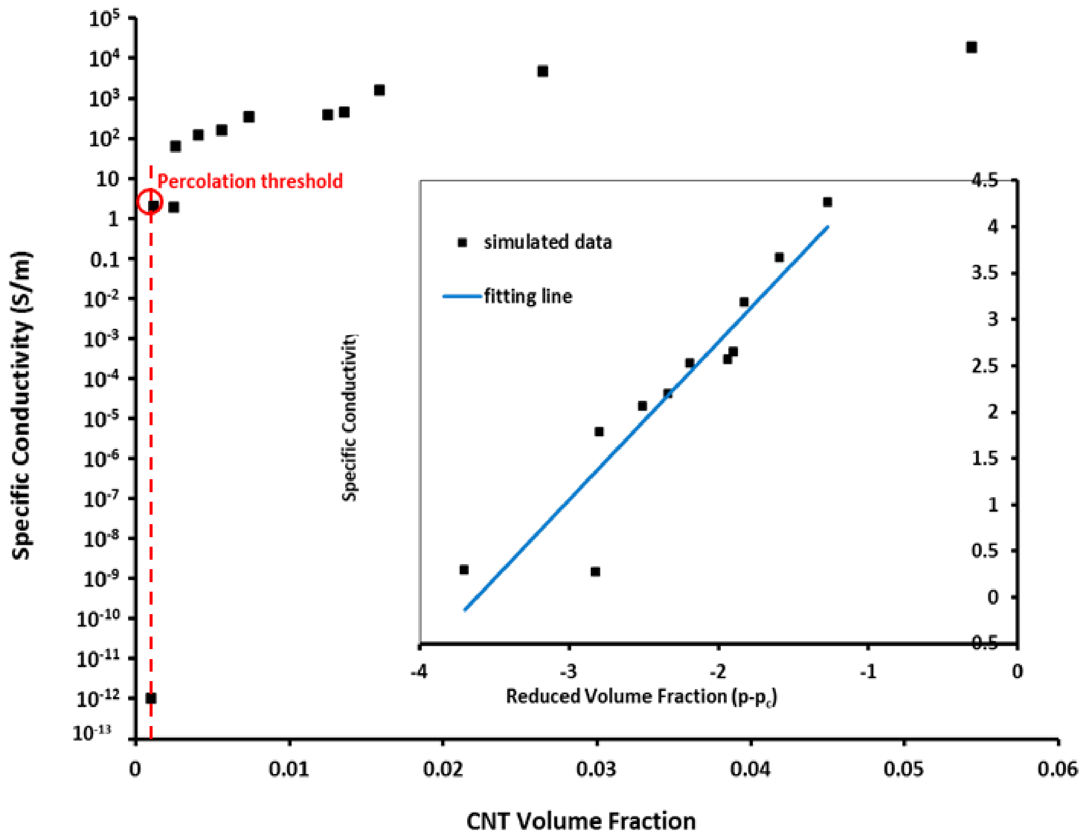

Figure 2.5 Electrical conductivity as a function of CNT volume fraction. CNTs used in the simulation have an aspect ratio of 200 and a tunneling length of 1.8 nm. The inset shows the log-log plot of the conductivity of the composite as a function of (p - p_c) with a linear fit.

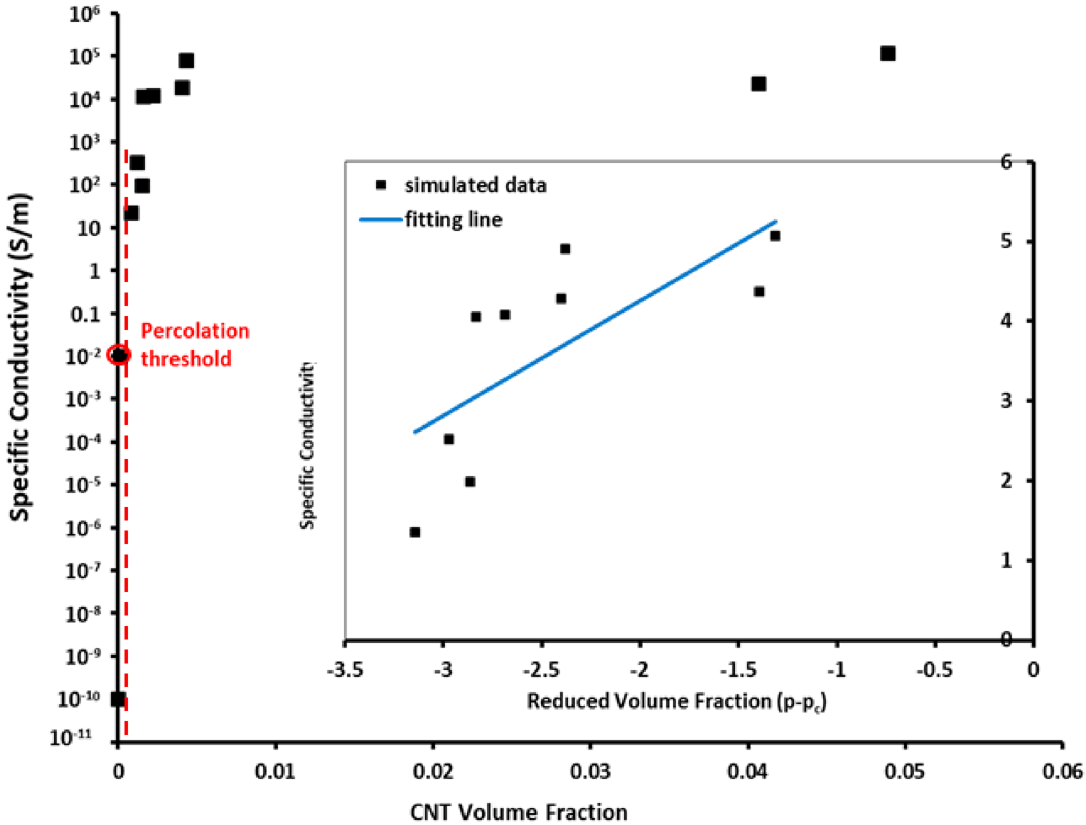

Figure 2.6 Electrical conductivity as a function of CNT volume fraction. CNTs used in the simulation have an aspect ratio of 500 and a tunneling length of 1.8 nm. The inset shows the log-log plot of the conductivity of the composite as a function of (p - p_c) with a linear fit.

These results illustrate classical percolation behavior. The specific conductivity reaches a saturation of 1.8×10^4 S/m at a volume fraction of 5 % and 10^5 S/m at a volume fraction of approximately 5%. The scaling factor, σ_0, is 10^6 S/m for CNTs with an aspect ratio of 200 and 10^7 S/m for CNTs with an aspect ratio of 500, which is in the range of experimentally measured CNT conductivity (Nan et al., 2010). In Figure 2.4-Figure 2.6, the conductivities were averaged over 50 random configurations, corresponding to each volume fraction. As shown in these figures, the conductivities increase as the aspect ratio increases. According to (Eken et al., 2011), the excluded volume theory suggests that to achieve high conductivity with a low volume fraction of randomly oriented nanotubes, the aspect ratio should be as high as possible, and the predicted results are consistent with this. As for the decrease in the percolation threshold with the increase in CNT aspect ratio, it could be due to fewer junctions in the electrical conductive network formed by CNTs with the higher aspect ratios. According to (Alamusi et al., 2011), the probability of the breakup of a conductive path increases with increases in CNT aspect ratios.

2.3.3 Tunneling length effects

As stated in the computational approach, by specifying a tunneling cut-off distance, a junction can be identified and tunneling would then occur at this junction. Beyond this cut-off distance, the tunneling effect would have a negligible effect on the overall electrical conductivity. By specifying a fixed tunneling cut-off distance, various junction distances or tunneling length can then be generated for different simulations, such that we can systematically investigate how differences in this distance would affect conductivity and percolation effects.

For a CNT aspect ratio of 100, tunnel cut-off distances of 1.8 nm, 1.5 nm and 3 nm were used. The electrical conductivities are shown in Figure 2.4, Figure 2.7-Figure 2.8. Each inset is a linear regression fit which results in different values of scaling exponent t.

The results for a tunneling length of 1.5 nm are shown in Figure 2.7, and as seen there is evident percolation behavior. The specific conductivity reaches a saturation of 10^4 S/m at approximately a volume fraction of 5 % and the scaling factor is 10^7 S/m. In comparison with the 1.8 nm results, there is an increase in the percolation threshold from 0.15% to 0.22%, which is in agreement with previous predictions (Eken et al., 2011). The critical exponent decreases from 3.07 to 2.55, which indicates that the tunneling distance also has a significant influence on the critical exponent in combination with the percolation threshold.

For a tunneling length of 3 nm (Figure 2.8), no abrupt increase in conductivity at low volume fractions are observed, and the predicted conductivity values are scattered. A log-log fit has resulted in a low R-squared (correlation coefficient) value and the randomness is quite high, which indicates a breakdown of classical percolation law. By applying the log-log fit, the critical exponent obtained is 0.18 and the constant σ_0 is below 1, which are both far below commonly assumed values. Therefore, the electrical conductivity of the CNT-epoxy composites cannot be characterized by the geometrical percolation theory for increases in tunnel length case for this aspect ratio and tunneling length.

The random dispersion of the CNTs and the interaction between the CNTs and the polymer matrix are crucial for determining the conductive properties of CNT-filled polymers (Alamusi et al., 2011). When the CNT concentration attains a critical value, a three-dimensional network will be formed throughout the matrix system. As a result, the macro electrical conductive behavior of CNT-epoxy composites can be described by statistical percolation theory (Chang et al., 2009). However, locally, some individual tubes may not be directly in contact, but can be isolated by the polymer matrix (Chang et al., 2009). The larger the tunneling length, the more pronounced the effects of tunneling distances are, and this is one of the reasons that classical percolation theory breaks down.

Furthermore, according to Balberg (Balberg, 2009), another factor to be taken into account is the exponential decay of the tunneling probability. He notes that experimentally observed behavior is associated with the network of fillers that have neighbors within a separation on the order of the tunneling decay constant, and this is also why there can also be a breakdown of classical percolation theories for large tunnel length cases.

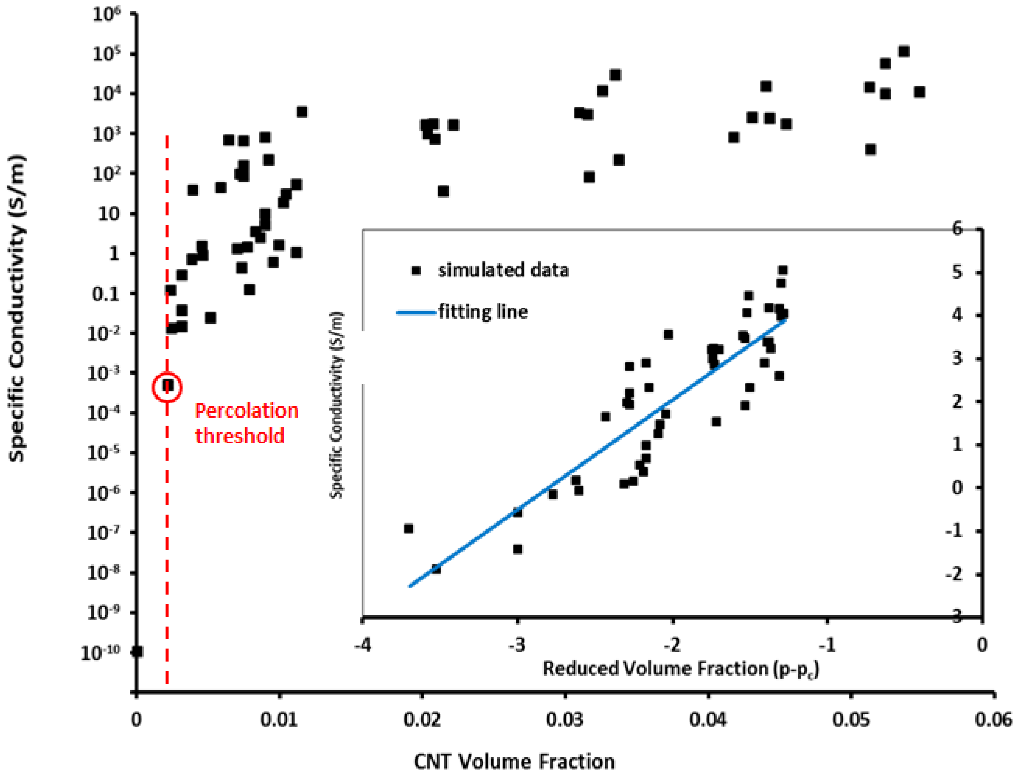

Figure 2.7 Electrical conductivity as a function of CNT volume fraction. CNTs used in the simulation have an aspect ratio of 100 and a tunneling length of 1.5 nm. The inset shows the log-log plot of the conductivity of the composite as a function of (p - p_c) with a linear fit.

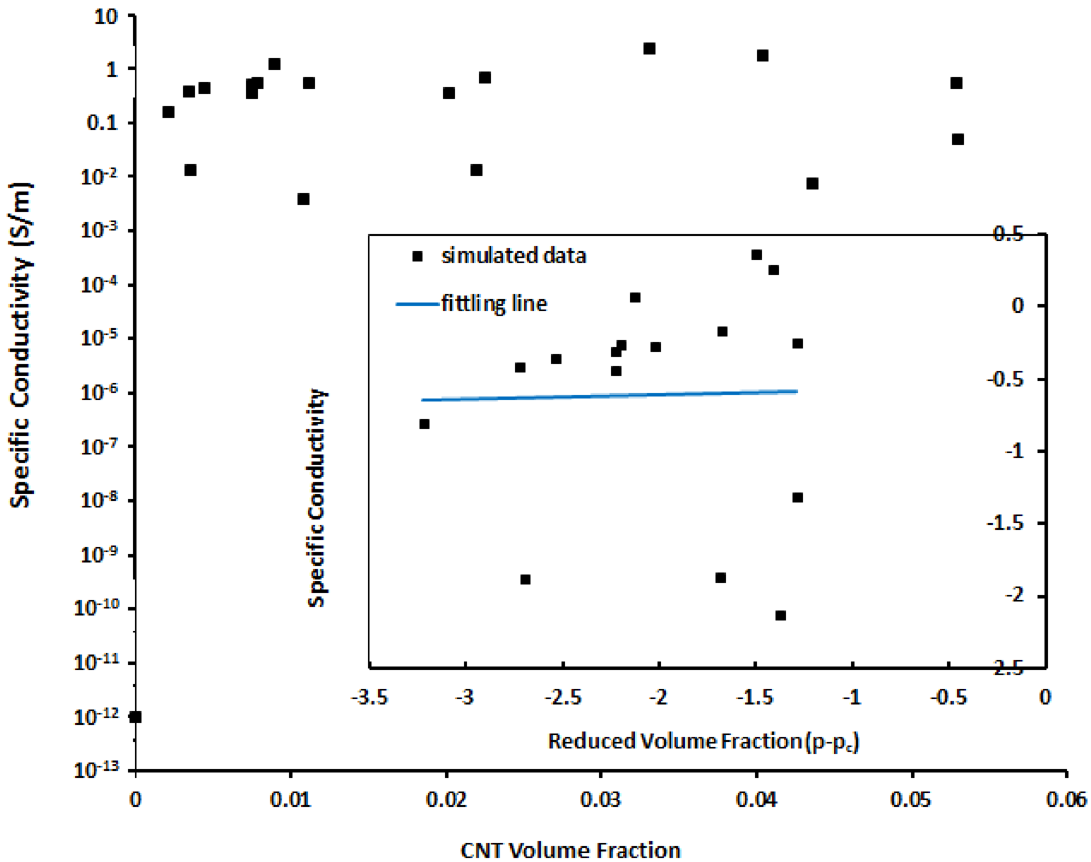

Figure 2.8 Electrical conductivity as a function of CNT volume fraction. CNTs used in the simulation have an aspect ratio of 100 and tunneling length of 3 nm. The inset shows the log-log plot of the conductivity of the composite as a function of (p - p_c) with a linear fit.

2.4 Summary and Conclusions

We have proposed a modeling approach to predict the electrical conductivity of a randomly distributed CNT-epoxy composite network. A path search algorithm and electrical junction identification method were developed to determine different electrical conductive paths. The composite conductivity was calculated as a function of tunneling lengths, CNT volume fractions, and CNT aspect ratios. Percolation-tunneling behavior was obtained for the critical exponents in the power law relation within the range of 1 to 4. The percolation threshold and scaling factors were compared with previous experimentally-based values and for low tunneling distances these values were consistent with most experimentally observed values. However, for increases in tunneling distances, there was a breakdown of classical percolation formulations. The reason could be that efficient carrier transport between CNTs is blocked by the polymer insulating layers, and fluctuation-induced tunneling has to be taken into account for the electrical conductivity (Chang et al., 2009). This is a further indication of how tunneling variations can significantly affect resistance and the percolation threshold.

The shape of CNTs and their local clusters may also affect the power law parameters, such as the critical exponent and the percolation threshold. According to Balberg (Balberg, 2009), the distribution of the separation between the conducting fillers that are on the order of the tunneling decay distance determines the critical behavior, such that the greater the separation distribution, the more pronounced the non-universal percolation behavior. This explains the breakdown of classical percolation theories for large tunnel lengths. The CNT-epoxy network becomes more dilute as the tunnel length increases, the percolation behavior with a well-defined percolation threshold then becomes less dominant, and a non-universal percolation behavior is more pronounced. Future investigations will focus on incorporating thermal and mechanical properties to better understand and predict how overall CNT-polymer behavior can be controlled for large scale processing.

CHAPTER 3

ELECTRO-THERMO-MECHANICAL MODELING AND ANALYSES OF CARBON NANOTUBE-POLYMER COMPOSITES

3.1 Introduction

A new FE modeling method has been developed to investigate how the electrical-mechanical-thermal behavior of CNT reinforced polymer composites is affected by electron tunneling distances, volume fraction, and physically realistic tube aspect ratios. A representative CNT polymer composite conductive path was chosen from a percolation analysis to establish the three-dimensional (3D) computational FE approach. A specialized Maxwell FE formulation with a Fermi-based tunneling resistance was then used to obtain current density evolution for different CNT-polymer dispersions and tunneling distances. Analyses based on thermo-electrical and electro-thermo-mechanical FE approaches were used to understand how CNT-epoxy composites behave under electro-thermo-mechanical loading conditions.

A better understanding of how conductivity in different CNT arrangements can be affected by tunneling is critical to better controlling potential sensing capabilities. We address these shortcomings and inconsistencies by developing a modeling approach to predict the electrical conductivity of CNT-epoxy composite based on variations in tunneling resistance, aspect ratios, CNT volume fractions and distributions. Based on the new percolation method that accounted for quantum tunneling described in Chapter 2, a representative conductive path is used as the basis for a representative FE model. The FE model, based on Maxwell's equations, is first used to investigate electrical conductivity behavior for different tunneling distances. Electro-thermo and electro-thermo-mechanical FE approaches are then used to investigate how temperatures, stresses, conductivities are affected by variations in tunneling distances and electro-thermo-mechanical loading conditions.

3.2 Finite Element Modeling

Maxwell formulation (Eqn. (3.1)), thermo-electro coupling (Eqn. (3.2)), and electro-thermo-mechanical coupling (Eqn. (3.3)), incorporated with a Fermi-based tunneling resistance (Eqn. (2.1)) were then used to obtain current density evolution for different tunneling distances. The Maxwell equations and the constitutive equation are as follows

$$\nabla \times \{H\} = \{J\} + \{\frac{\partial D}{\partial t}\} \ , \tag{3.1a}$$

$$\nabla \times \{E\} = -\{\frac{\partial B}{\partial t}\} \ , \tag{3.1b}$$

$$\nabla \cdot \{B\} = 0 \ , \tag{3.1c}$$

$$\nabla \cdot \{D\} = \rho \ , \tag{3.1d}$$

$$\{J\} = [\sigma]\{E\}\,, \quad \{D\} = [\varepsilon]\{E\}\,, \ \ \{E\} = -\nabla V\,, \tag{3.1e}$$

$$\nabla \cdot (\{J\} + \{\frac{\partial \{D\}}{\partial t}\}) = 0\,. \tag{3.1f}$$

where J is conduction current density, D is electric flux density vector, ρ is electric charge density, and V is electric scalar potential.

The thermo-electro coupling is through Seebeck coefficients, which are represented as [K^{Vt}] in Eqn. (3.2). The thermo-electro FE matrix equation is

$$\begin{bmatrix} [C^t][0] \\ [0][C^V] \end{bmatrix} \begin{Bmatrix} \{\dot{T}\} \\ \{\dot{V}\} \end{Bmatrix} + \begin{bmatrix} [K^t][0] \\ [K^{Vt}][K^V] \end{bmatrix} \begin{Bmatrix} \{T\} \\ \{V\} \end{Bmatrix} = \begin{Bmatrix} \{Q\} \\ \{I\} \end{Bmatrix} , \tag{3.2}$$

where **[** C^t] is thermal specific heat matrix , [C^V] is the dielectric coefficient matrix, [K^t] is thermal conductivity matrix, [K^V] is electrical conductivity coefficient matrix, [T] is thermal potential (temperature) vector , [V] is electric potential vector, [Q] is the heat generation rate per unit volume, and [K^{Vt}] is the Seebeck coefficient coupling matrix.

The electro-thermo-mechanical FE matrix equations are:

$$\begin{bmatrix} [K][0][0][0] \\ [0][K^t][0][0] \\ [0][0][K^V][0] \\ [0][0][0][K^m] \end{bmatrix} \begin{Bmatrix} \{u\} \\ \{T\} \\ \{V\} \\ \{\phi\} \end{Bmatrix} = \begin{Bmatrix} \{F\} \\ \{Q\} \\ \{I\} \\ \{\psi_f\} \end{Bmatrix} , \tag{3.3}$$

where [K] is structural stiffness matrix, { F }is the sum of force vector, { Q }is the sum of heat rate and convection surface vector, { I } is the applied nodal electric current vector, { ψ_f } is the applied nodal flux vector, { u } is displacement vector, and { ϕ } is magnetic scalar potential vector. The zero values correspond to a decoupling of the displacements from the thermal and electrical fields. These system of FE equations are used to solve the electro-mechanical-thermal response of the CNT polymer unit cell. Eqns. (3.1) pertain to the Maxwell electromagnetic behavior. Eqns. (3.2) pertain to the thermal heat conduction, and are coupled to the Maxwell equations through the Seebeck coefficients (Eqn. (3.2)) and the mechanical behavior is given by Eqn. (3.3).

As mentioned in Chapter 2, the tunneling resistance that we used in our approach is based on Simmons' formula (Simmons, 1963) as

$$J = (6.2 \times 10^{10} / \Delta s^2)\{\varphi_I \exp(-1.025\Delta s \varphi_I^{\frac{1}{2}})\} - (\varphi_I + V)\exp[-1.025\Delta s(\varphi_I + V)^{\frac{1}{2}}]\}\,, \quad (3.4a)$$

$$\varphi_I = \varphi_0 - (V/2s)(s_1 + s_2) - [5.75 / K(s_2 - s_1)]\ln[s_2(s - s_1)/s_1(s - s_2)]\,, \quad (3.4b)$$

$$s_2 = 6/K\varphi_0\,, \quad s_2 = s[1 - 46/(3\varphi_0 Ks + 20 - 2VKs)] + 6/K\varphi_0\,, \quad \Delta s = s_2 - s_1\,, \quad (3.4c)$$

$$R_{tunnel} = \frac{V}{A \cdot J}\,, \quad (3.4d)$$

where J is the tunneling current density, V is the electrical potential difference, s_1, s_2 are the limits of barrier at Fermi level, s is the thickness of the insulating barrier, A is the cross sectional area of the tunnel, and φ_0 is the barrier height, which for epoxy is 0.5-2.5 eV and 1.5 eV was used in this work (Hu et al., 2008a). In this equation, s is the tunneling distance in our FE models (Xu, Siqi;Rezvanian, Omid; Zikry, 2012).

3.3 Results and Discussion

The conductive path search algorithm, the 3D CNT network model, and the electro-thermo-mechanical FE formulations with Fermi-based tunneling resistance were used to investigate the current density evolution and thermo electric behavior for different CNT-polymer dispersions and tunneling distances.

3.3.1 Finite Element Analyses

To investigate the local behavior of CNT-polymer composite, one conductive path was chosen from the percolation analysis for a physically representative 3D computational model. FE analyses were then conducted to obtain the 3D spatial current flows, current densities, and thermal distributions. To be consistent with experimentally observed values (Li et al., 2007), the aspect ratio (length/diameter) of CNTs was set equal to 50. The polymer matrix was assumed to be epoxy, isotropic linear elastic, and below the glass transition temperature, with an electrical resistivity of 10^{10} $\Omega\cdot$m, a barrier height of 5 eV, and a dielectric constant of 3.98. The length of each CNT is 200 nm, and the electrical resistivity is assumed to be 10^{-6} $\Omega\cdot$m.

The finite element mesh and the tunnel regions of the model are shown in Figure 3.1. The three CNTs in the polymer matrix are connected by two tunnel regions with a torus shape (Figure 3.2(a)). The inset is a close-up view of the bottom tunnel region, where it is assumed that the electrons can tunnel. It should be noted that the CNTs are not in contact, and that there is a polymer gap between the two CNTs. Based on the angle, θ, as indicated in Figure 3.2 (b-c), the tunneling distance, d_t, the length of the curve, was varied for approximate tunneling distances of 1 nm, 2 nm and 3 nm.

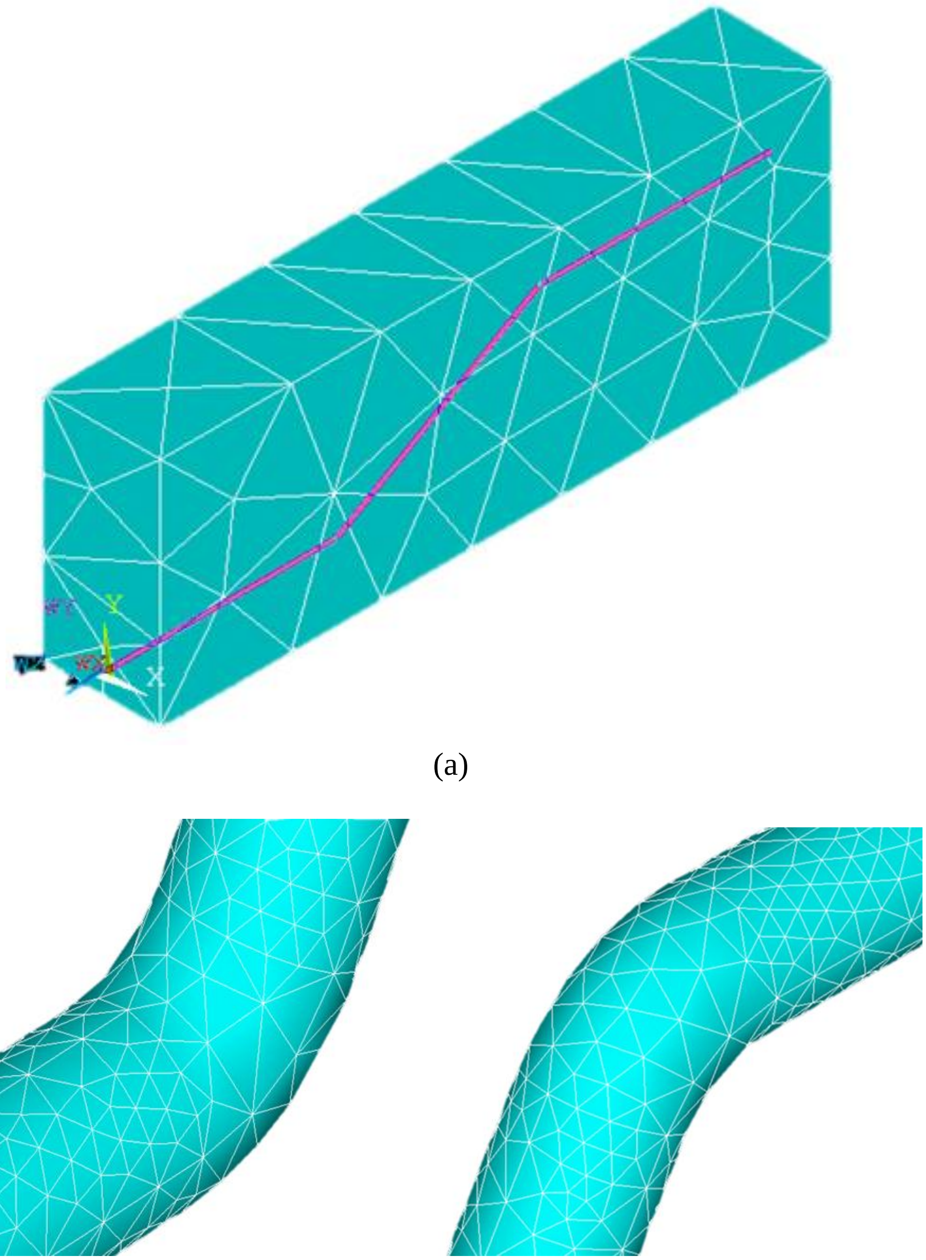

(a)

(b) (c)

Figure 3.1 (a) Finite element mesh for a 3D CNT-epoxy composite model (b) (c) close up view of the two tunnel regions.

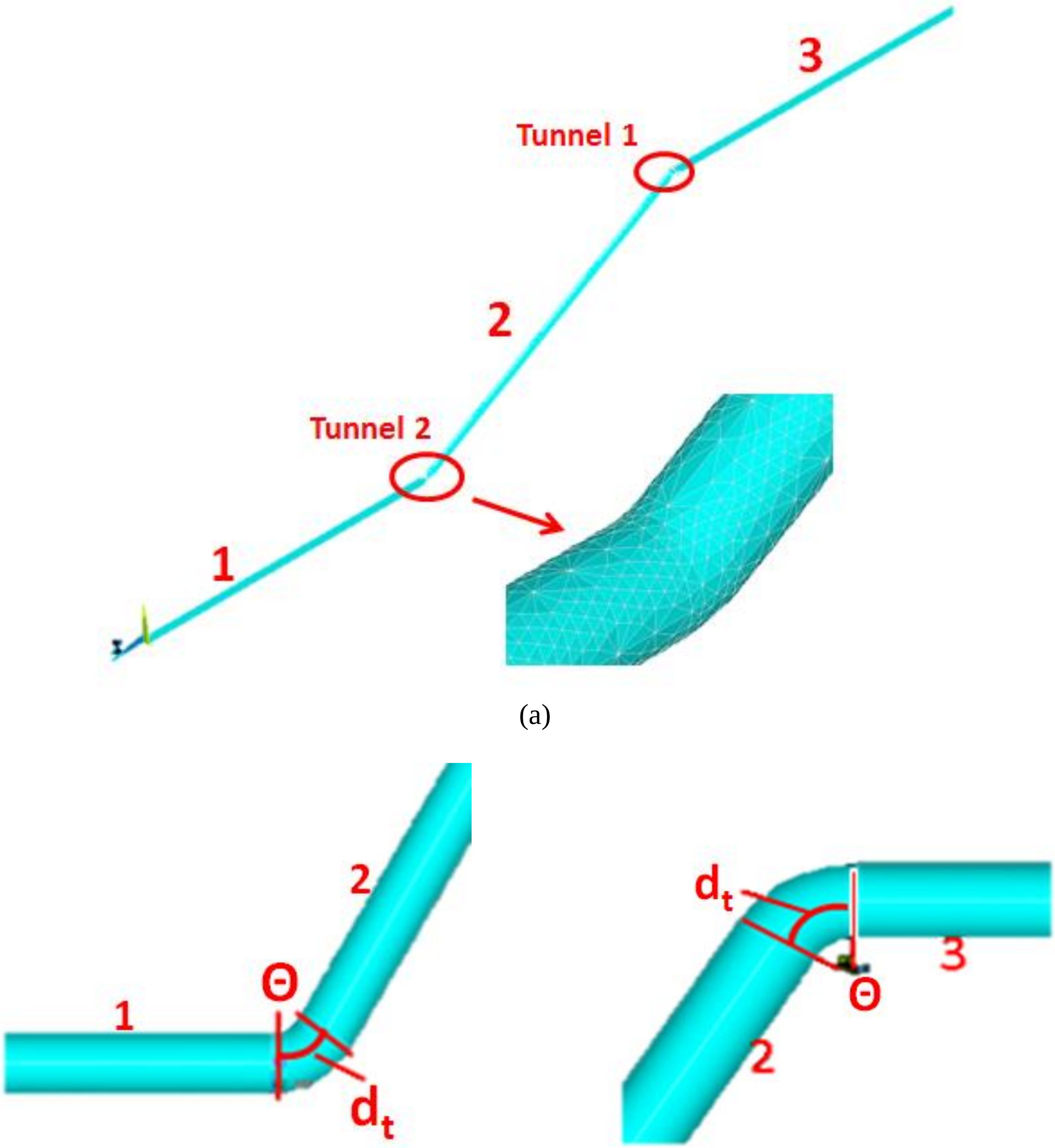

(b) (c)

Figure 3.2 (a) The three-CNT connected with two tunnel regions (b) Tunnel 2 (c) Tunnel 1.

The dimensions of CNT-epoxy composite cell for a tunneling distance 1 nm is100 nm×200 nm ×580 nm, for a tunneling distance of 2 nm is100 nm×200 nm ×578 nm, and for a tunneling distance of 3 nm is100 nm×230 nm ×460 nm. It should be noted that to adjust for the specific CNT arrangements, the dimensions of the composite cell in the three cases are slightly different, but the results are normalized with respect to the different cell sizes. Based on convergence analyses, approximately 35,000 to 40,000 3D ten noded tetrahedral elements were used for electrical analysis, and approximately 30,000 to 110,000 3D ten noded tetrahedral elements were used for the electro-thermo analyses and the electro-thermo-mechanical analyses.

3.3.1.1 Electrical Analyses

The total current density along the length of the three CNTs for an applied voltage of 1 V applied to the two far ends of the three-CNT epoxy model is shown in Figure 3.3-Figure 3.5 for the three tunneling distances of 1, 2, and 3 nms. The current densities are normalized by the maximum total current density of the epoxy matrix. The total current density in the epoxy matrix with the embedded CNTs is shown in Figure 3.3 (a). It can be seen that there are large decreases in total current density as the tunneling distance increases from 1 nm to 2 nm. This is consistent with experimental observations (see, for example, (Balberg, 2009; Yu et al., 2010; Eken et al., 2011; Li et al., 2008a)).The normalized maximum total current density decreases from 5.74×10^4 to 5.700×10^3. However, for the 3 nm tunnel distance case, the total current density in CNTs is lower than that of the 2 nm tunnel distance case. The normalized maximum total current density is 5.700×10^3 for the 3 nm case and 7.500×10^3 for the 2 nm case. This is most likely due to that as the tunneling distance increases, which occurs by varying the angles between contacting CNTs, the orientation effects become more pronounced. This underscores the point that tunneling is also affected by the orientation of CNT tubes, and not only by the tunneling distance (Yu et al., 2010). As indicated in Figure 3.3(b), Figure 3.4-Figure 3.5, the maximum occurs along the CNT on the top (CNT 3), and the region where the maximum occurs varies for each tunneling distance. These differences are not affected by the CNT orientations, but by the large current density gradients between the epoxy matrix and the CNTs.

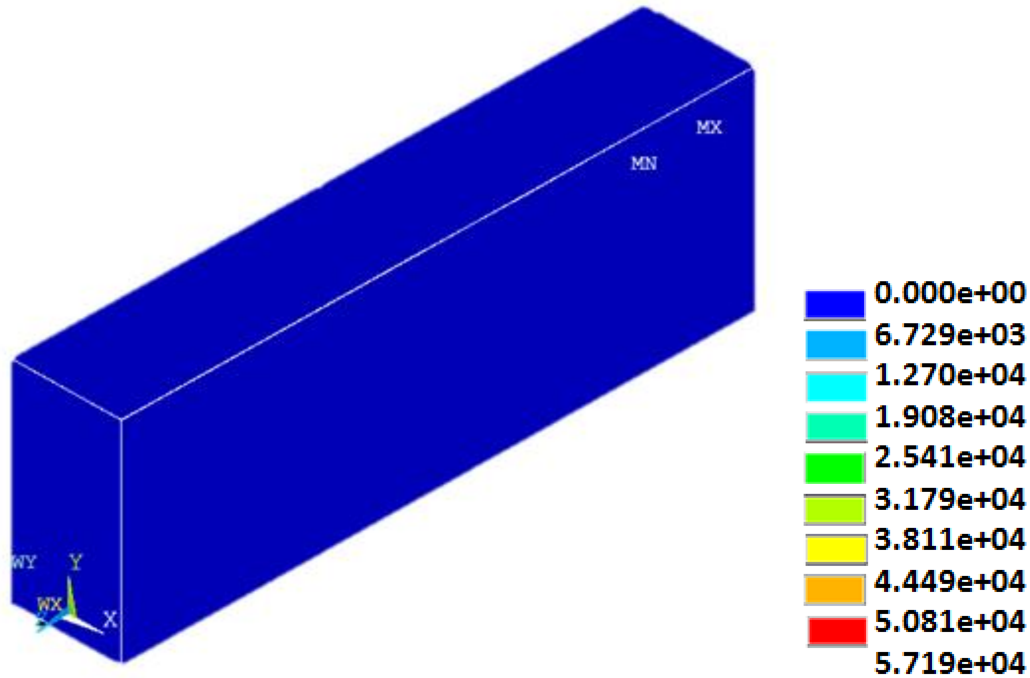

(a)

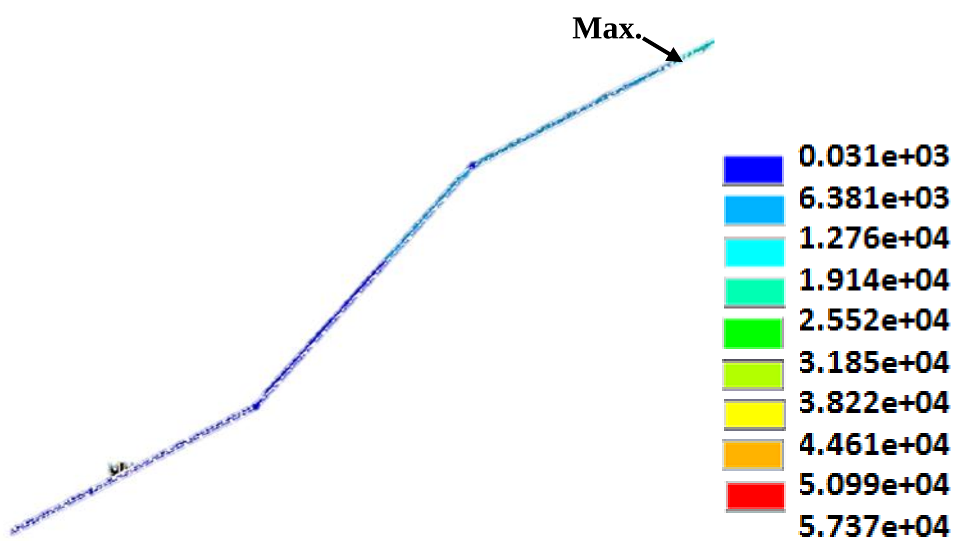

(b)

Figure 3.3 Normalized total current density for (a) epoxy/CNT composite (b) CNTs for a tunneling distance of 1 nm.

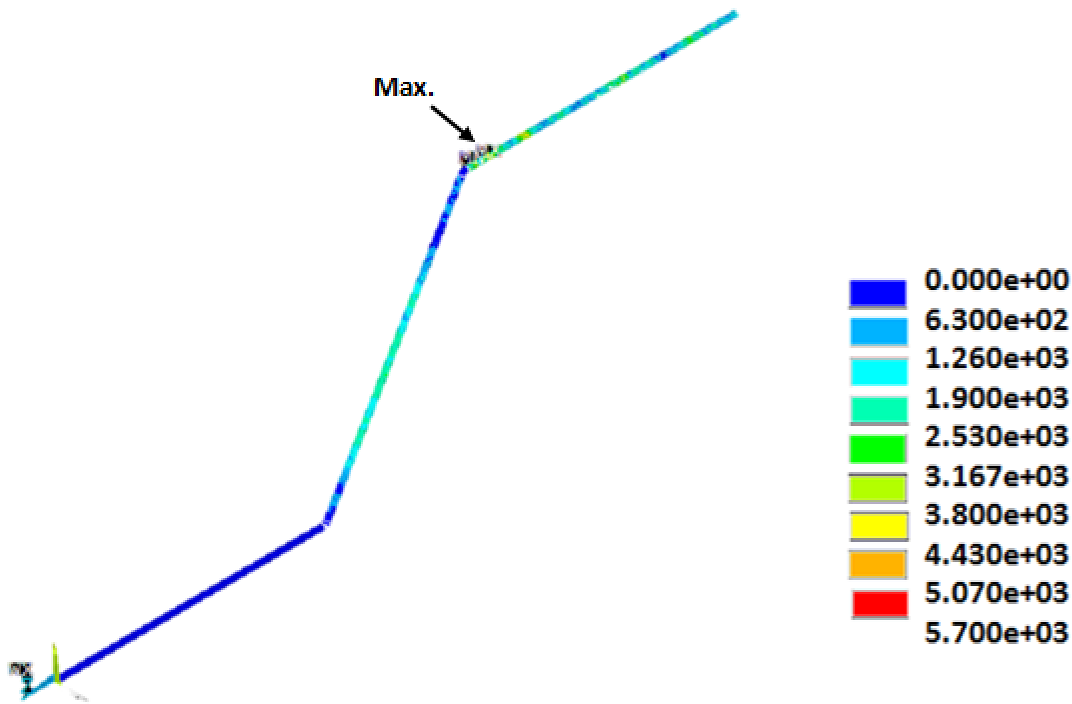

Figure 3.4 Normalized total current density for CNTs in an epoxy matrix for a tunneling distance of 2 nm.

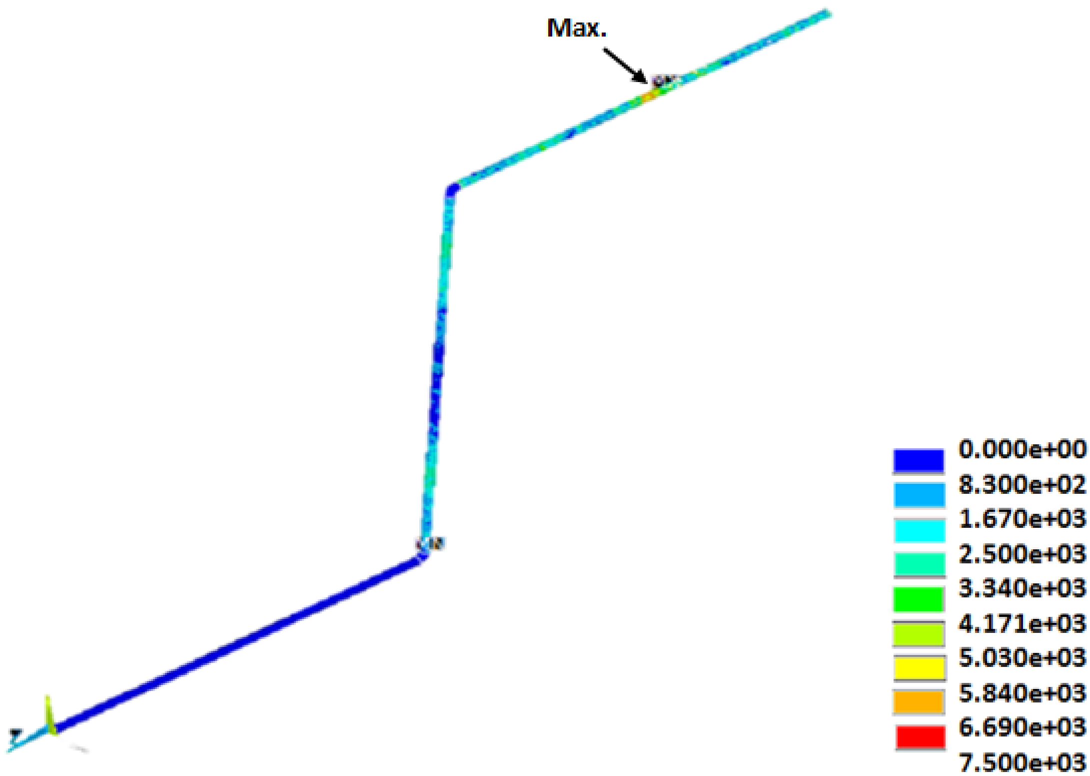

Figure 3.5 Normalized total current density for CNTs in an epoxy matrix for a tunneling distance of 3 nm.

3.3.1.2 Electro-Thermo Analyses

To further investigate the tunneling distance effects, electro-thermo analyses were conducted by coupling the heat flow equations to electric charge equations through the Seebeck coefficients. The Seebeck coefficients used here are for CNTs from (Yu et al., 2008). A thermal difference of 293K-373K and a voltage of 1V were simultaneously applied to the two ends of the three-CNT epoxy computational cell. The temperature distributions are shown in Figure 3.6, Figure 3.8 and Figure 3.10 for the three tunneling distances. It can be seen that there are large decreases in total current density as the tunnel distance increases from 1 nm to 2 nm (Figure 3.7-Figure 3.9). The normalized maximum total current density decreases from 6.787×104 to 6.033×103 for these tunneling distances, but it increases to 1.576×104 for the tunneling distance of 3 nm (Figure 3.11). This increase is due to the CNT orientations and arrangements, and the large gradients with the epoxy current density. Furthermore, the coupled thermal fields result in a significant increase in current density and this is due to the coupled effects of the Seebeck coefficients (Ashcroft and Mermin 1976), which couples the temperature differences directly into electricity. There are, therefore, three main factors that affect thermo-electrical behavior: CNT orientations, tunneling distances, and thermo-electrical gradients with the epoxy.

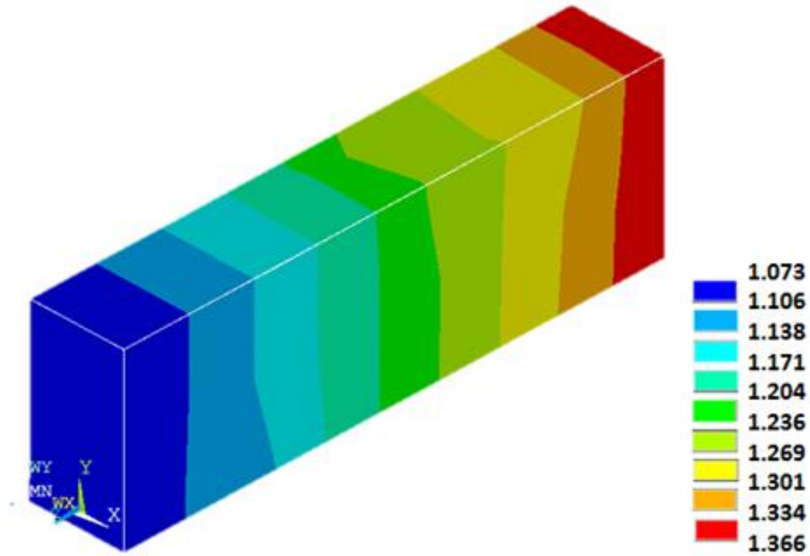

(a)

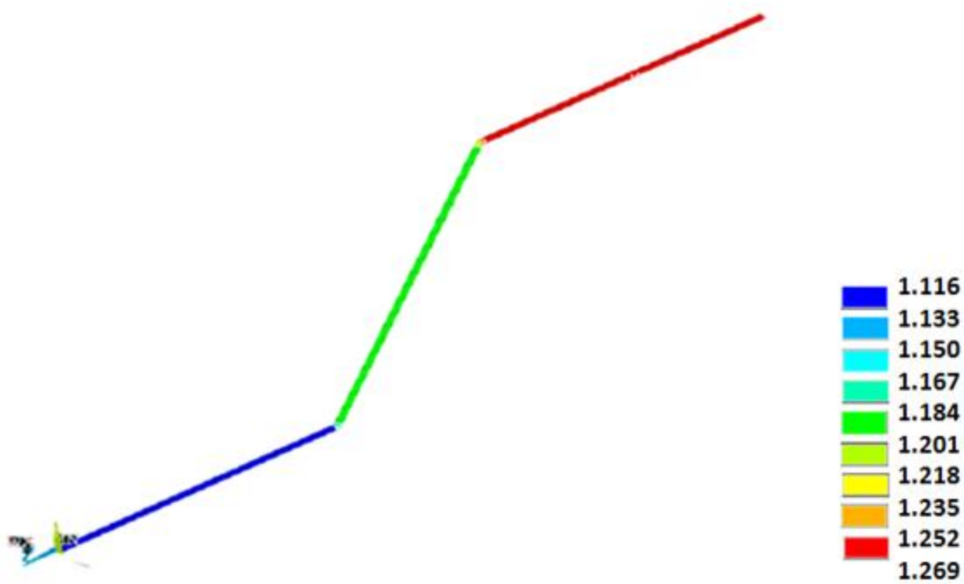

(b)

Figure 3.6 Normalized nodal temperature for (a) epoxy/CNT composite (b) CNTs for a tunneling distance of 1 nm.

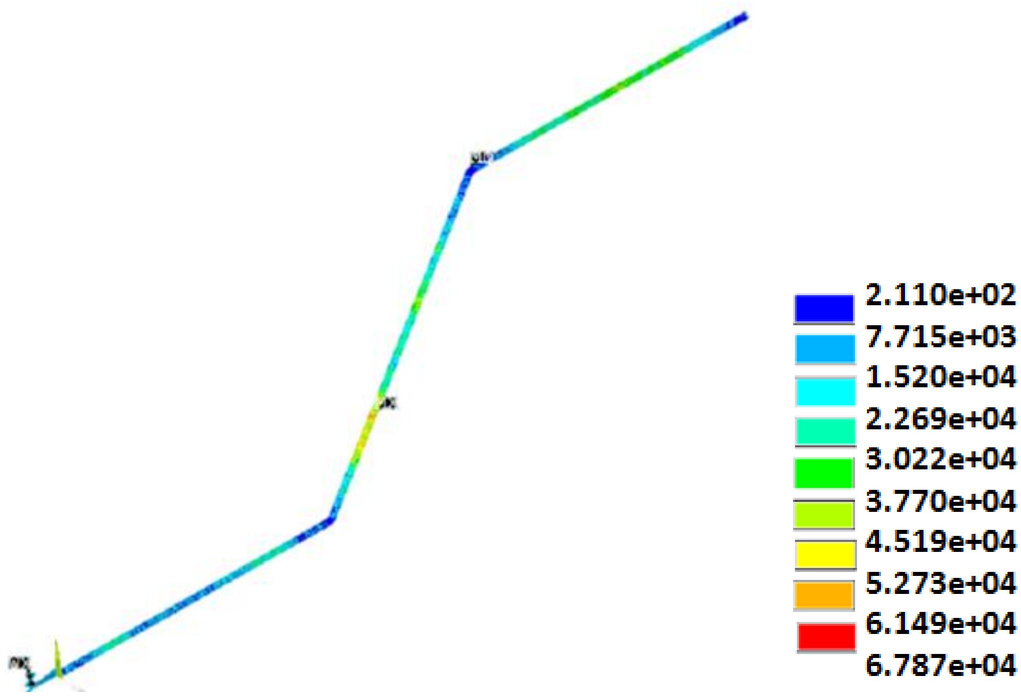

Figure 3.7 Normalized total current density for CNTs in epoxy matrix for a tunneling distance of 1 nm.

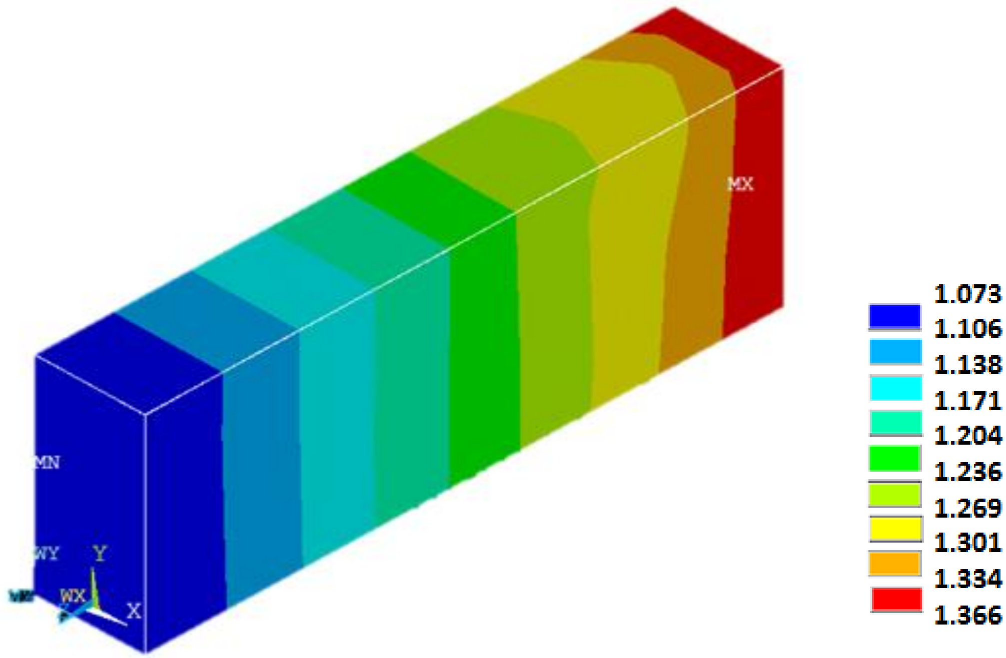

(a)

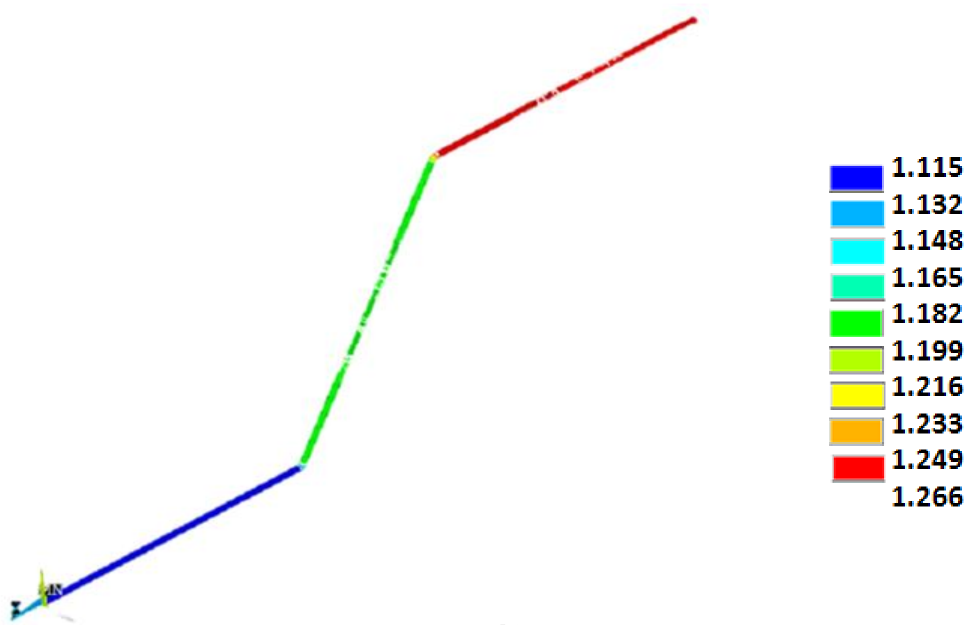

(b)

Figure 3.8 Normalized nodal temperature for (a) epoxy/CNT composite (b) CNTs for a tunneling distance of 2 nm.

For these electro-thermo loading conditions, the maximum Joule heat occurs at the narrower part of the bottom tunnel regions for all the three cases. Results of the maximum joule heat for the two tunnel regions are listed in Table 3.1-Table 3.3. This effect is more pronounced for the larger tunneling distances of 2 and 3 nms.

Table 3.1 Joule Heating (J) for tunneling distance of 1 nm

Tunnel 1	0.320e-21
Tunnel 2	0.355e-21

Table 3.2 Joule Heating (J) for tunneling distance of 2 nm

Tunnel 1	1.027e-026
Tunnel 2	2.137e-025

Table 3.3 Joule Heating (J) for tunneling distance of 3 nm

Tunnel 1	8.312e-036
Tunnel 2	2.911e-035

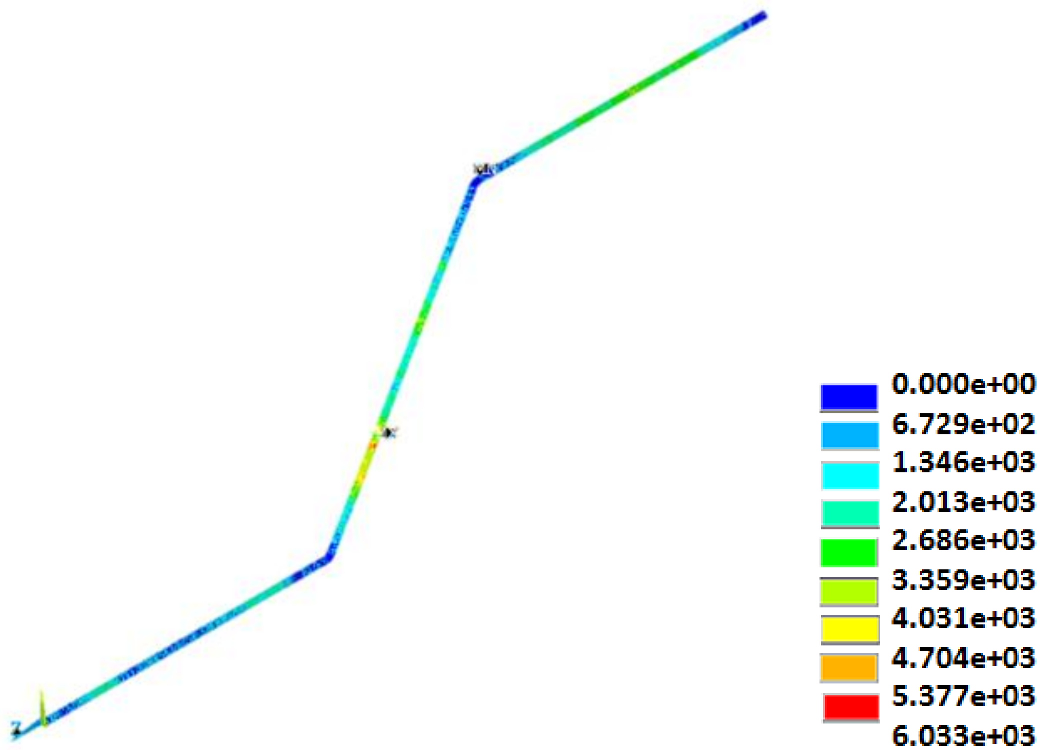

Figure 3.9 Normalized total current density for CNTs in epoxy matrix for a tunneling distance of 2 nm.

Figure 3.10 Normalized nodal temperature for (a) epoxy/CNT composite (b) CNTs for a tunneling distance of 3 nm.

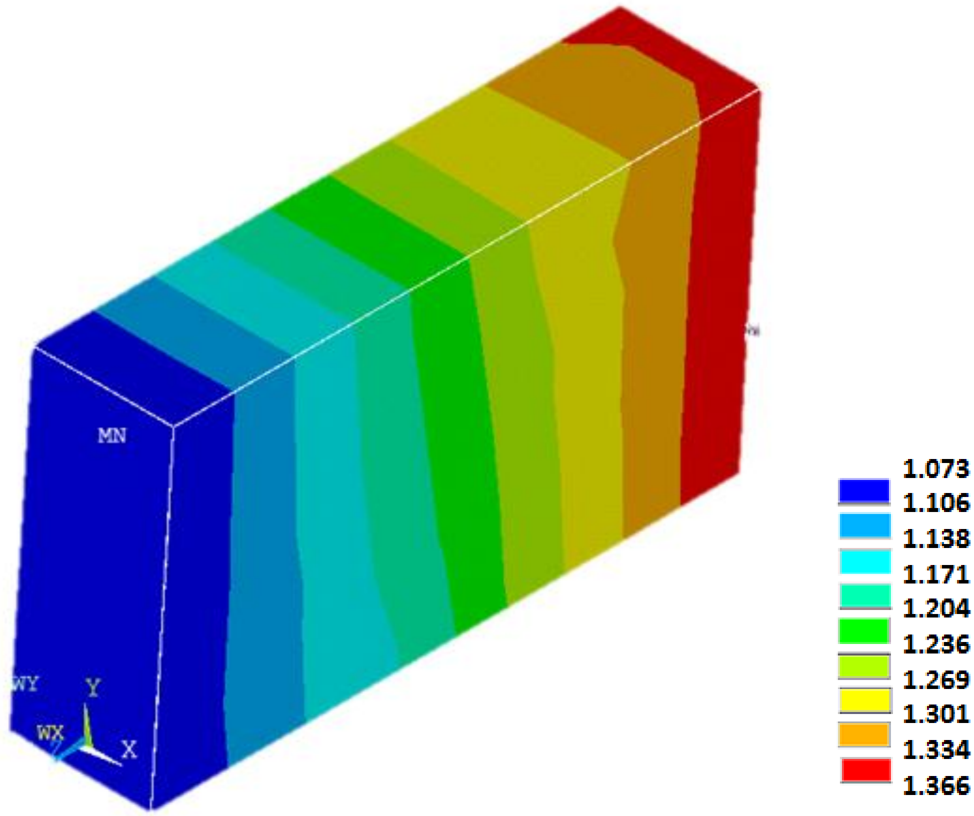

(a)

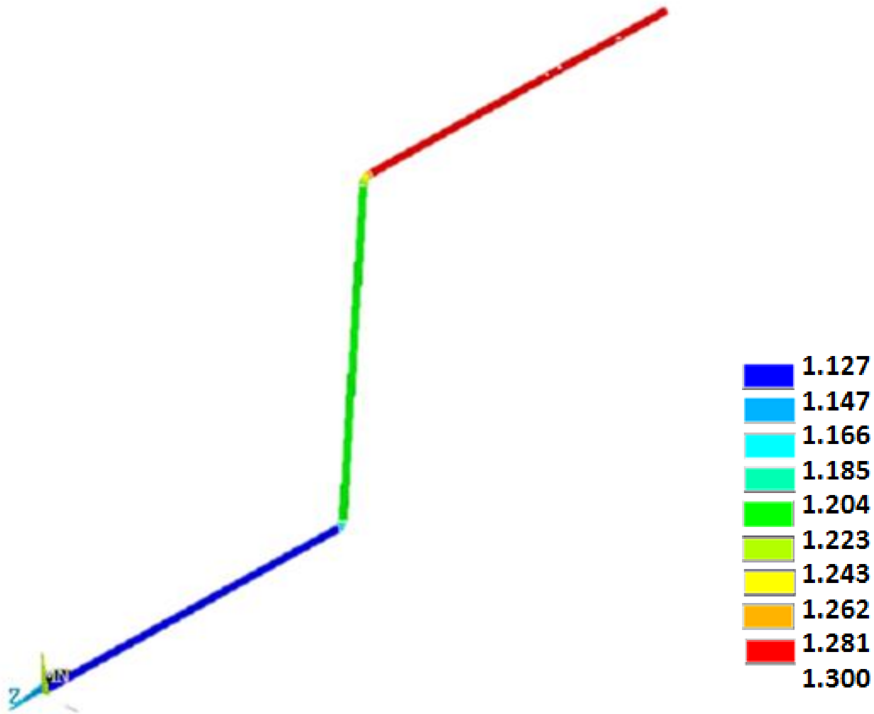

(b)

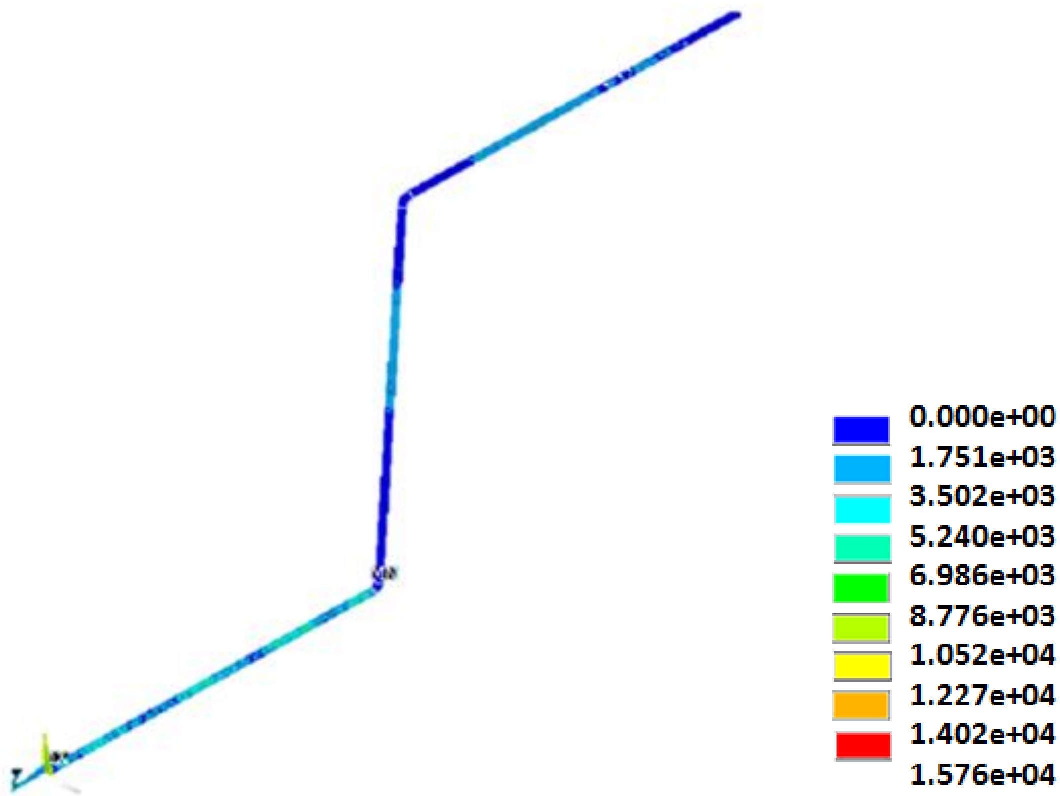

Figure 3.11 Normalized total current density for CNTs in epoxy matrix for a tunneling distance of 3 nm.

3.3.1.3 Electro-thermo-mechanical Analyses

For the case of 1 nm tunnel distance, an electro-thermo-mechanical analysis was conducted. A displacement of 4 nm was applied to one end of the CNT-epoxy composite cell. The thermo-electrical analyses were coupled through the Seebeck coefficients, but the mechanical analyses were decoupled from the thermo-electrical analyses, since accurate GF for the CNT polymer composites that account for tunneling effects are not available for random arrangements and distributions. The 3D nodal displacement results are normalized by the initial length of the cell (Figure 3.12). The von Mises stress, normalized by the Young's modulus of CNTs, is shown in Figure 3.13.The normalized maximum von Mises stress in the matrix is 0.022% and 1.460% in the CNTs, which further indicates that there are large gradients in the stress fields at the interface of the epoxy matrix and the CNTs.

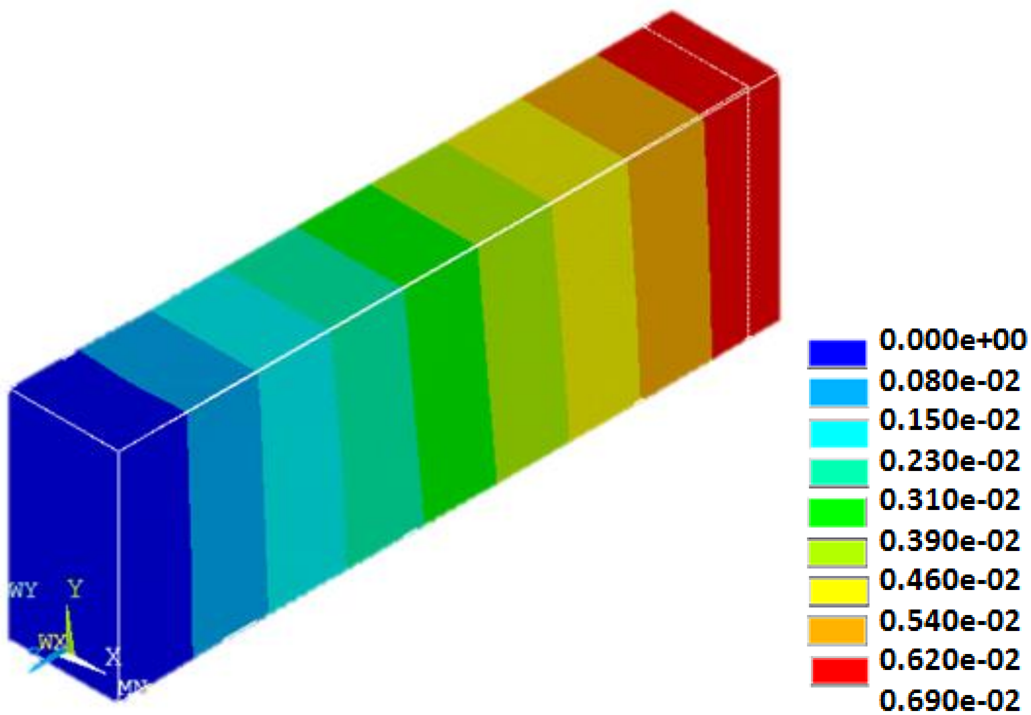

Figure 3.12 Normalized 3D displacement for epoxy/CNT composite for a tunneling distance of 1 nm.

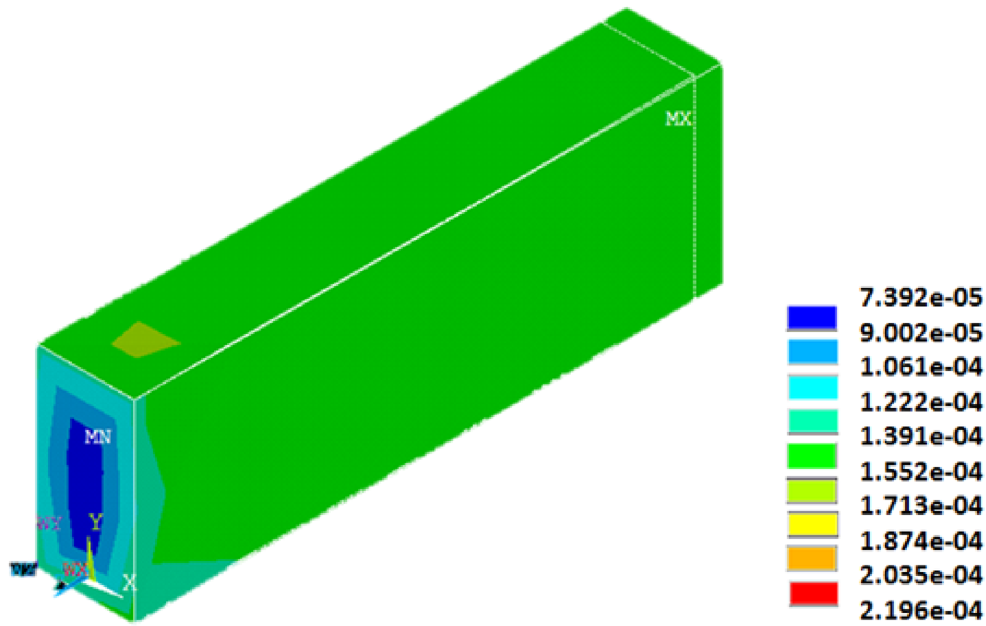

(a)

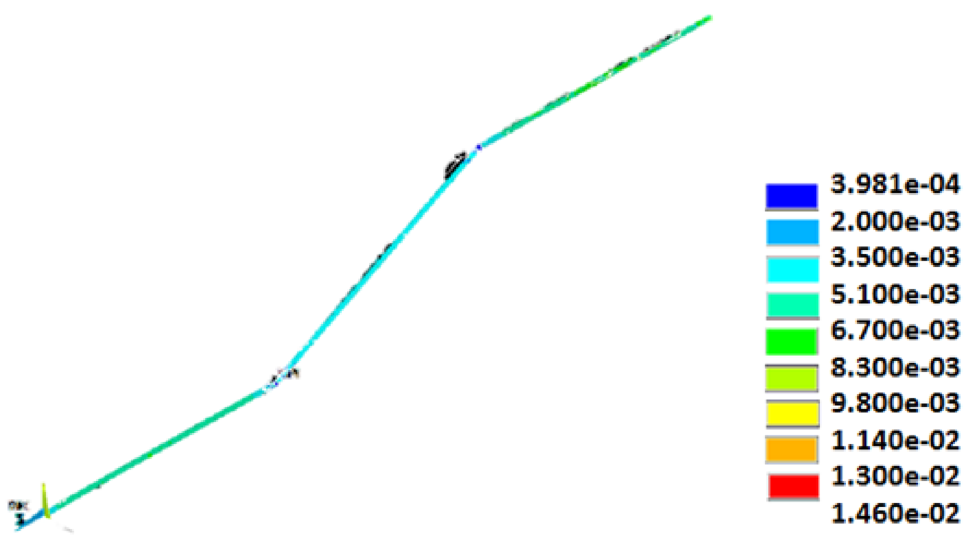

(b)

Figure 3.13 Normalized Von Mises stress for (a) epoxy/CNT composite (b) CNTs for a tunneling distance of 1 nm.

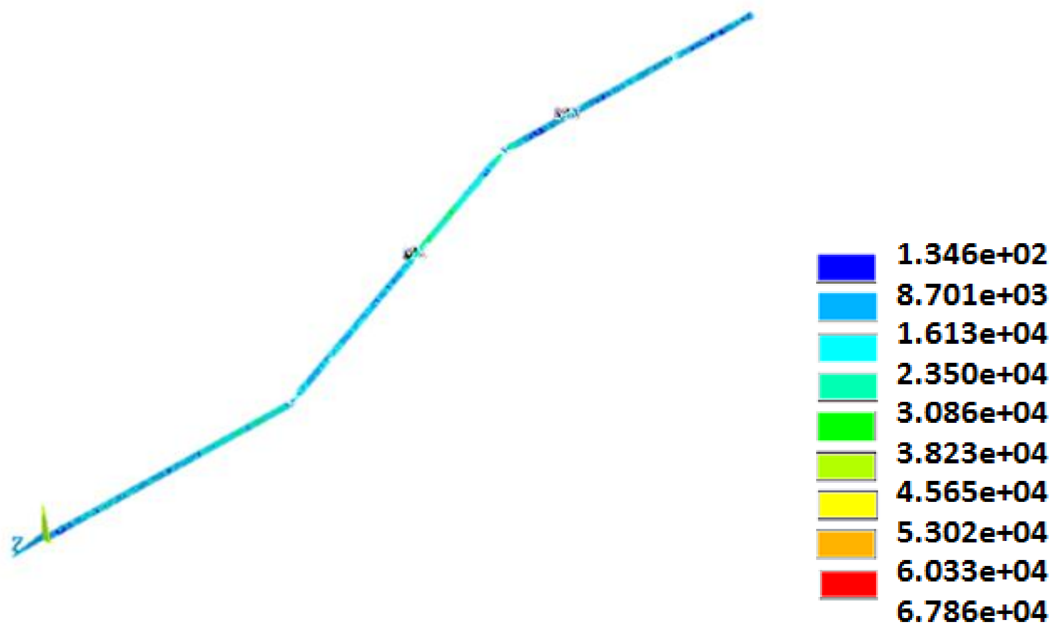

Figure 3.14 Normalized total current density for CNTs in epoxy matrix for a tunneling distance of 1 nm.

The normalized total maximum total current density is 6.786×10^{4}. As illustrated in Figure 3.14, the normalized total current density is lower than that for the electrical loading and slightly larger than that for the thermo-electrical loading, which indicates that the effects of stress are not significant, and this can be due to that the stresses are not fully coupled to the electro-thermal fields, and this coupling is not attainable, since accurate piezo GFs that account for tunneling effects for CNT-epoxy composites are not known (Karube and Fukunaga, 2011). Nevertheless, stress and strain distributions can be obtained for different electro-thermo-mechanical loading conditions to understand and analyze CNT composite behavior subjected to electro-thermo-mechanical loading conditions.

3.4 Summary and Conclusions

The effects of the random distribution of CNTs and electron tunneling on the overall electro-thermo-mechanical behavior of CNT polymer composites were investigated within a thermo-mechanical-electrical finite-element framework. A 3D CNT network model was developed based on representative distributions of CNTs embedded in epoxy matrix composites. These representative distributions were obtained from a percolation analysis that accounts for tunneling distances. Electro-thermo-mechanical FE models for different quantum tunneling distances for non-contacting CNTs were then used to determine the current flow and total current density due to electrons tunneling through the polymer matrix for different electro-thermo-mechanical loading conditions. The analyses indicate that tunneling has a dominant role in the overall electrical conductivity, thermal and mechanical behavior of the composite. There is no clear correlation with tunneling distance, however, since the behavior is dominated by CNT orientation and distribution. This further underscores how the behavior of randomly distributed functionalized CNTs in an epoxy matrix with varying tunneling distances can be difficult to predict, since the physical scales range from tunnel lengths of a few nanometers to CNTs with lengths of hundreds of nanometers. Future investigations will focus on determining local GFs that incorporate tunneling effects and couple changes in resistance to different electro-thermo-mechanical loading conditions.

CHAPTER 4

MODELING THE PIEZORESISTIVITY OF CARBON NANOTUBE POLYMER COMPOSITES

4.1 Background

Due to their light weight, high strength, high sensitivity, extraordinary electrical and thermal properties, CNTs have the potential to be used in many new technological applications in areas related to quantum mechanical, micro-electronic, structural and mechanical, and piezoresistive sensing applications. Individual CNTs can be either metallic metallic or semiconducting behavior, depending on their diameter and helicity of the arrangement of graphitic rings in their walls (Odom and Huang, 1998; Thostenson and Chou, 2007). One of the potential applications is CNT based polymer composites, which can be used for new multifunctional sensing and mechanical strength capabilities (Alamusi et al., 2011). The potential use of these CNT based composites for multifunctional applications are predicted on the relatively high piezoresistivity response of CNTs as conductive fillers within a polymer based matrix.

Metals, alloys inorganic semiconductor materials have been widely used in piezoresistive applications and systems. Most metals have piezoresistive strain coefficients (GFs) that are approximately in the range of 1.0 to 2.0 (Reilly and Sanchez, 1999). Silicon semiconductor piezoresistors may have even higher GFs that range from -120 to 120, depending on the temperature, doping level, crystalline structure, orientation, and how these interrelated factors affect the band-gap (Hwang et al., 2004; Kanda, 1982). These materials, however, have high densities and weight, are not mechanically durable or easily conformable for desired applications, and require complex manufacturing processes (Blazewicz et al., 1997).

To overcome these limitations, conductive CNT-polymer composites have been examined as piezoresistors and they have demonstrated relatively high piezoresistive properties, large sensing capabilities and high strength. The piezoresistive GF has been shown to vary widely with the electric structure of a CNT (Minot et al., 2003; Cao et al., 2003; Grow et al., 2005). For example, Grow et al. showed that CNT GFs could be positive or negative (Grow et al., 2005). Depending on the applied strain, it can increase from zero to hundreds and reach as much as 600 to 1000 in the linear range of SWNTs (Cao et al., 2003; Cullinan and Culpepper, 2010). It can even be greater than 2900 (Stampfer et al., 2006). Another advantage of these sensors is the small size and high sensitivity response that render it ideal for real-time measurements (Grammatikos et al., 2011). In addition, CNT-Polymer composite sensing systems have the potential to be directly embedded in structural composites during composite processing to provide internal strain sensing to control processing defects and service applications to monitor life cycle damage and durability.

It is important, therefore to understand and predict the electromechanical response of CNT-based polymer composites. Early efforts have been made, such as the theoretical studies focused on the deformation of the electronic structure of SWNTs (Yang and Han, 2000). These analytical models may provide knowledge of how the structures at the micro/nanoscale influence the macroscale properties and provide useful information for optimizing the composite structure. There have been numerous experimental studies that have demonstrated the viability of the sensing capabilities of CNTs. Micro-scale strain responses of SWNTs were demonstrated using an atomic force microscope (AFM) (Tombler et al., 2000; Minot et al., 2003; Cao et al., 2003), and later experiments that uniformly strained the entire CNT showed that CNT GF could be as high as 2900 ((Stampfer et al., 2006). CNT-polymer based composites were investigated experimentally with a specific focus on the electrical conductivity of the CNTs and tunneling effects in CNT-polymer network (Kang et al., 2009; Thostenson and Chou, 2007; Park et al., 2008). The limitations of these approaches are that it is difficult, due to the random dispersion of CNTs within a polymer matrix, to ascertain how the current densities and coupled strains and stresses are locally distributed for CNT arrangements. If these local distributions can be obtained, then the electromechanical response of CNT polymer-based composites can be optimized.

These optimal arrangements for sensing and electrical conductivity are difficult to determine from experiments, since arrangements are highly random and percolation is not easy to determine (Xu, Siqi;Rezvanian, Omid; Peters, Kara; Zikry, 2012). Furthermore, overall GFs, changes in resistance, and strain sensitivities cannot be determined experimentally for different loading conditions, such as tension, compression, bending. Furthermore, tunneling distances, which have a significant effect on electrical conductivity at the quantum scale, and tube lengths which are usually at the nano-micro scale (Iijima, 1991) render experimental measurements, difficult, if not impossible.

Computational analyses, therefore, can provide insights for determining the optimal combinations of factors such as dispersion, CNT arrangements and orientation, tunneling distances, aspect ratios, and different loading conditions. The design of piezoresistive nancomposite strain gauges with tailored sensitivities is predicted on, developing an understanding and identification of the underlying mechanisms that govern macroscale piezoresistive response at the micro and nanoscales.

At present, several mechanisms are believed to contribute to the piezoresistive response of CNT-polymer composites. It has been indicated that piezoresistive response of macroscale nanocomposite material originates from the tunneling effect between conducting inclusions (CNTs) in the nanoscale under compression or tension (Kang et al., 2009). The geometric change of the specimen may have an effect on its macroscale resistance behavior (Fernberg et al., 2008) . An additional mechanism is associated with the CNTs themselves which have considerable inherent effect that cannot be neglected. It has been observed both experimentally and in modeling that mechanical deformation of CNTs can directly lead to significant changes in their conductance (Chen and Weng, 2007), indicating CNTs are themselves good strain sensors due to inherent piezoresistivity.

The objective of this study is to determine GFs and resistance variations of CNT-polymer composite systems using finite element methodologies, by coupling Maxwell equations to mechanical loads through piezoresistive coefficients for different arrangements, tunnel distances, and loading conditions for composites including perfectly aligned and alignments based on percolated paths. We have investigated the influences of loading conditions, such as tension, compression, and bending, variations in tunnel distance and CNT tube orientations and distributions on the piezoresistivity and resistance variations of CNT polymer composites. The coupled FE approach is based on using initial piezoresistive coefficients and initial resistance estimates. A scaling relation between GFs, and applied strains is then obtained to understand how variations in loading and CNT arrangements affect sensing capabilities. These variations in GFs are then used to understand how strains, stresses and current densities vary for aligned and percolated paths for different tensile, compressive, and bending loading conditions.

4.2 Computational Approach: Finite Element Modeling

First discovered by Lord Kelvin in 1856, the piezoresistive effect is a widely used sensor principle. The mechanism is based on the physical volume change of the material due to mechanical strain, bringing about a change in the energy bands of the materials. This alters the number of charge carriers for conduction, and as a result, the electrical resistivity of the material changes.

Sensors that demonstrate a change in resistance due to applied strain are commonly used as strain gauges. Their sensitivity, known as the GF, is one of key performance descriptors for strain sensing materials and is conventionally defined as

$$GF = \frac{\Delta R / R}{\Delta l / l} = \frac{\Delta R}{\varepsilon R}, \tag{4.1}$$

where R is the initial resistance of the strain gauge, ΔR is resistance change, l is the initial length of the strain gauge, Δl is the change in length, and ε is applied strain. Based on the orientation of the gauge, the GFs can be broken down into longitudinal (GF_L) and transverse (GF_T) factors as

$$GF_L = \frac{\Delta R_L / R}{\varepsilon_L}, \tag{4.2}$$

$$GF_T = \frac{\Delta R_T / R}{\varepsilon_T}, \tag{4.3}$$

where ΔR_L and ΔR_T are the changes in resistance when the gauges are placed longitudinally and transversely to the applied strain.

In our approach, the resistance variations and GFs of the FE models are obtained by coupling Maxwell equations to mechanical loads through piezoresistive coefficients. The Maxwell equations and the constitutive equation are given by

$$\nabla \times \{H\} = \{J\} + \{\frac{\partial D}{\partial t}\} \ , \tag{4.4a}$$

$$\nabla \times \{E\} = -\{\frac{\partial B}{\partial t}\} \ , \tag{4.4b}$$

$$\nabla \cdot \{B\} = 0 \ , \tag{4.4c}$$

$$\nabla \cdot \{D\} = \rho \ , \tag{4.4d}$$

$$\{J\} = [\sigma]\{E\}, \quad \{D\} = [\varepsilon]\{E\}MCK, \quad \{E\} = -\nabla V, \tag{4.4e}$$

$$\nabla \cdot (\{J\} + \{\frac{\partial \{D\}}{\partial t}\}) = 0. \tag{4.4f}$$

where J is conduction current density, D is electric flux density vector, ρ is electric charge density, and V is electric scalar potential.

The following FE equations couple Maxwell equations to mechanical loads through the following general piezoresistive equations

$$\begin{bmatrix} [M][0] \\ [0][0] \end{bmatrix} \begin{Bmatrix} \{\ddot{u}\} \\ \{\ddot{V}\} \end{Bmatrix} + \begin{bmatrix} [C][0] \\ [0][0] \end{bmatrix} \begin{Bmatrix} \{\dot{u}\} \\ \{\dot{V}\} \end{Bmatrix} + \begin{bmatrix} [K][0] \\ [0][K^V] \end{bmatrix} \begin{Bmatrix} \{u\} \\ \{V\} \end{Bmatrix} = \begin{Bmatrix} \{F\} \\ \{I\} \end{Bmatrix}, \qquad (4.5)$$

where [M] is structural mass matrix, [C] is structural damping matrix, [K] is structural stiffness matrix, { F }is the sum of force vector, { I } is the applied nodal electric current vector, [K^V] is electrical conductivity coefficient matrix, [V] is electric potential vector, and{ u } is displacement vector. For quasi-static applications, only the third matrix of equations needs to be retailed and it is coupled to the electrical conductivity through the electrical conductivity matrix [K^V].

The conductivity matrix [K^V] is given by

$$[K^V] = \int_{vol} (\nabla\{N\}^T)^T [\rho]^{-1} (\nabla\{N\}^T) d(vol), \qquad (4.6)$$

where { N }is matrix of shape functions, { ρ } is electric resistivity matrix.

In piezoresistive materials, the stresses or strains results in a change of electrical resistivity as given by

$$[\rho] = [\rho^0]([I] + [r]), \qquad (4.7a)$$

where

$$[\rho] = \text{electric resistivity matrix of a loaded material} = \begin{bmatrix} \rho_{xx} & \rho_{xy} & \rho_{xz} \\ & \rho_{yy} & \rho_{yz} \\ \text{symm} & & \rho_{zz} \end{bmatrix}, \qquad (4.7b)$$

$$[I] = \text{identitiy matrix}, \qquad (4.7c)$$

$$[r] = \text{relative change in resistivity} = \begin{bmatrix} r_x & r_{xy} & r_{xz} \\ & r_y & r_{yz} \\ \text{symm} & & r_z \end{bmatrix}, \tag{4.7d}$$

calculated as

$$\{r\} = [\pi]\{\sigma\}, \tag{4.7e}$$

where

$$\{r\} = \text{vector of matrix } [r] \text{ components} = [r_x \;\, r_y \;\, r_z \;\, r_{xy} \;\, r_{yz} \;\, r_{xz}]^T, \tag{4.7f}$$

$$[\pi] = \text{piezoresistive stress matrix}, \tag{4.7g}$$

$$\{\sigma\} = \text{stress vector} = [\sigma_x \;\, \sigma_y \;\, \sigma_z \;\, \sigma_{xy} \;\, \sigma_{yz} \;\, \sigma_{xz}]^T, \tag{4.7h}$$

similarly, for strains

$$\{\mathrm{r}\} = [\mathrm{g}]\{\varepsilon^{el}\}, \tag{4.7i}$$

where

$$[\mathrm{g}] = \text{piezoresistive strain matrix},$$

$$\{\varepsilon^{el}\} = \text{elastic strain vector}.$$

It should be noted that in general, there are 81 piezoresistive strain coefficient components in the [g] matrix. Due to the symmetry of both the strains and resistivities, the number of the piezoresisitive strain coefficients is reduced to 36. By observing that the piezoresistive stress coefficient matrix for Germanium and Silicon display diagonal symmetry (Smith, 1954), we assume the same for CNTs and further assume a transversely isotropic material symmetry such that the CNT piezoresistive strain matrix can be written as

$$[g]=\begin{bmatrix} g_{11}^C & g_{12}^C & g_{13}^C & 0 & 0 & 0 \\ g_{12}^C & g_{11}^C & g_{13}^C & 0 & 0 & 0 \\ g_{13}^C & g_{13}^C & g_{33}^C & 0 & 0 & 0 \\ 0 & 0 & 0 & g_{44}^C & 0 & 0 \\ 0 & 0 & 0 & 0 & g_{44}^C & 0 \\ 0 & 0 & 0 & 0 & 0 & g_{66}^C \end{bmatrix}, \qquad (4.8)$$

since g_{66}^C is related to g_{11}^C and g_{12}^C, the number of independent components of the [g] matrix can be reduced to 5.

Most of the measurements regarding inherent piezoresistivity of CNTs are limited to axial tensile experiments, as noted in the introduction. Thus there is very limited data available regarding the remaining four independent piezoresistive strain coefficients that are needed to fully characterize the transversely isotropic piezoresistive response of CNT and effect of individual CNT piezoresistive coefficients on the overall composite GFs. Since our objective is to study the effects of tunneling distance, CNT arrangements and orientations, and loading conditions on the composite piezoresistive response, we assumed an isotropic piezoresistive response of CNT, by using 2000 for the g_{11}^C and g_{33}^C components and zero for the other components in the [g] matrix of CNTs (Cullinan and Culpepper, 2010; Hierold, 2004; Stampfer et al., 2006). We then used these initial values to determine the overall CNT-polymer response.

As described in previous chapters, the tunneling resistance that we used in our approach is based on Simmons' formula (Simmons, 1963) as

$$J=(6.2\times10^{10}/\Delta s^2)\{\varphi_I\exp(-1.025\Delta s\varphi_I^{\frac{1}{2}})\}-(\varphi_I+V)\exp[-1.025\Delta s(\varphi_I+V)^{\frac{1}{2}}]\}, \quad (4.9a)$$

$$\varphi_I = \varphi_0 - (V/2s)(s_1 + s_2) - [5.75/K(s_2 - s_1)]\ln[s_2(s - s_1)/s_1(s - s_2)], \qquad (4.9b)$$

$$s_2 = 6/K\varphi_0, \quad s_2 = s[1 - 46/(3\varphi_0 Ks + 20 - 2VKs)] + 6/K\varphi_0, \quad \Delta s = s_2 - s_1, \qquad (4.9c)$$

$$R_{tunnel} = \frac{V}{A \cdot J}, \qquad (4.9d)$$

where J is the tunneling current density, V is the electrical potential difference, s_1, s_2 are the limits of barrier at Fermi level, s is the thickness of the insulating barrier, A is the cross sectional area of the tunnel, and φ_0 is the barrier height, which for epoxy is 0.5-2.5 eV and 1.5 eV was used in this work (Hu et al., 2008a). In this equation, s is the tunneling distance in our FE models (Xu, Siqi;Rezvanian, Omid; Zikry, 2012).

4.3 Results and Discussion

The piezoresistive coupled FE formulations with the Fermi-based tunneling resistance were used to investigate the electrical conductivities, current density evolution, stress and strain response, and piezoresistivity behavior of different CNT arrangements/orientations, tunneling distances, and tensile, compressive, and bending loading conditions.

4.3.1 Electrical and Mechanical Properties

To obtain a detailed understanding of the CNT-polymer composite behavior, different arrangements of CNT composites were analyzed as shown in Figure 4.1: (a) one CNT in a polymer matrix; (b) two aligned CNTs in a polymer matrix; (c) three aligned CNTs in a polymer matrix; and (d) a percolated path with nonaligned CNTs in a polymer matrix. As described by Xu et al. (Xu, Siqi;Rezvanian, Omid; Peters, Kara; Zikry, 2012), the percolated path is the conductive path based on a percolation analysis for a physically representative 3D computational model for a randomly arrangement of CNTs that is representative of CNT dispersions within a polymer matrix.

The different loading conditions, tunneling distances, and materials properties that are used in this study are given in Table 4.1.

As noted in the previous section, the piezoresistive strain coefficients for the FE models, the three components for the initial piezoresistive strain matrix were taken as 2000 for the CNTs and 4 for the epoxy matrix and tunnel regions (Kang et al., 2009).

For CNT-polymer composite sensing applications, the initial resistance is usually measured in an unstrained state, and varies with the types and dimensions of the strain gauges. In our model, to have a reference resistance to investigate the electromechanical response in the strained states, and to account for the tunneling effects, an analytical formulation was used to calculate the initial resistance (Ruschau et al., 1992). In this formulation, the total resistance is a function of both the resistance through each filler particle and the particle-particle contact resistance. Considering the contact resistance at the electrodes, the resistance is given by the following equation, developed by Ysuda and Ngata:

$$R_c = 2R_e + \frac{(M-1)R_p + MR_i}{N}, \tag{4.10}$$

where R_c is the composite resistance, R_e is the lead resistance to electrodes, R_p is the particle-particle contact resistance, R_i is the resistance across one particle, M is the number of particles forming one conduction path, and N is the number of conduction paths.

The electrodes in Eqn. (4.10) were assumed as two surfaces electrically contacting the conductive path in our model. R_e was the resistance of the epoxy matrix, R_i was the CNT resistance, M was the number of CNTs in each arrangement, and N was one in our models. Thus the initial resistance was calculated to be $3.979 \times 1017\Omega$ and this value was used in all the simulations as a reference resistance in unstrained state. It should be noted that only the initial resistance of the conduction path, the sum of the resistance of epoxy resistance to the two surfaces, the resistance of CNTs and their connecting tunnels were calculated, while the resistance of the matrix surrounding the path was ignored due to the insulating matrix. This analytical initial resistance can be higher than actual values, but it provides a general trend of the resistance variation as a function of the applied strain could be seen.

It should also be noted that in the simulations, to simplify the problem, CNTs were modeled as solid cylinders with an aspect ratio (length/diameter) of CNTs set as 50, for the tensile, compressive, and bending loading conditions, which is related to the physical continuum modeling used in this study. For electrical properties, the CNTs were assumed to be metallic so that band-gap changes were neglected.

Table 4.1 Material Properties and Loading Conditions.

Loading Conditions	Tension, Compression, Bending	
Tunneling Distances	1 nm, 2 nm , 3 nm	
Voltages applied	1V	
Strains applied	0.3% - 5%	
Materials Properties	CNT	Epoxy
Young's Modulus (GPa)	136.64	2.9
Poisson's Ratio	0.236	0.3
Electrical Conductivity (S/m)	10^6	1
Density (g/cm^3)	1.3	1.85
Piezoresistive Strain Coefficient	2000	4
Dielectric Constant		3.98
Rectangular Barrier Height (V)	5.0	

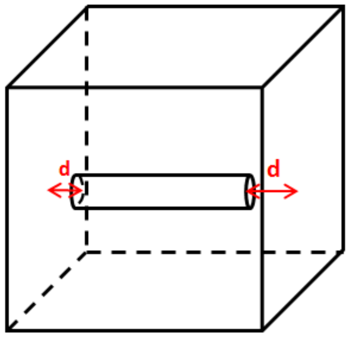

(a)

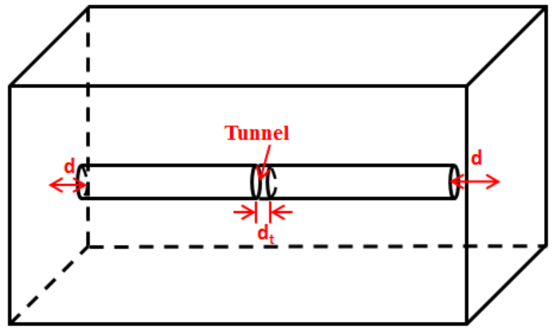

(b)

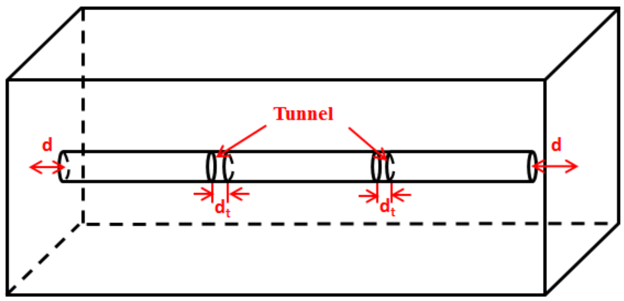

(c)

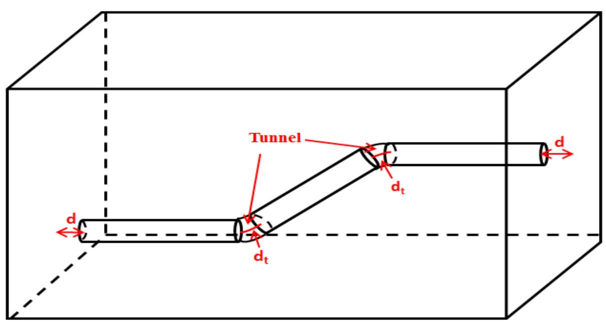

(d)

Figure 4.1 (a-d) FE models for aligned CNTs and percolated path.

Based on convergence analyses, approximately 20,000 to 40,000 3D ten noded tetrahedral elements were used for the piezoresistive analyses. In each analysis, the left end of the model was constrained, with the degrees of freedom (DOFs) in x, y, and z directions were set to zero. A displacement and a voltage of 1V were applied simultaneously to the right end of the model. FE analyses were then conducted to obtain the 3D spatial current flows, current densities, and elastic strains and stresses. Figure 4.2 shows a meshed FE model of one CNT in epoxy matrix with the boundary conditions and different electrical and mechanical loading conditions.

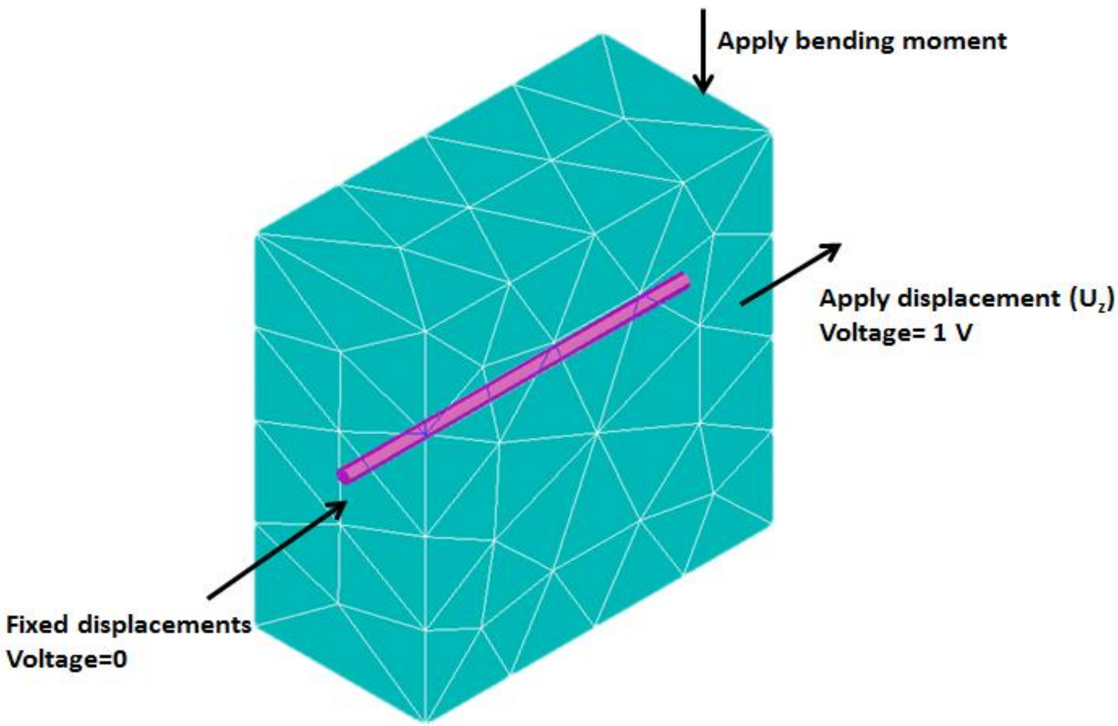

Figure 4.2 FE model of one CNT in epoxy matrix.

4.3.2 Gauge Factors and Local Resistance Variations

GFs and resistance variations obtained for the different arrangements (Figure 4.1(a-d)) were obtained for each arrangement for tunneling distances of 1, 2, and 3 nms. The GFs and resistance variations were calculated for applied elastic strains that ranged from 0.3% to 5% for tensile, compressive, and bending loading conditions. As a benchmark case, the response of one CNT in the polymer matrix (no tunnel) was also obtained.

4.3.2.1 Effects of Tunneling Distance on Gauge Factors

As shown in Figure 4.3-Figure 4.5, under tensile loading conditions, in the strain range of approximately 0.5%-5%, for all the three arrangements, the GFs are negative and increase from about -200 towards zero with increasing strain, this trend is consistent with the modeling evaluation (Cullinan and Culpepper, 2010) and the results observed by (Grow et al., 2005).

GFs measured in the axial direction with randomly oriented CNTs range from 0.48 to 5 (Kang et al., 2009, 2006; Bautista-Quijano et al., 2010; Wang et al., 2008). These values are approximately in the same magnitude range for nominal strains in the range of 0.5%. In our analyses, the GFs are negative, because of the assumption of the initial resistance, and they approach zero because the normalized resistance change gradually increases with increasing applied strain.

It can be seen that for each arrangement, the GF of the one CNT in the polymer matrix model has the lowest magnitude, and this is most likely due to the lack of a tunnel effect. As shown in Figure 4.3, the GFs of two aligned CNTs with 1, 2, and 3 nms tunnels are approximately the same. By adding more CNTs and tunnel regions (Figure 4.4-Figure 4.5), for the three aligned CNTs in the matrix and the percolated path, the effects of tunneling distance become more pronounced especially for the strains that range from 1% to 5%. Hence, the increased number of tunneling regions and tunneling resistance can dominate the overall resistance, and this overall resistance increases significantly with tunneling distances. For both the arrangements, the models with a 1 nm tunneling distance has the highest magnitude GF. As can been seen from Figure 4.3-Figure 4.5, the one CNT polymer matrix model has the lowest GF. This further substantiates that a higher ratio of tunneling resistance leads to higher sensitivities (Hu et al., 2010).

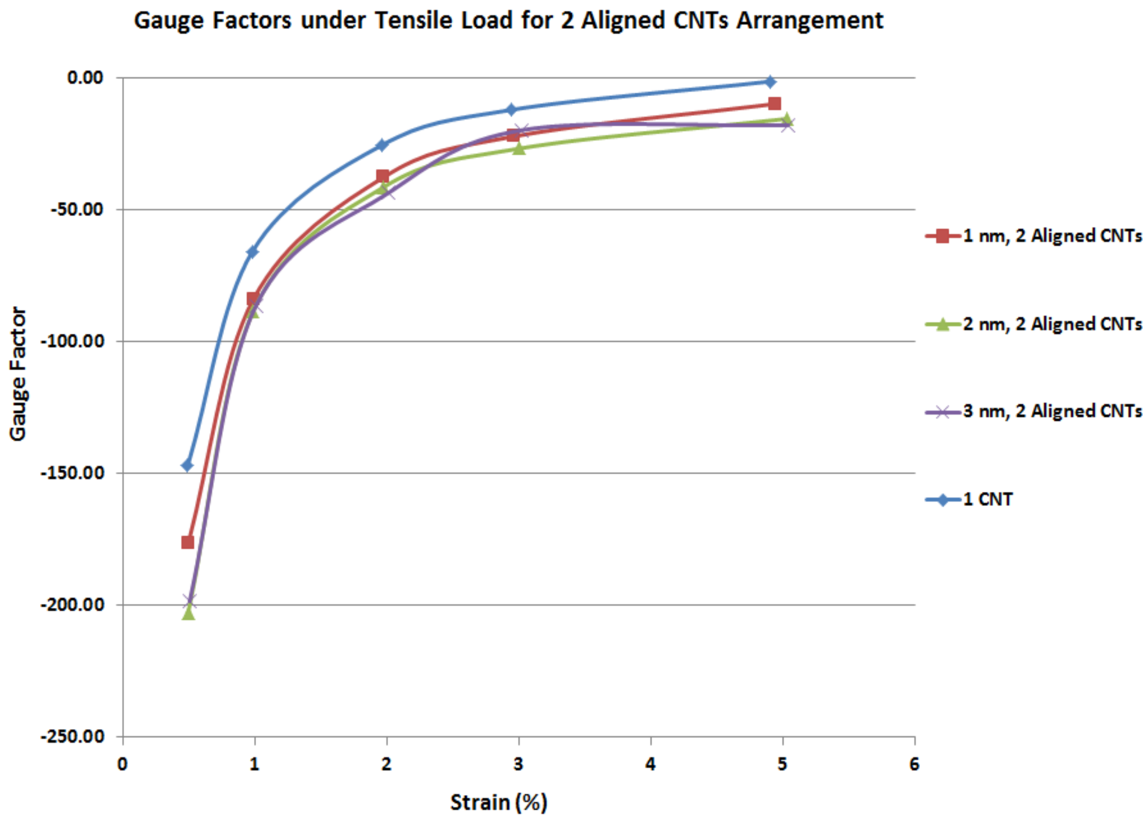

Figure 4.3 Gauge factors of two perfectly aligned CNTs in the polymer matrix.

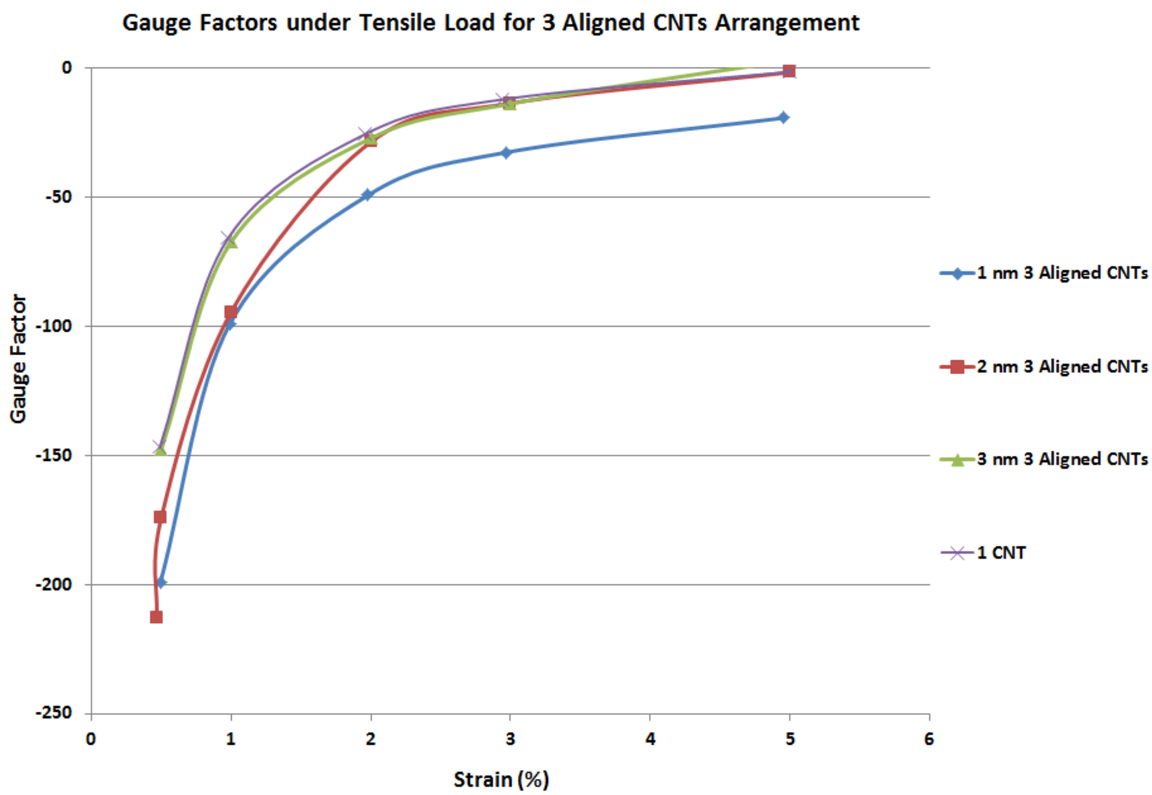

Figure 4.4 Gauge factors of three perfectly aligned CNTs in the polymer matrix.

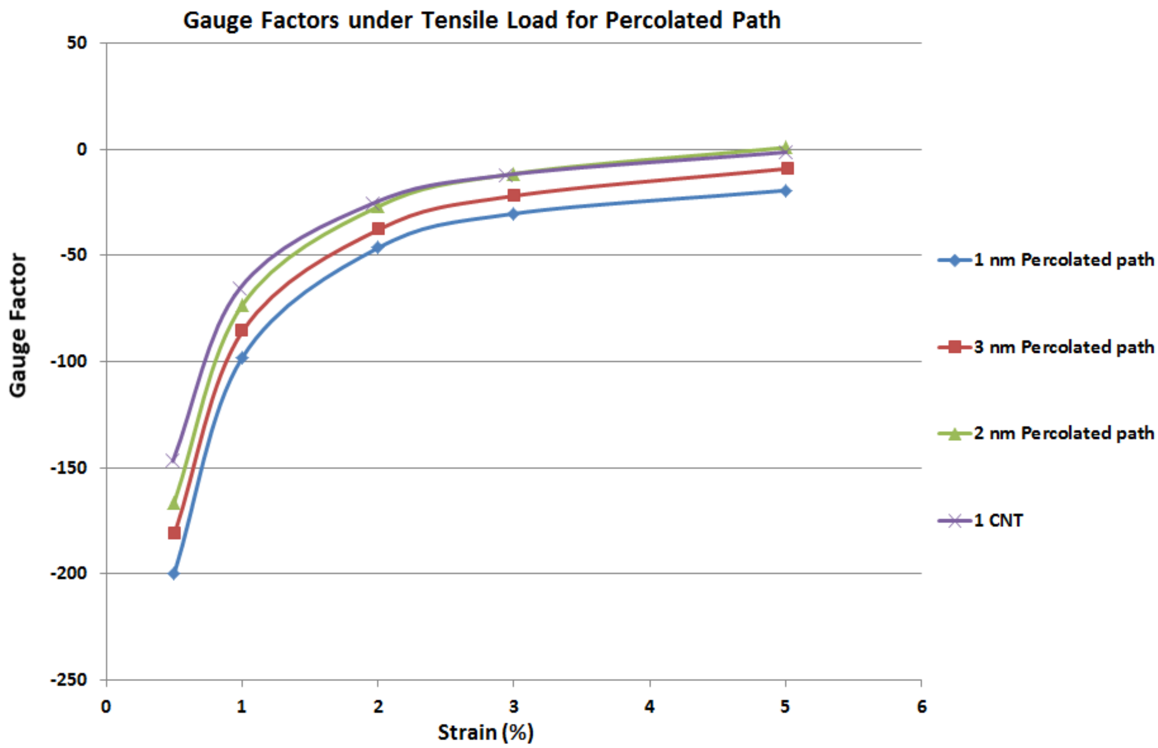

Figure 4.5 Gauge factors of the percolated path in the polymer matrix.

4.3.2.2 Effects of Different CNT Arrangements and Orientations on Gauge Factors

To further investigate the effects of different CNT arrangements and orientations on gauge response, GFs of the four arrangements with a tunneling distance of 1 nm were compared (Figure 4.6).

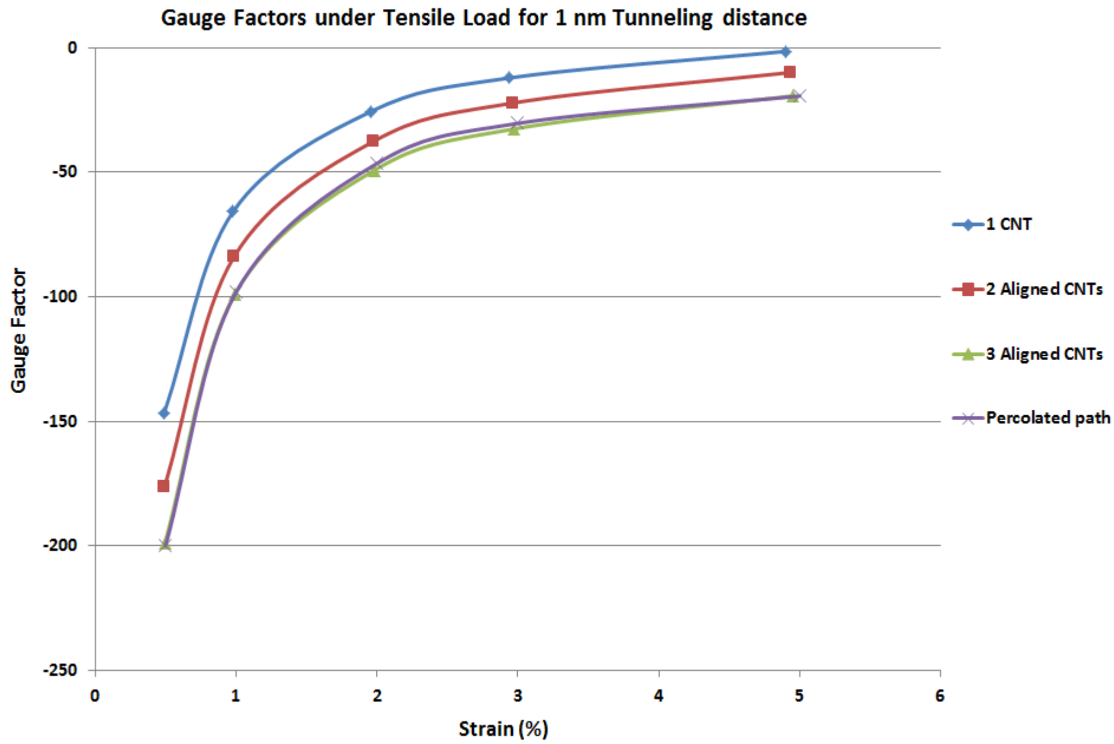

Figure 4.6 Gauge factors for arrangements with a 1 nm tunneling distance.

It can be seen that a logarithmic relation can be obtained for the GF as a function of the applied strain for all the CNT arrangements. It should be noted that this scaling behavior is for the composite even though initial and distinct GFs were used for the polymer, the CNTs, and the tunnel, which indicates that a scaling relation can be obtained based on the initial GFs. This logarithmic proportional relation between the GF and the applied strain for the percolated path with atunneling distance 1 nm is

$$GF \propto 77.6 * \ln(\varepsilon)\text{-}121, \qquad (4.11)$$

where ε is the applied strain. For aligned arrangement, the relation between the GF and the applied strain remains logarithmic, with only the constants in the proportional relation (Eqn. 4.11) being different.

These results indicate that under tensile load, GFs follow a general logarithmic trend and are more dependent on tunneling distance variation than on the CNT arrangements and orientations.

GFs were also obtained for compressive and bending loads. The GFs for various tunneling distances and arrangements are shown in Figure 4.7-Figure 4.8.

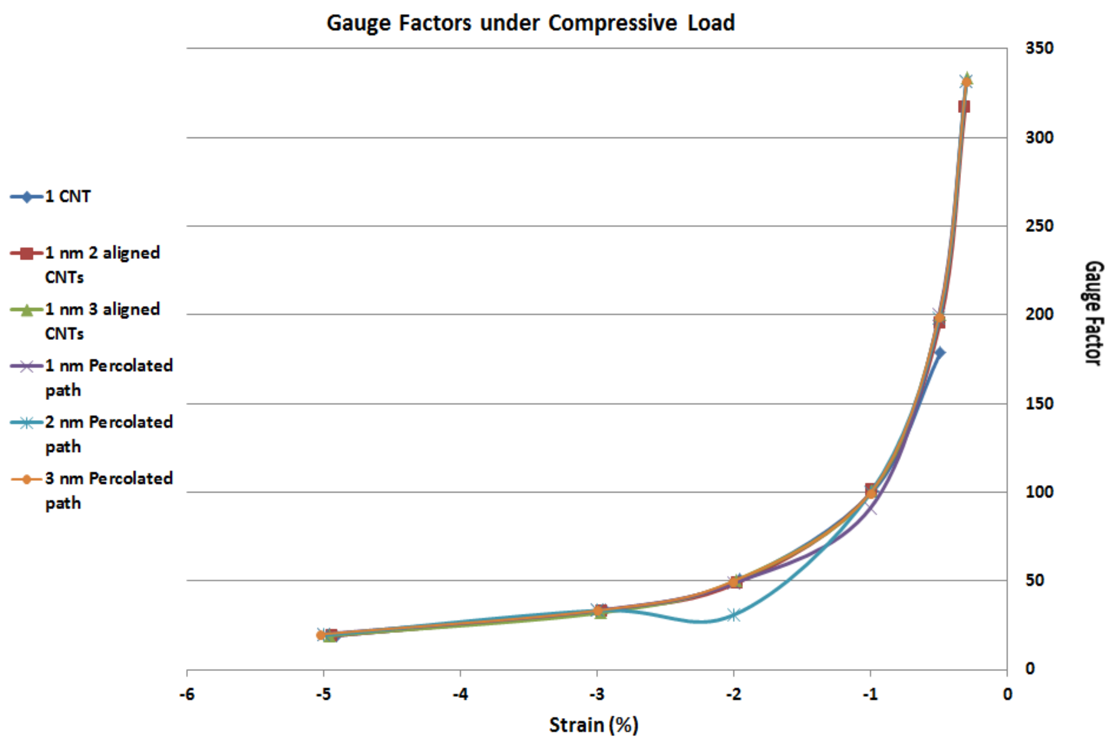

Figure 4.7 Gauge factors for CNTs in the polymer matrix under compressive axial displacement.

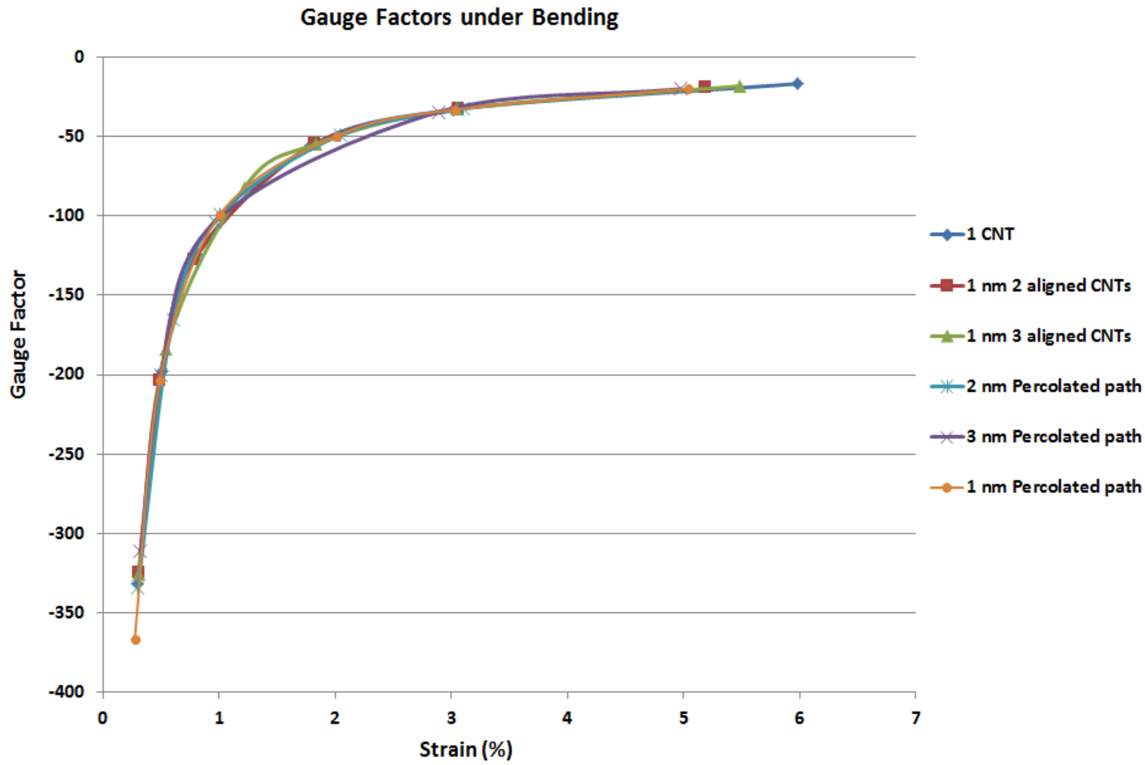

Figure 4.8 Gauge factors for CNTs in the polymer matrix under bending.

As seen in Figure 4.7, under tension, the one CNT in matrix model has the lowest GFs in magnitude in comparison with all the other arrangements. However, in comparison with the tensile loading conditions, tunneling distance does not significantly affect the GFs. All the GFs for all the aligned and percolated arrangements, for both compressive and bending loading conditions, have almost the same gauge magnitude as a function of applied strain. It can be seen that the GFs decrease as the compressive strain increases, and finally converge for strains greater than 3%. This is consistent with the numerical and experimental observations of (Hu et al., 2010) that sensor sensitivity in CNT sensors is much lower when subjected to compressive strain in comprasion with tensile loading conditions and that the GFs, under compression, saturates with increases in strain. The GF behavior, under compression, can also be due to the lateral expansion rather than the contraction associated with tensile loads, and that CNTs are generally stronger in compression (Ci et al., 2008b; Yap et al., 2007).

For bending loading conditions (Figure 4.8), the behavior is similar to the compressive loading cases. The one CNT in the polymer matrix has the lowest GFs in magnitude. The GFs for all the other arrangements decrease in magnitude and they coincide for strains greater than 3% strain in the transverse bending direction (Figure 4.2). Tunneling distances and arrangements do not have a significant effect on the GFs for bending loading conditions. This can be due to the tensile and compressive strains associated with bending, and it will be discussed further in section 4.3.3.

The percolated path, under tensile loading conditions, had the highest GFs and a logarithmic trend (Figure 4.5, cf., Eqn. 4.11). This can be due to that under tensile loading conditions, lateral contractions results in increased tunneling effects due to decreasing tunneling resistances. For compressive loading conditions, there can be minimum tunneling distances, due to lateral expansion and non-penetration restrictions (Hu et al., 2010). These trends can be better understood by examining how resistance changes with strain, this is discussed further in Section 4.3.2.3.

4.3.2.3 Effects of Tunneling Distance and Arrangements on Resistance Variations under Tensile Loading Conditions

The resistance variations for the different arrangements were also obtained, and the results of three aligned CNTs and the percolated arrangements are shown in Figure 4.9-Figure 4.10. It can be seen that the one CNT model has the highest resistance change and is linear as a function of the applied strain. For the other aligned arrangements, it can also be seen that the variation is not linear. This is probably due to the variations associated with tunnel resistances and local changes in current and resistance distribution as a function of the tensile loading. By comparing the slopes of the resistance change curves, the percolated configuration has larger changes in resistance than the aligned case except for the 3 nm tunneling distance case. As can be seen in Figure 4.9, as tunneling distance increases, the applied strain has more impact on the overall resistance change. This behavior is supported by the numerical studies (Theodosiou and Saravanos, 2010)and recent experimental results (Hu et al., 2008a). It also further substantiates that for tensile loading conditions, the percolated arrangement with the lowest tunnel distance has the desired behavior of higher sensitivities.

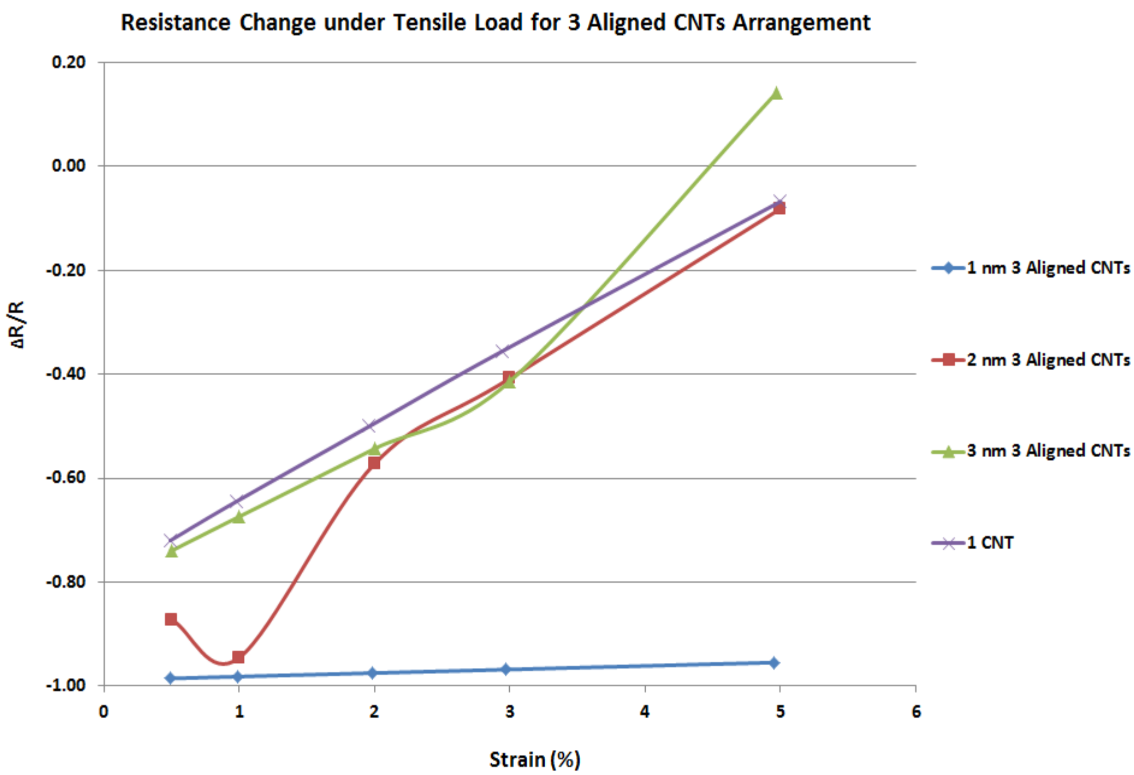

Figure 4.9 Resistance variations for three perfectly aligned CNTs in the polymer matrix under tension.

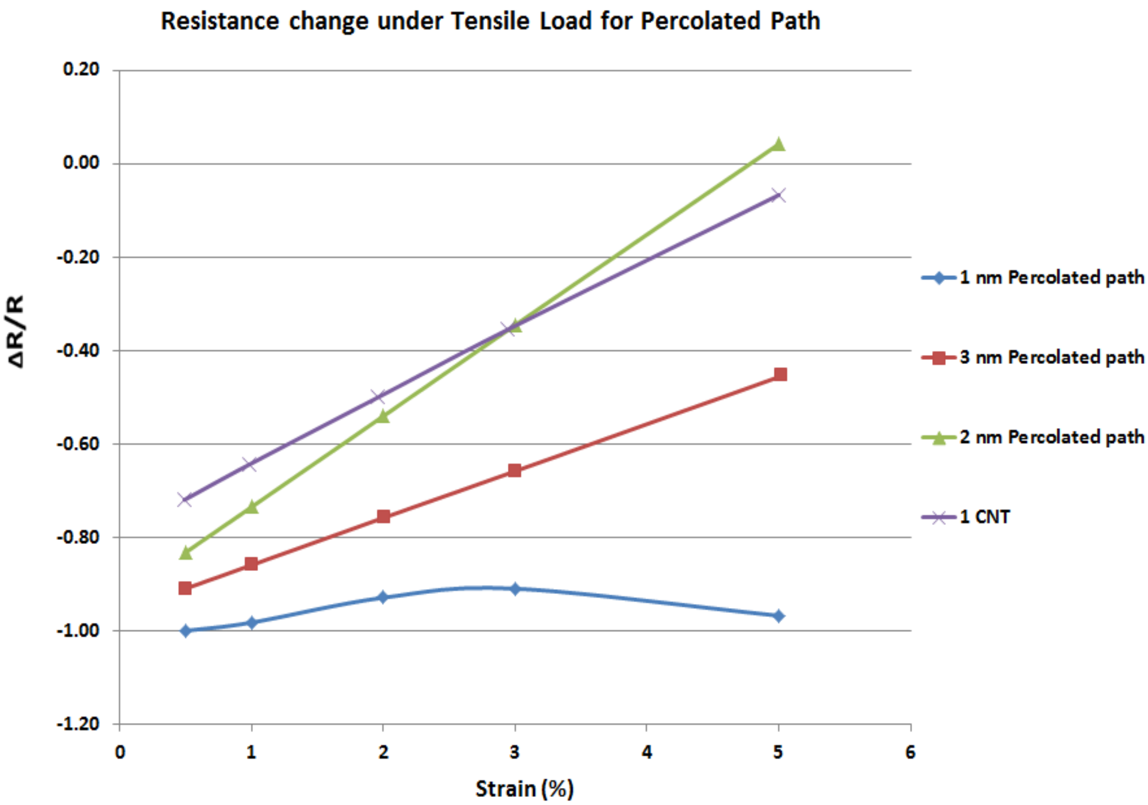

Figure 4.10 Resistance variations for the percolated path in the polymer matrix under tension.

4.3.2.4 Effects of Tunneling Distance and Arrangements on Resistance Variations under Compressive and Bending Loading Conditions

The resistance variations for different arrangements and tunneling distances for compressive and bending loading conditions are shown in Figure 4.11-Figure 4.12. There's no consistent trend for the compressive loading conditions for any of the arrangements as a function of the applied strains. This could be due to the range of large elastic strains, even though it is known that CNTs can withstand high strains (Cullinan and Culpepper, 2010).

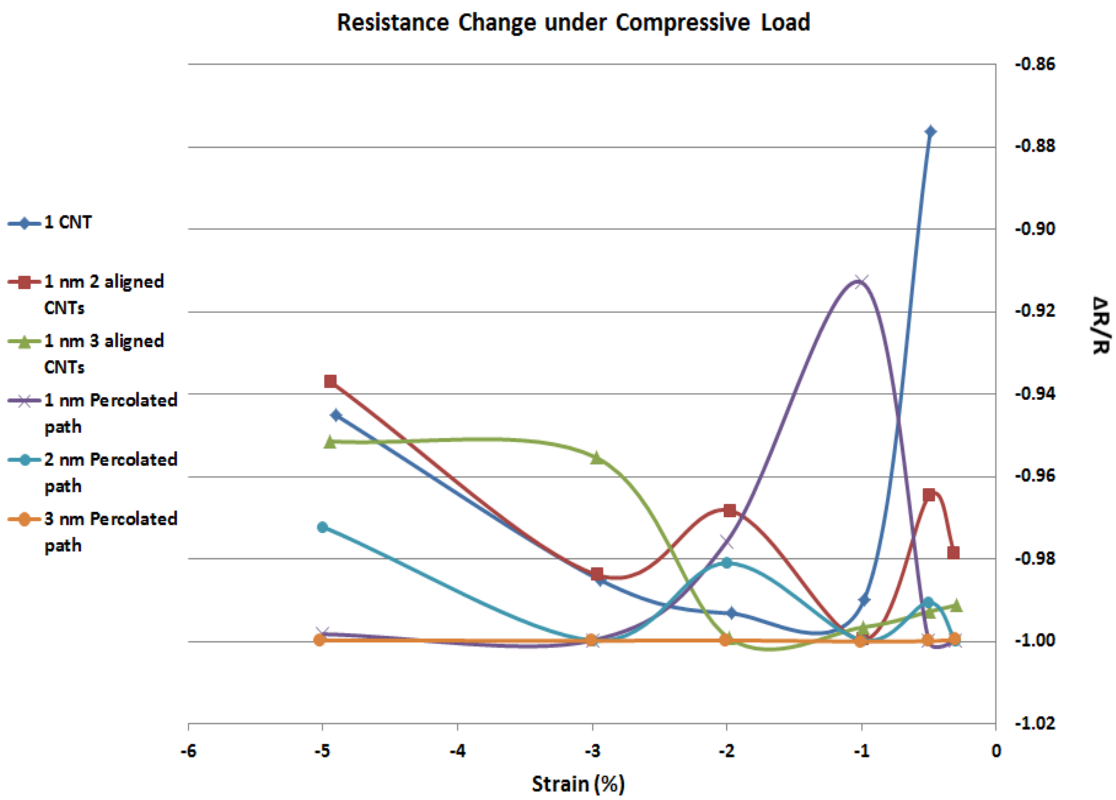

Figure 4.11 Resistance variations for CNTs in the polymer matrix under compression.

The resistance variation is affected by both tunneling distance and CNT arrangements under compressive loads. Within the small strain range, below 0.5%, where most of the measurements under compressive load have been investigated (Ci et al., 2008a; Yap et al., 2007), as strain increases, the resistance variation increases in magnitude (Hu et al., 2010). This is consistent for the percolated path configuration for compressive strain lower than 0.5% (Figure 4.12). This lack of variation can be due to the large elastic strains and the distribution and effects of local strains and stresses on the current and resistances. The GFs had a clear logarithmic trend (cf., Eqn. 4.11), but changes in resistances are directly affected by the strain and stress distributions, and the initial resistances. As noted earlier, the initial resistances are not easily ascertained for CNT-polymer composites with tunneling effects, and these effects would become pronounced with large elastic strains (Hu et al., 2010).

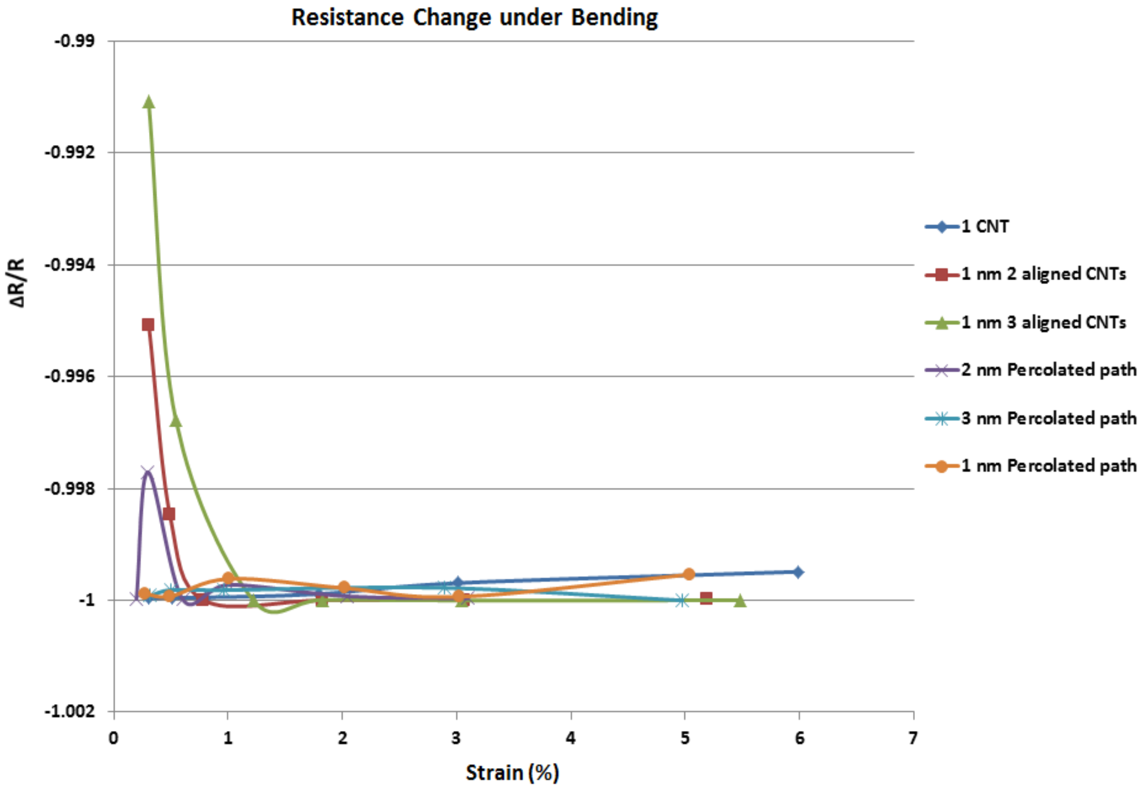

Figure 4.12 Resistance variations for CNTs in polymer matrix under bending.

For the bending loading conditions, there is little variation in the resistance responses for the three arrangements (Figure 4.12). These results show the resistance changes are almost coincident for strains larger than 1.5%, which indicates that the different CNT arrangements and tunneling distances do not affect the results at large elastic strains. For small strains, as tunneling distance increases for different CNT arrangements, the resistance variations increase in magnitude. At strains lower than 1% bending strain, there are resistance increases in magnitude with increases in load. For strain greater than 1%, there is little or no variation. As noted earlier, this can be due to the large elastic strains, the initial resistance calculations, and the distributions and effects of the local strains and stresses on the current density calculations. Marhar et al. (Mahar et al., 2007) have also noted that small bending distoritions of CNTs would have negligible effects on its electrical properties.

4.3.3 Current Density, Strain and Stress Distributions in CNT-Polymer Composites

To better understand the electrical-mechanical behavior of the CNT-polymer composite, we investigated the spatial distribution of electrical conductivity, stress and strain for the different CNT arrangements for the tensile, compressive and bending loading conditions for a representative tunneling distance of 1 nm. The dimensions of the CNT-epoxy composite cell for a tunneling distance of 1 nm is 100 nm×200 nm ×606 nm (Figure 4.13).

For the contour spatial distributions, the current densities are normalized by the maximum current density of the epoxy matrix, and the von Mises stresses are normalized by the Young’s modulus of epoxy of 2.9 GPa. Results for an applied strain of 1% for the three loading conditions are presented and discussed in this section. Results for tunneling distances of 2 nm and 3 nm are presented in the appendices.

4.3.3.1 Three Aligned CNTs Electromechanical Behavior

Contours for the current density in the z direction and the total normalized current flow are shown in Figure 4.13 (a-b), and the normalized von Mises stresses and strains are shown in Figure 4.14 (a-b). The maximum current density in the z direction occurs at the tunnel region that is adjacent to the right end where voltage is applied (Figure 4.13 (b)), and this is also where the total current is a maximum. As shown in Figure 4.14 (a), the maximum normalized von Mises stress is 1.31 at an applied strain of 1%, and it increases to 6.55 as the applied strain increases to 5%, and these maximum values occur along the CNTs near the fixed boundary. The maximum von Mises strain in the matrix is 1.13% and 15.9% in the CNTs, which further indicates that there are large gradients in the stress fields at the interface of the epoxy matrix and the CNTs. The maximum strains occur in the tunnel region, which coincide with the locations of the maximum current density, which further underscores the piezoresistive effects associated with CNTs and tunneling. The large stress and strain values are due to the inherent high strength of the CNTs, the gradients between the epoxy and the tubes, and the perfectly aligned arrangements. It has been reported that some SWNTs exhibit large elastic ranges, with elongations of over 50% (Marques et al., 2004).

Figure 4.13 (a) Current flow for three aligned CNTs in the polymer matrix under tension. (b)Current density in the z direction for three aligned CNTs in the polymer matrix under tension.

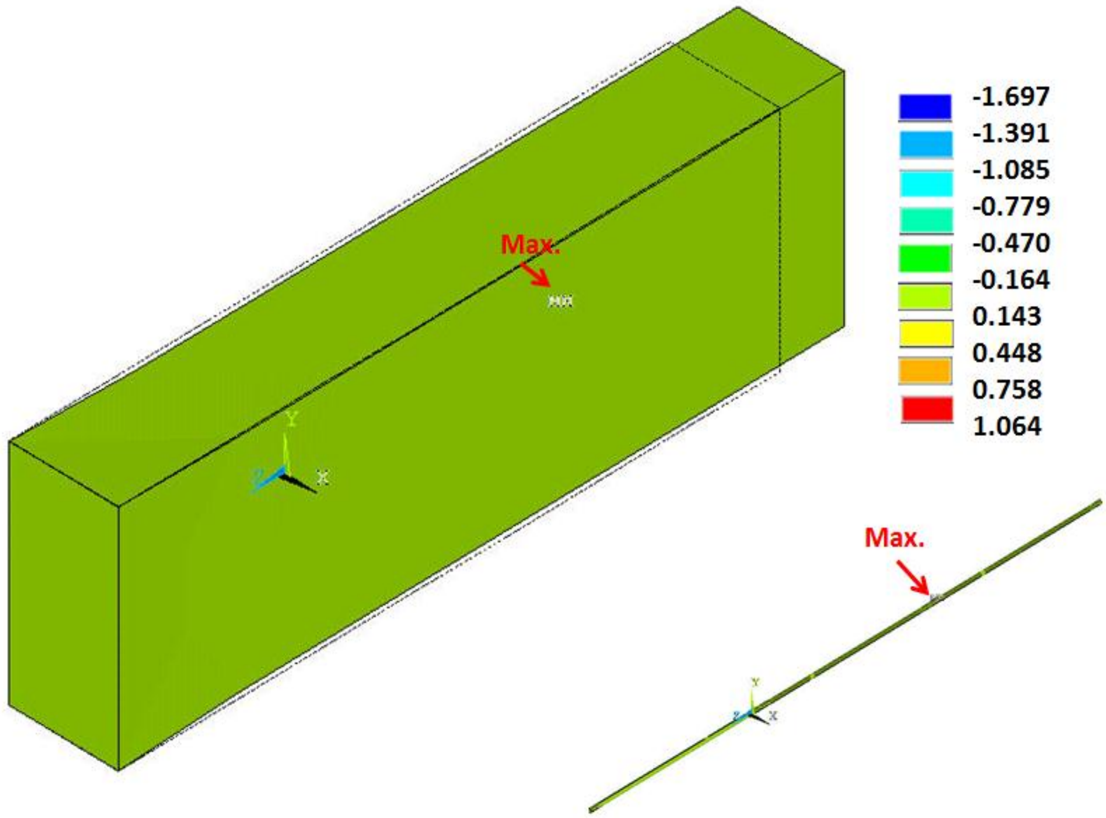

(a)

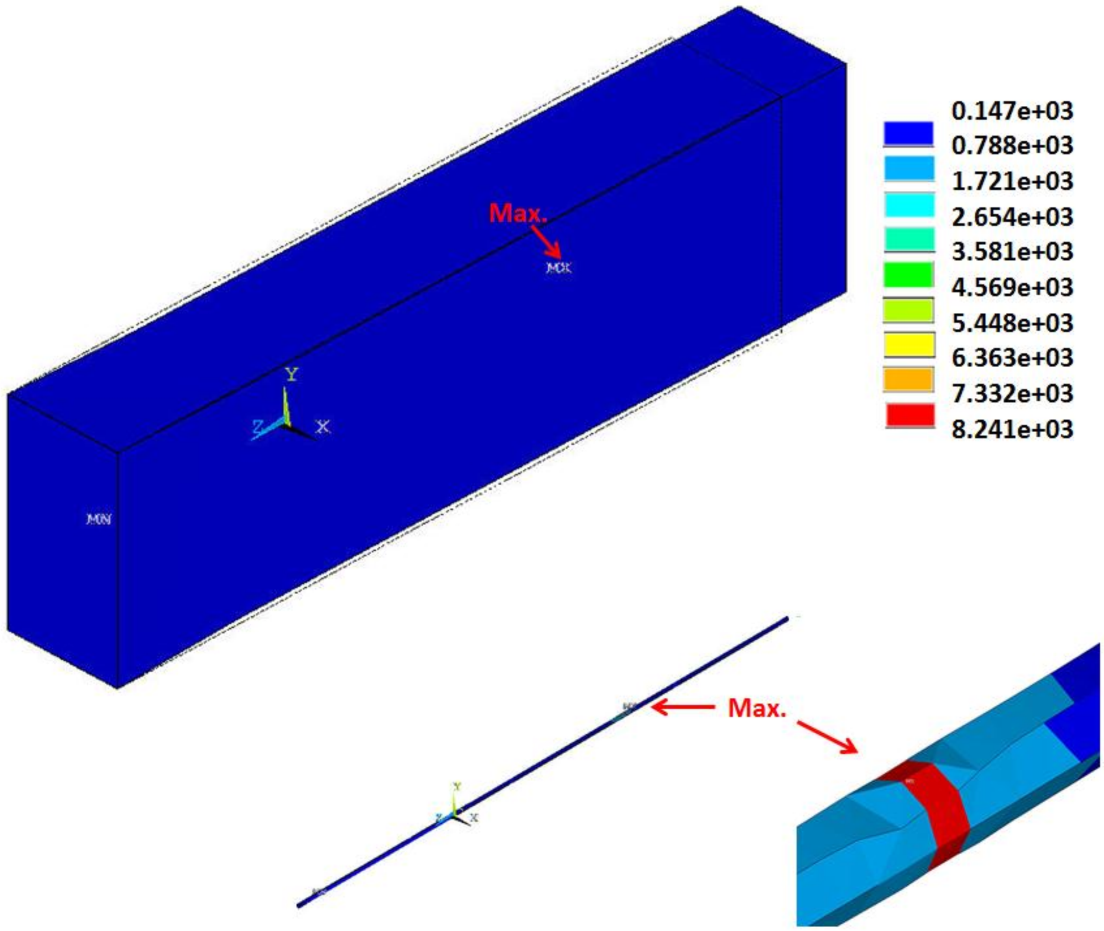

0.147e+03
0.788e+03
1.721e+03
2.654e+03
3.581e+03
4.569e+03
5.448e+03
6.363e+03
7.332e+03
8.241e+03
Max.
MX
MN
Y
Z
X
Max.

(b)

Figure 4.14 (a) von Mises stress for three aligned CNTs in the polymer matrix under tension. (b) von Mises strain for three aligned CNTs in the polymer matrix under tension.

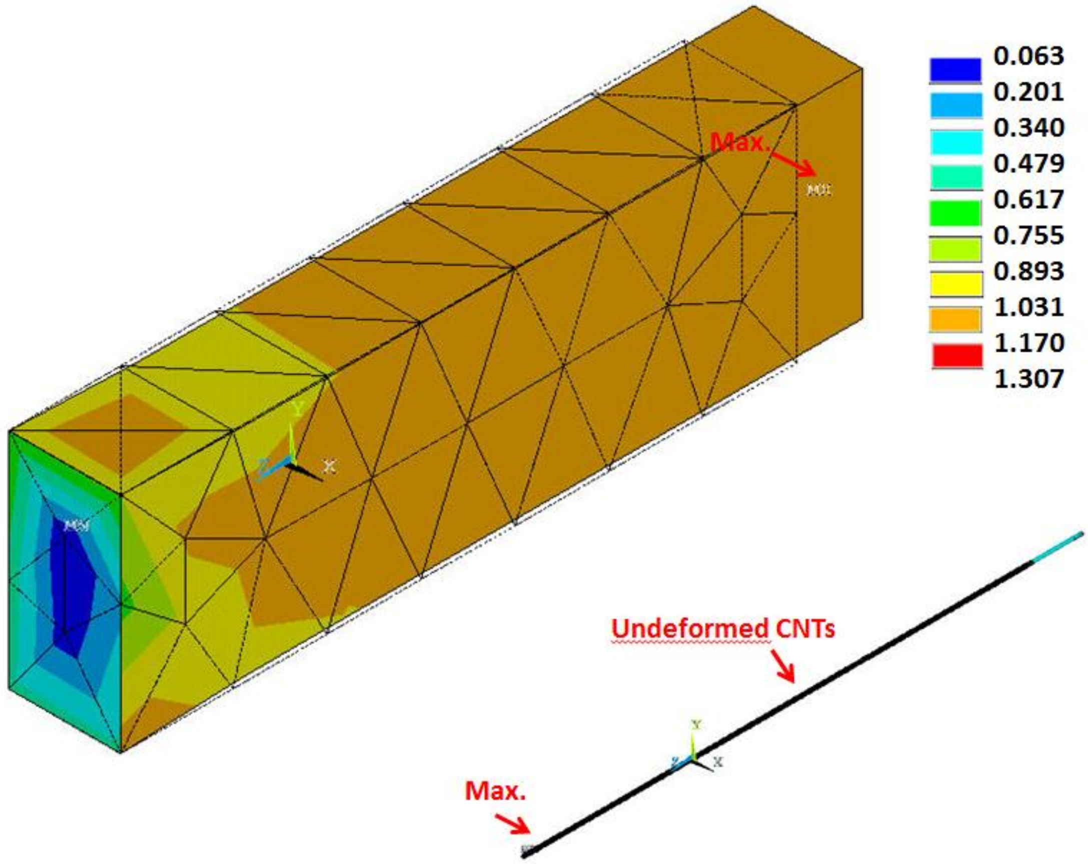
0.063
0.201
0.340
0.479
0.617
0.755
0.893
1.031
1.170
1.307
Max.
Undeformed CNTs
Max.

(a)

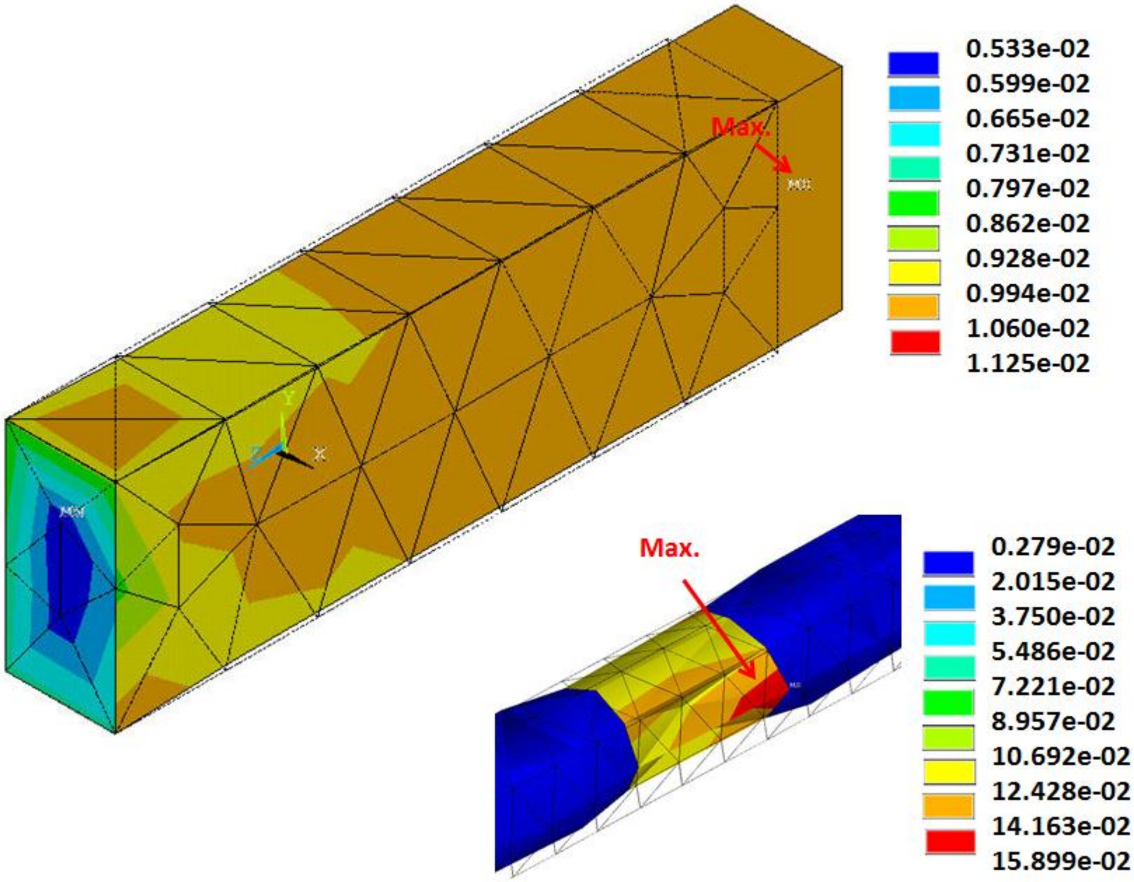

0.533e-02
0.599e-02
0.665e-02
0.731e-02
0.797e-02
0.862e-02
0.928e-02
0.994e-02
1.060e-02
1.125e-02
Max.
Max.
0.279e-02
2.015e-02
3.750e-02
5.486e-02
7.221e-02
8.957e-02
10.692e-02
12.428e-02
14.163e-02
15.899e-02

(b)

To contrast these results with the tensile loading conditions, the current density in the z direction and the von Mises strains are shown in Figure 4.15-Figure 4.16 for the same arrangements and tunneling distance of 1 nm. In comparison with the tensile loading condition, the normalized maximum current density in the z direction, for the tensile loading case is 8.241×10^3 as compared with 4.412×10^4 for the compressive loading case at an applied strain of 1%. The maximum von Mises values are approximately the same with the maximum values occurring in the tunnel region. This indicates that the piezoresistive effect is dominated by the tunnel effects and not the loading conditions at this applied strain. As noted earlier, changes in resistance and GFs did not become significant, for the different loading conditions, until the strains were significantly large.

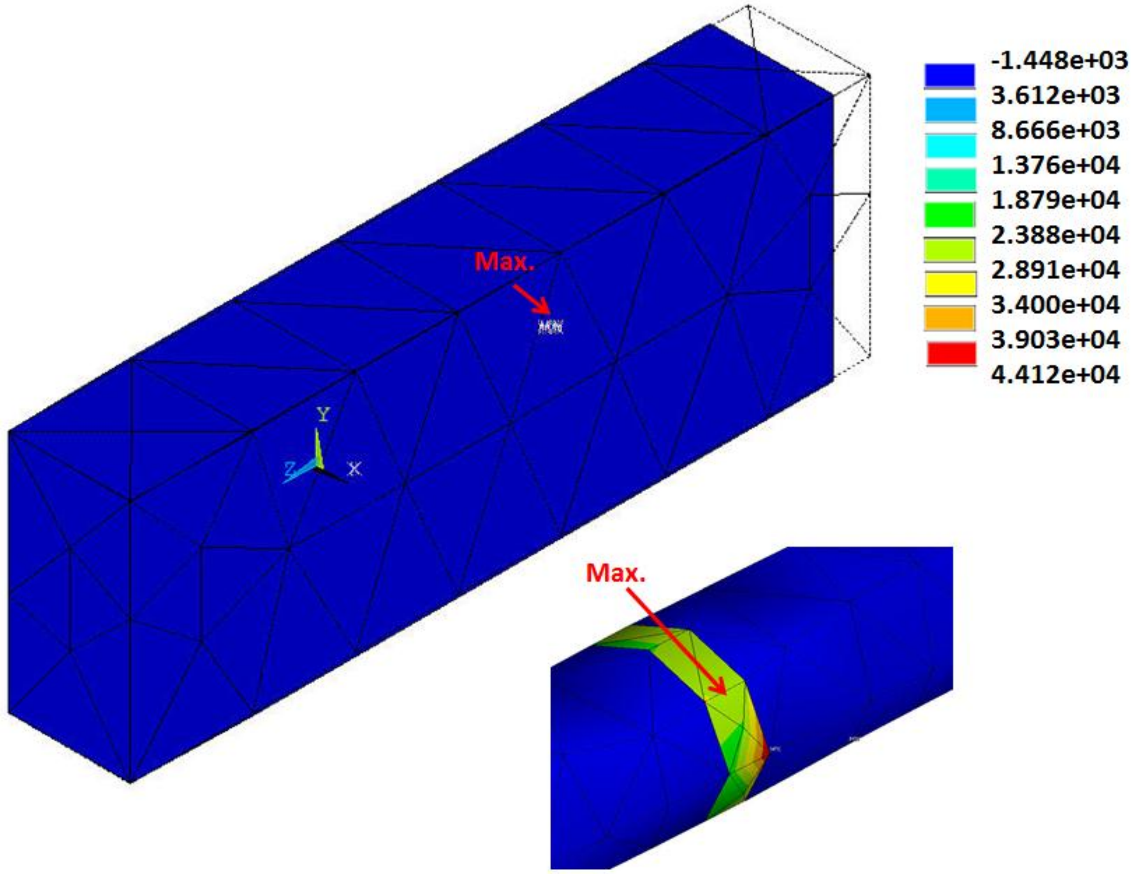

Figure 4.15 Current density in the z direction for three aligned CNTs in the polymer matrix under compression.

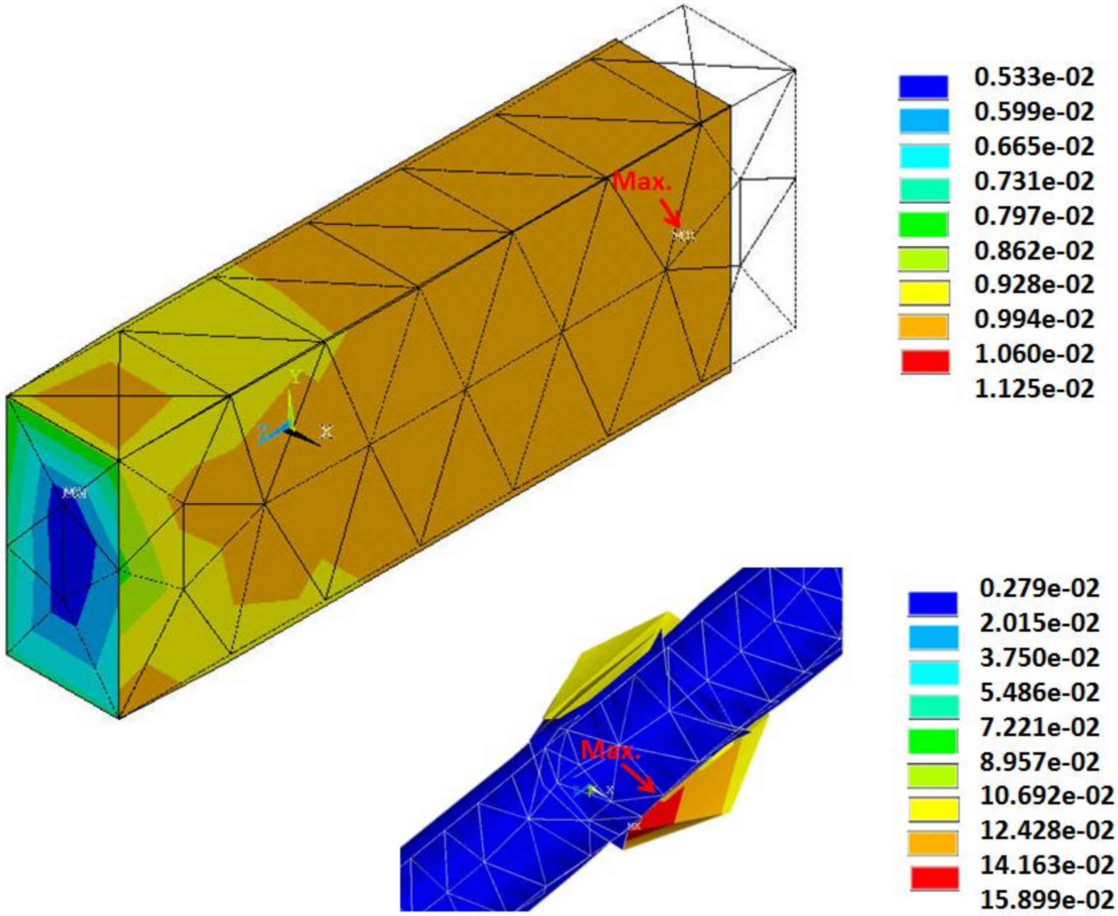

Figure 4.16 von Mises strain for three aligned CNTs in the polymer matrix under compression.

Figure 4.17-Figure 4.18 show the current density in the z direction and the von Mises strain for the three aligned CNTs with a 1 nm tunneling distance at an applied strain of 1%. In comparison with the tensile and compressive loading cases, the current densities in the z direction are significantly higher at least by three orders of magnitude with a maximum value of 2.212×10^{7}. The von Mises stress and strain values are lower than that of the tensile and

compressive loads. This is due to the maximum strains occurring on the top and bottom surfaces of the computational cell, which is where the epoxy is. Bending in this case results in much higher current densities in the CNTs, in comparison with the tensile and compressive loading cases, with the maximum strain values dominated by the overall deformation of the CNTs.

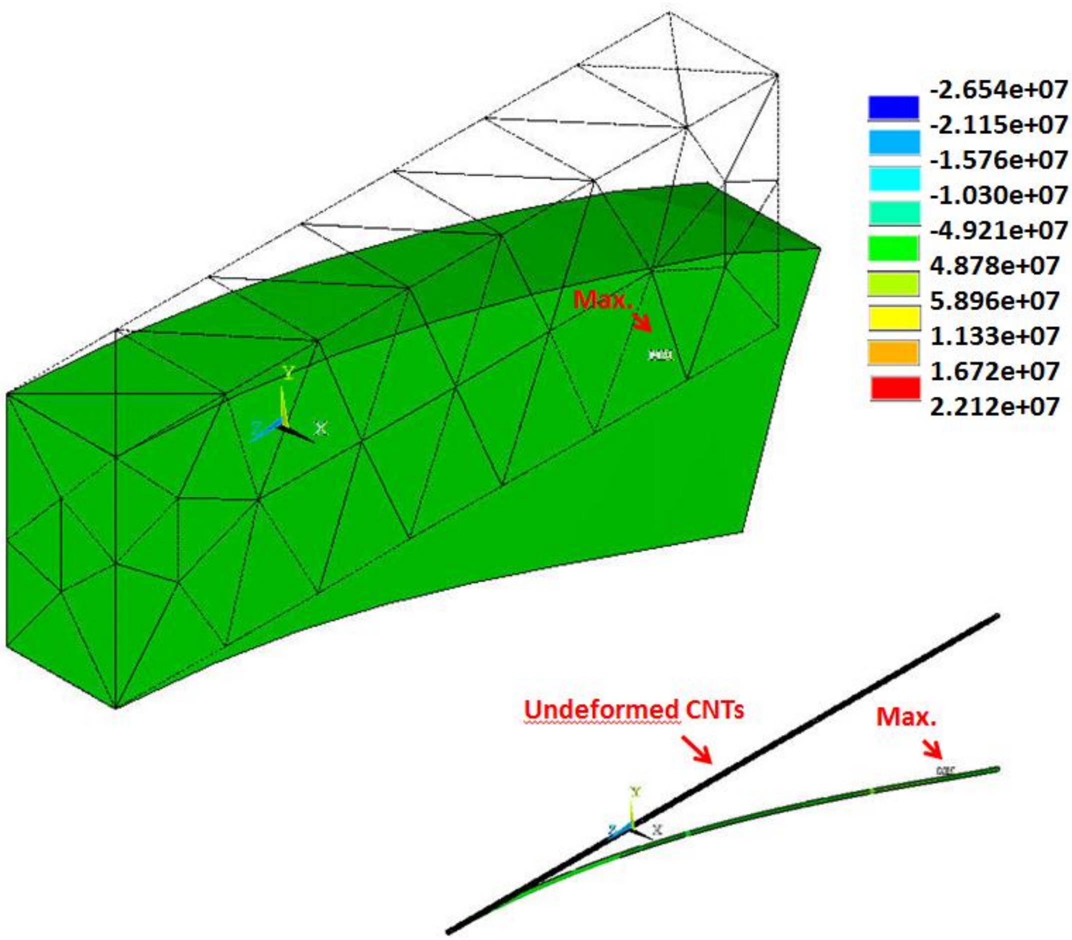

Figure 4.17 Current density in the z direction for three aligned CNTs in the polymer matrix under bending.

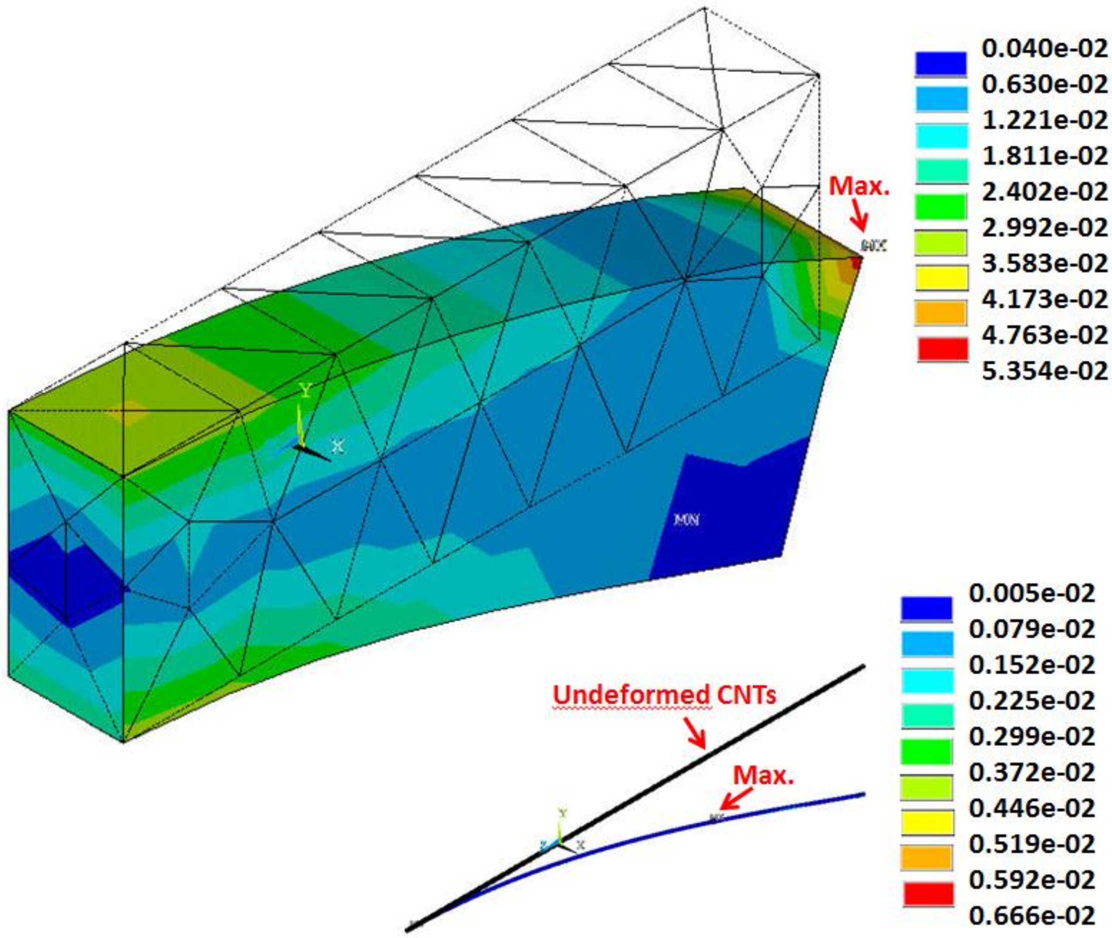

Figure 4.18 von Mises strain for the three aligned CNTs in the polymer matrix under bending.

4.3.3.2 Percolated Path Piezoresistive Behavior

To further understand how piezoresistivity is affected by different CNT arrangements and orientations within the polymer matrix, we investigated the behavior of the polymer matrix with the percolated path for the three loading conditions for a tunneling distance of 1 nm. For the tensile loading case at an applied strain of 1%, the current density in the z direction is shown in Figure 4.19 and the von Mises strain is shown in Figure 4.20. The maximum current density in the z direction occurs along the CNT on the top surface of one of the CNTs (Figure 4.19), and the maximum value is approximately four times the initial value of the matrix. The maximum von Mises strain in the matrix is 1.4% and 15.7% in the CNTs, which further indicates that there are large gradients in the strain fields at the interface of the epoxy matrix and the CNTs. The maximum von Mises strain occurs at the two tunnel regions (Figure 4.20). This indicates, in comparison with the aligned three CNT case, that the percolated path has significantly higher current densities and strains, which further substantiates that piezoresistivity is directly affected by percolation, tunneling distance, and orientations (Cullinan and Culpepper, 2010; Alamusi et al., 2011).

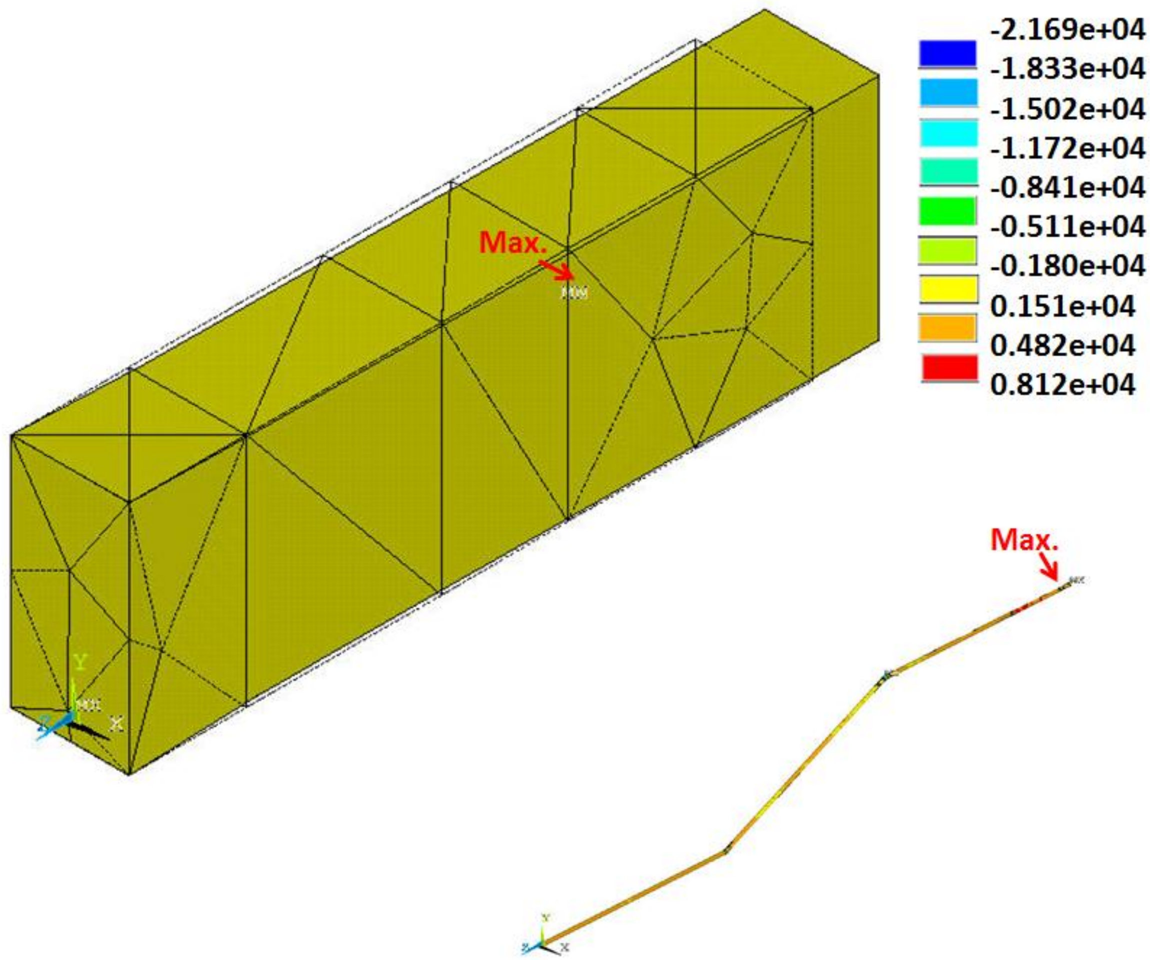

Figure 4.19 Current density in the z direction for the percolated path for the tesile loading case.

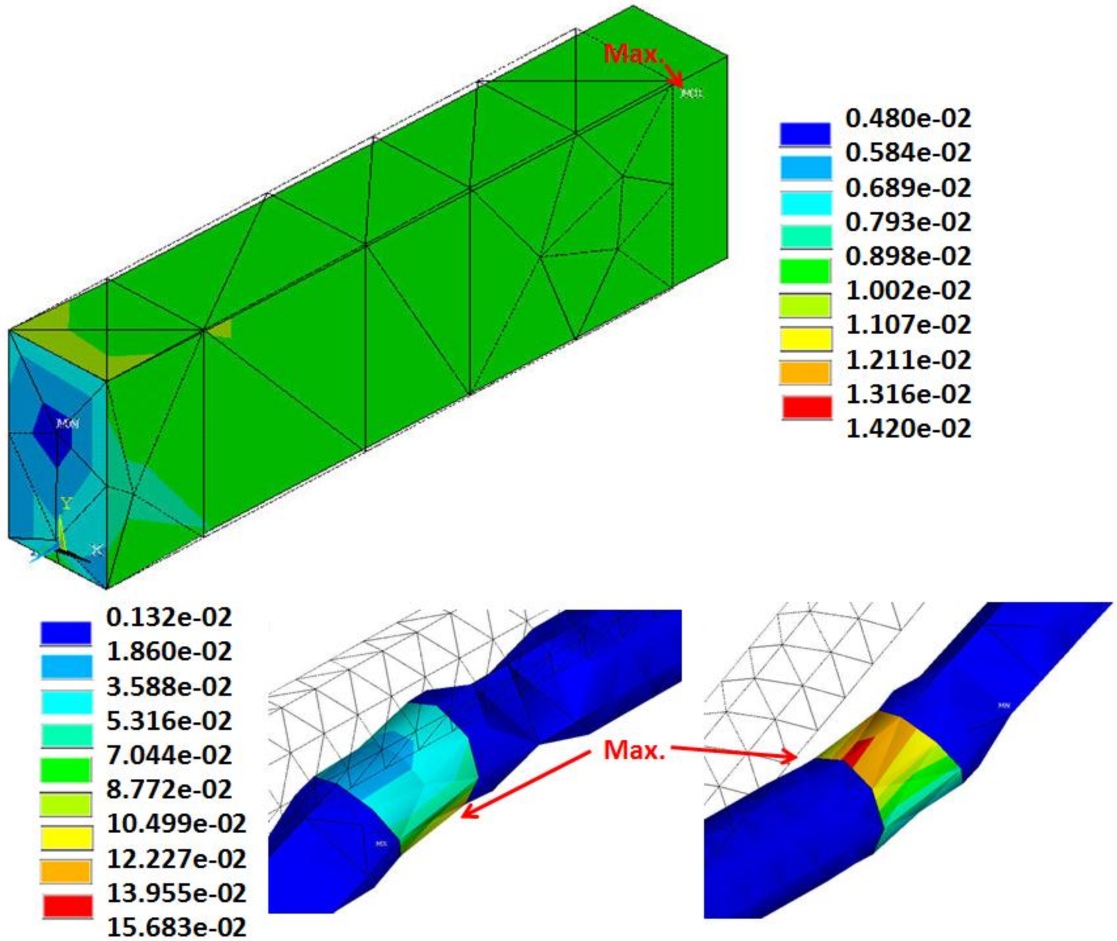

Figure 4.20 von Mises strain for the percolated path for the tensile loading case.

For the compressive loading case for the percolated path, at an applied strain of 1%, the maximum current density was approximately three orders of magnitude higher, in comparison with the tensile case, with a maximum normalized value of 7.830×10^{6} (Figure 4.21). The von Mises strains were approximately the same as for the tensile case with a maximum value of 15.6%. Therefore, for the compressive loading cases, for the percolated case, the electrical conductivity is significantly higher, in comparison with the tensile loading case, with large local strains, which further corroborates the percolated path as an optimal piezoresistive orientation.

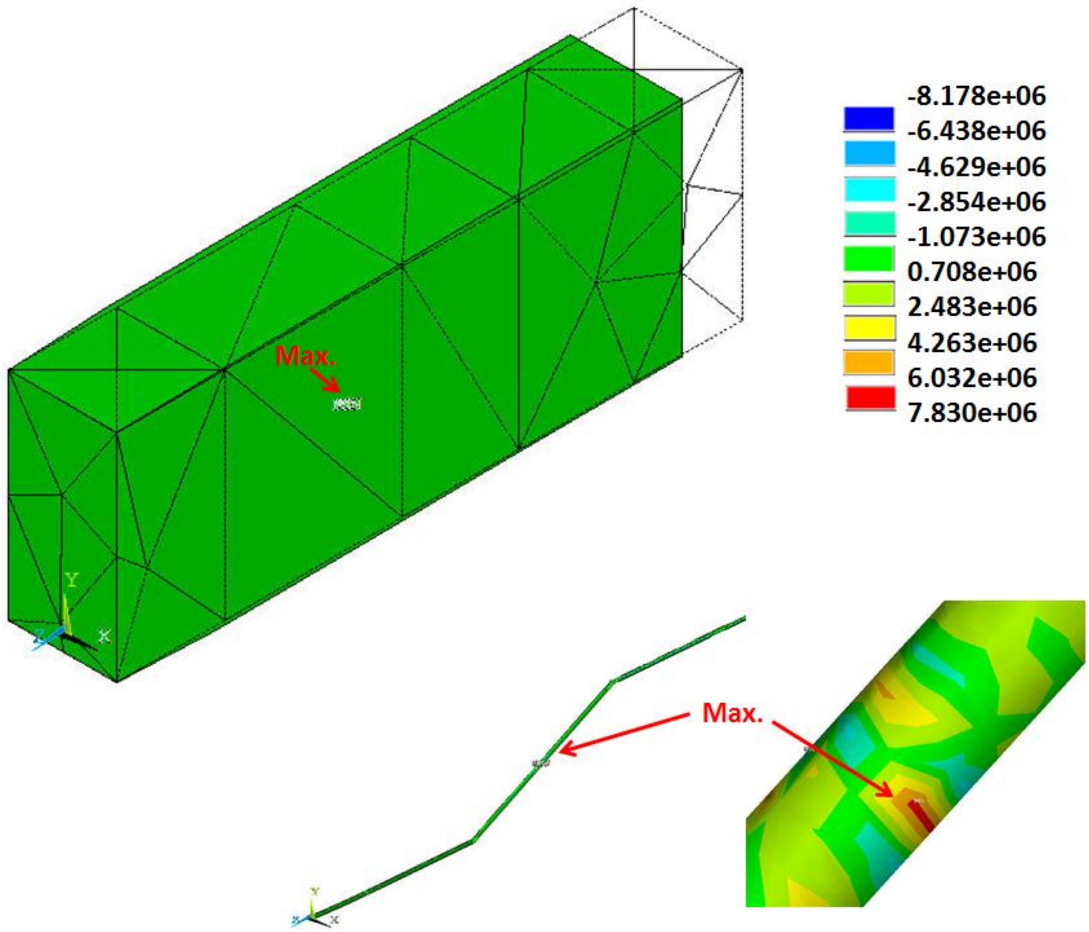

Figure 4.21 Current density in the z direction for the percolated path for the compressive loading case.

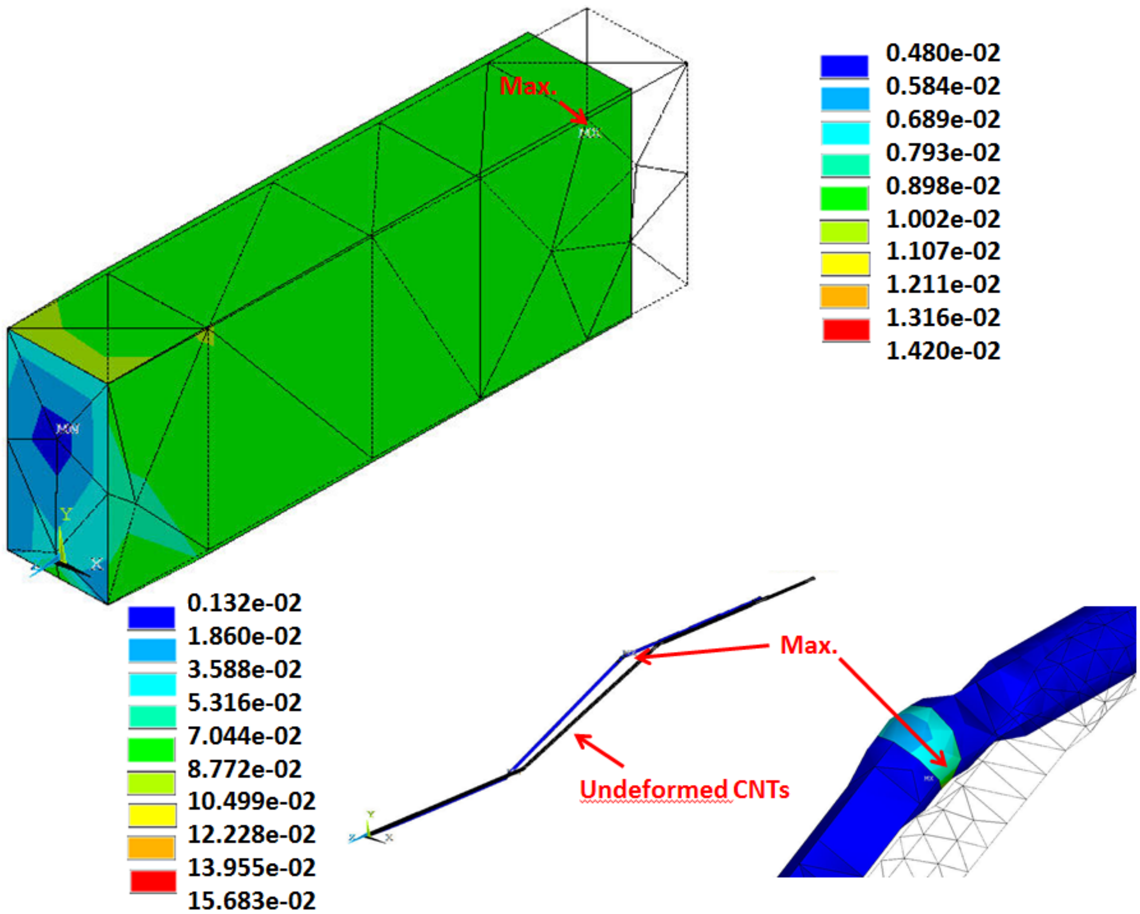

Figure 4.22 von Mises strain for the percolated path for the compressive loading case.

The current density distribution in the z direction is shown in Figure 4.23 and the von Mises strain distribution is shown in Figure 4.24 for the percolated path subjected to the bending load at a nominal strain of 1%. The current densities in the z direction are higher than that for the tensile case and lower than that for the compressive case, with values almost at the average of both the tensile and compressive cases. The von Mises strains are significantly higher with values as large as 27.7% (Figure 4.24). The maximum strains occur at the top surfaces of the CNTs. The results for these three loading conditions for the percolated path clearly demonstrate that electrical conductivity and sensing capabilities can be optimized as a function of percolation, tunneling distance, orientation, and loading condition.

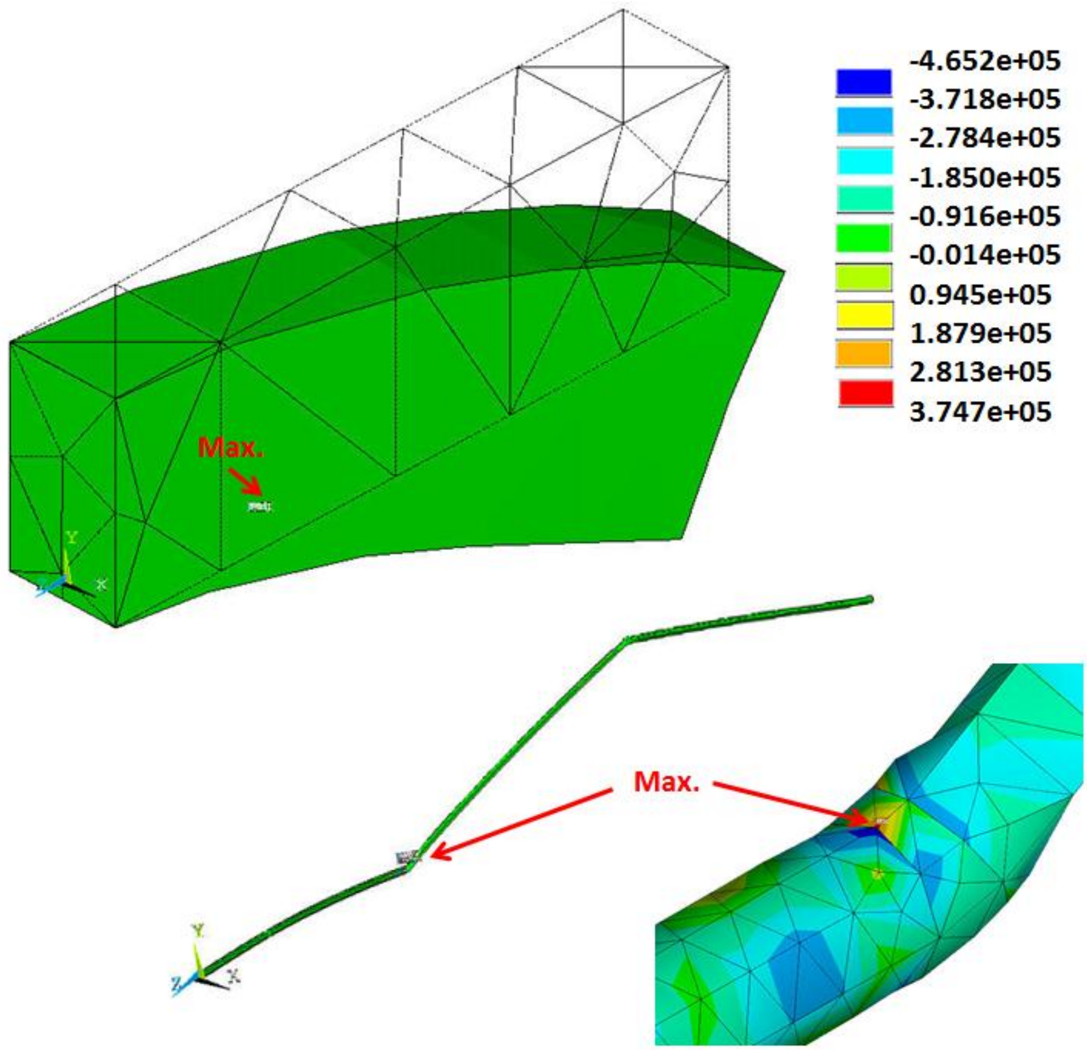

Figure 4.23 Current density in the z direction for the percolated path for the bending loading case.

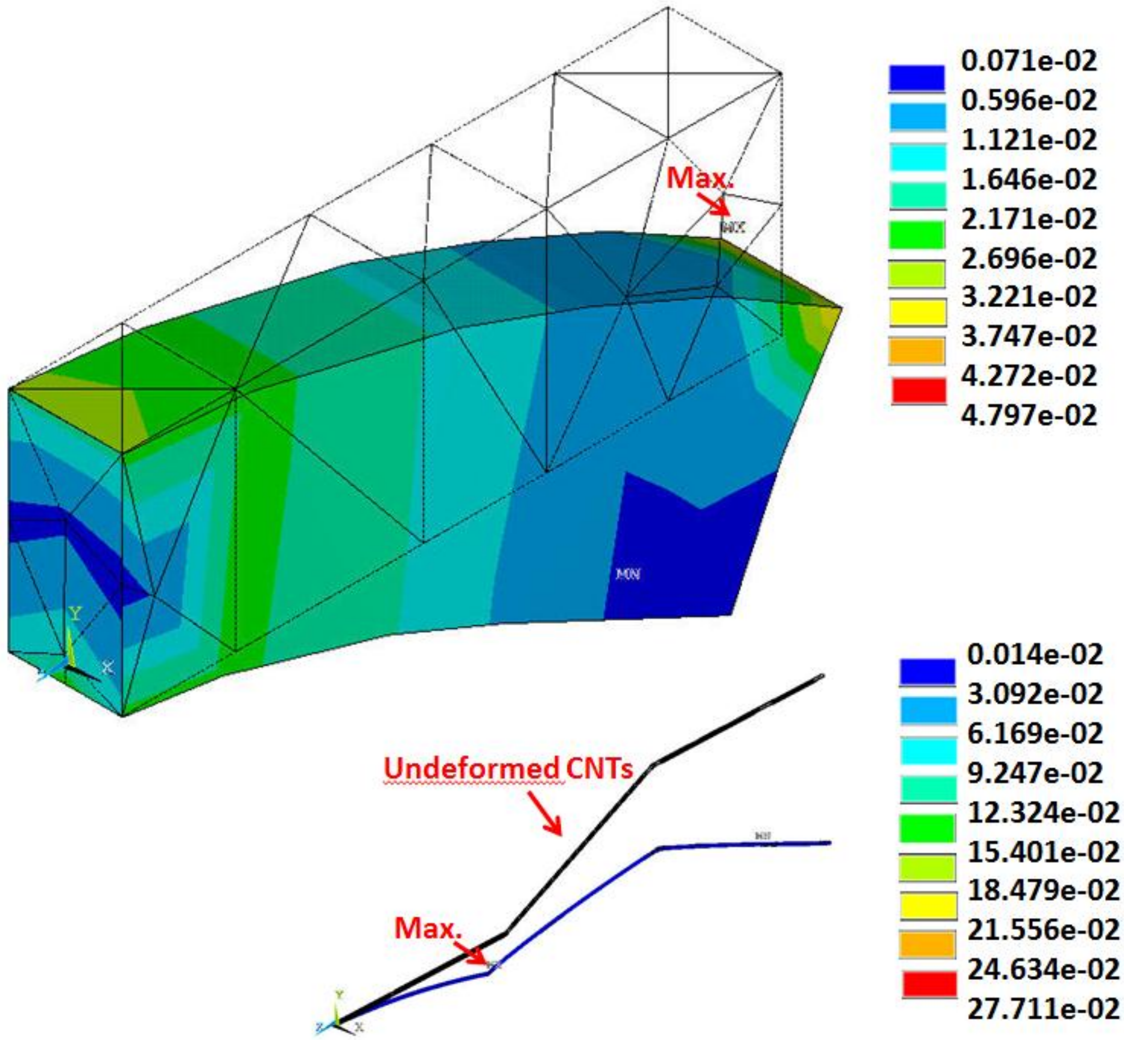

Figure 4.24 von Mises strain for the percolated path for the compressiveloading case.

4.4 Summary and Conclusions

The GFs, resistance variations, interrelated stress and strain, and current distributions in CNT-polymer composite FE models were investigated. A FE approach that coupled Maxwell equations to mechanical loads through piezoresistive coefficients for tunnel distances, and tensile, compressive, and bending loading conditions for composites for different arrangements and orientations that included perfectly aligned CNTs and percolated paths through conductive CNTs was developed.

A logarithmic correlation for GFs, as a function of the applied strain, for all three loading conditions was obtained for all the arrangements and tunneling distances, with tensile loading conditions. Resistance change did not show a distinct trend, because it's affected by the local distributions of current density, strains, stresses, and variations in tunnel distance, and this was substantiated by the contours of current density, von Mises stresses and strains at representative elastic strains.

The maximum conductivities and highest stresses, strains were obtained for the percolated path for the tensile loading case. For the tensile loading case, the percolated arrangement with the lowest tunnel distance (1 nm) had the highest strain sensitivity, highest von Mises stress and current density. The results also indicated that under tensile loading, GFs were more affected by tunneling distance variations than CNT arrangements. The resistance changes generally linearly increased with applied strains, and it was shown that almost all the percolated arrangements have larger changes in resistance than the aligned arrangements, which further indicated that the percolated arrangement with the lowest tunnel distance has the desired higher sensitivity.

The compression and bending cases exhibited different behavior from tension in that GFs were not significantly affected by tunneling distance, or CNT arrangement and orientation. There were small variations in GFs for these loading conditions, because the stress and strain distributions are affected by the lateral expansion of the tubes and the bending strain distribution in the matrix and of the tubes. There was lower sensitivity for the compression and bending loading cases, and with increasing lateral contractions, tunnel effects were pronounced, and this resulted in difference in GF response and resistance changes. For the compressive loading case for the percolated path, at an applied strain of 1%, the maximum current density was approximately three orders of magnitude higher, in comparison with the tensile case. The von Mises strains were approximately the same as for the tensile case with a maximum value of 15.6%. Therefore, for the compressive loading cases, for the percolated case, the electrical conductivity is significantly higher, in comparison with the tensile loading case, with large local strains, which further corroborates the percolated path as an optimal piezoresistive orientation. For the bending case for the percolated path, the current densities in the z direction are higher than that for the tensile case and lower than that for the compressive case, with values almost at the average of both the tensile and compressive cases, and the von Mises strains are significantly higher with values as large as 27.7%

The results for the these three loading conditions for the percolated path clearly demonstrate that electrical conductivity and sensing capabilities can be optimized as a function of percolation, tunneling distance, orientation, and loading condition. For the percolated path under tensile loading conditions, elastic strains as high as 16% and electrical conductivities that were four orders in magnitude greater than the initial matrix conductivity were predicted. These predictions, therefore, can be used as guidelines, to optimize CNT-polymer composites for desired piezoresistive applications.

CHAPTER 5

RECOMMENDATIONS FOR RUTURE RESEARCH

There are several recommendations for the future research based on the current findings:

- As an alternative to using Simmons' tunnel resistance formulation (Simmons, 1963), develop FEM scheme to handle generalized cases for tunneling resistance so the tunneling resistance can be obtained for arbitrary geometries;
- Develop FEM techniques that can couple mechanical fields to thermal-electrical fields, by implementing resistivity as a function of stress, strain and temperature;
- Take into account CNT chirality, crystallinity and curvature effects, consider the structural change of CNTs, and couple local the stress/strain response of CNTs to Raman band shifts (Zhao et al., 2001), to further investigate potential of sensing capabilities within a multiscale framework;
- Investigate the effects of defects, voids, interfacial strength, debonding, and failure of CNTs in the polymer matrix on the sensing response of CNT-polymer composites.

LIST OF REFERENCES

Alamusi, Hu, N., Fukunaga, H., Atobe, S., Liu, Y., and Li, J. (2011). Piezoresistive strain sensors made from carbon nanotubes based polymer nanocomposites. Sensors (Basel, Switzerland) *11*, 10691–10723.

Ambrosetti, G., Grimaldi, C., Balberg, I., Maeder, T., Danani, A., and Ryser, P. (2010). Solution of the tunneling-percolation problem in the nanocomposite regime. Physical Review B *81*, 155434-155455.

Ashcroft, N. M. D. (1976). Solid State Physics (Philadelphia: Saunders).

Ashrafi, B., and Hubert, P. (2006). Modeling the elastic properties of carbon nanotube array/polymer composites. Composites Science and Technology *66*, 387–396.

Balberg, I. (2009). Tunnelling and percolation in lattices and the continuum. Journal of Physics D: Applied Physics *42*, 064003-064018.

Balberg, I., and Binenbaum, N. (1983). Computer study of the percolation threshold in a two-dimensional anisotropic system of conducting sticks. Physical Review B *28*, 3799–3812.

Baughman, R. H., Zakhidov, A. a, and de Heer, W. a (2002). Carbon nanotubes--the route toward applications. Science (New York, N.Y.) *297*, 787–792.

Bauhofer, W., and Kovacs, J. Z. (2009). A review and analysis of electrical percolation in carbon nanotube polymer composites. Composites Science and Technology *69*, 1486–1498.

Bautista-Quijano, J. R., Avilés, F., Aguilar, J. O., and Tapia, a. (2010). Strain sensing capabilities of a piezoresistive MWCNT-polysulfone film. Sensors and Actuators A: Physical *159*, 135–140.

Berhan, L., and Sastry, A. M. (2007). Modeling percolation in high-aspect-ratio fiber systems. II. The effect of waviness on the percolation onset. Physical Review E *75*, 41121-41127.

Blazewicz, S., Patalita, B., and Touzain, P. (1997). Study of piezoresistance effect in carbon fibers. Carbon *35*, 1613–1618.

Bryning, M. B., Islam, M. F., Kikkawa, J. M., and Yodh, a. G. (2005). Very Low Conductivity Threshold in Bulk Isotropic Single-Walled Carbon Nanotube-Epoxy Composites. Advanced Materials *17*, 1186–1191.

Cao, J., Wang, Q., and Dai, H. (2003). Electromechanical Properties of Metallic, Quasimetallic, and Semiconducting Carbon Nanotubes under Stretching. Physical Review Letters *90*, 157601-157604.

Cebeci, H., Villoria, R. G. de, Hart, A. J., and Wardle, B. L. (2009). Multifunctional properties of high volume fraction aligned carbon nanotube polymer composites with controlled morphology. Composites Science and Technology *69*, 2649–2656.

Celzard, A., McRae, E., Deleuze, C., Dufort, M., Furdin, G., and Marêché, J. F. (1996). Critical concentration in percolating systems containing a high-aspect-ratio filler. Physical Review B *53*, 6209–6214.

Chang, L., Friedrich, K., Ye, L., and Toro, P. (2009). Evaluation and visualization of the percolating networks in multi-wall carbon nanotube/epoxy composites. Journal of Materials Science *44*, 4003–4012.

Chen, Y.-R., and Weng, C.-I. (2007). Electronic properties of zigzag carbon nanotubes under uniaxial strain. Carbon *45*, 1636–1644.

Ci, L., Suhr, J., Pushparaj, V., Zhang, X., and Ajayan, P. M. (2008a). Continuous carbon nanotube reinforced composites. Nano letters *8*, 2762–2766.

Ci, L., Suhr, J., Pushparaj, V., Zhang, X., and Ajayan, P. M. (2008b). Continuous carbon nanotube reinforced composites. Nano letters *8*, 2762–2766.

Cullinan, M., and Culpepper, M. (2010). Carbon nanotubes as piezoresistive microelectromechanical sensors: Theory and experiment. Physical Review B *82*, 1–6.

Dalmas, F., Dendievel, R., Chazeau, L., Cavaillé, J.-Y., and Gauthier, C. (2006). Carbon nanotube-filled polymer composites. Numerical simulation of electrical conductivity in three-dimensional entangled fibrous networks. Acta Materialia *54*, 2923–2931.

Dharap, P., Li, Z., Nagarajaiah, S., and Barrera, E. V. (2004). Nanotube film based on single-wall carbon nanotubes for strain sensing. Nanotechnology *15*, 379–382.

Ding, W., Eitan, A., Fisher, F. T., Chen, X., Dikin, D. A., Andrews, R., Brinson, L. C., Schadler, L. S., and Ruoff, R. S. (2003). Direct Observation of Polymer Sheathing in Carbon Nanotube−Polycarbonate Composites. Nano Letters *3*, 1593–1597.

Dufresne, A., Paillet, M., Putaux, J. L., and Schweitzer, A. A. (2002). Processing and characterization of carbon nanotube / poly (styrene-co-butyl acrylate) nanocomposites. *7*, 3915–3923.

Eken, a. E., Tozzi, E. J., Klingenberg, D. J., and Bauhofer, W. (2011). A simulation study on the combined effects of nanotube shape and shear flow on the electrical percolation thresholds of carbon nanotube/polymer composites. Journal of Applied Physics *109*, 084342-084350.

Fernberg, P., Nilsson, G., and Joffe, R. (2008). Piezoresistive Performance of Long-Fiber Composites with Carbon Nanotube Doped Matrix. Journal of Intelligent Material Systems and Structures *20*, 1017–1023.

Frogley, M. D., Zhao, Q., and Wagner, H. D. (2002). Polarized resonance Raman spectroscopy of single-wall carbon nanotubes within a polymer under strain. Physical Review B *65*, 113413-113416.

Gao, L., Chou, T.-W., Thostenson, E. T., Godara, A., Zhang, Z., and Mezzo, L. (2010). Highly conductive polymer composites based on controlled agglomeration of carbon nanotubes. Carbon *48*, 2649–2651.

Gojny, F. H., Wichmann, M. H. G., Fiedler, B., Kinloch, I. A., Bauhofer, W., Windle, A. H., and Schulte, K. (2006). Evaluation and identification of electrical and thermal conduction mechanisms in carbon nanotube/epoxy composites. Polymer *47*, 2036–2045.

Grammatikos, S. a., Gkikas, G., and Paipetis, a. (2011). Monitoring strain and damage in multi-phase composite materials using electrical resistance methods. Proceedings of SPIE *7982*, 79820K–79820K–6.

Grow, R. J., Wang, Q., Cao, J., Wang, D., and Dai, H. (2005). Piezoresistance of carbon nanotubes on deformable thin-film membranes. Applied Physics Letters *86*, 093104–093106.

Halary, J., Stanford, J. L., Lovell, P. A., and Young, R. J. (2004). Raman-Active Nanostructured Materials for Use as Novel Stress-Sensitive Polymeric Coatings. *791*, 6–11.

Heo, S. I., Yun, J. C., Oh, K. S., and Han, K. S. (2006). Influence of particle size and shape on electrical and mechanical properties of graphite reinforced conductive polymer composites for the bipolar plate of PEM fuel cells. Advanced Composite Materials *15*, 115–126.

Hierold, C. (2004). From micro- to nanosystems: mechanical sensors go nano. Journal of Micromechanics and Microengineering *14*, S1.

Hsu, C. C., Chao, R. M., Liu, C. W., and Liang, S. Y. (2011). Evaluation of the gauge factor for single-walled carbon nanonets on the flexible plastic substrates by nano-transfer-printing. Journal of Micromechanics and Microengineering *21*, 75012–75021.

Hu, N., Karube, Y., Arai, M., Watanabe, T., Yan, C., Li, Y., Liu, Y., and Fukunaga, H. (2010). Investigation on sensitivity of a polymer/carbon nanotube composite strain sensor. Carbon *48*, 680–687.

Hu, N., Karube, Y., Yan, C., Masuda, Z., and Fukunaga, H. (2008a). Tunneling effect in a polymer/carbon nanotube nanocomposite strain sensor. Acta Materialia *56*, 2929–2936.

Hu, N., Masuda, Z., Yamamoto, G., Fukunaga, H., Hashida, T., and Qiu, J. (2008b). Effect of fabrication process on electrical properties of polymer/multi-wall carbon nanotube nanocomposites. Composites Part A: Applied Science and Manufacturing *39*, 893–903.

Hu, N., Masuda, Z., Yan, C., Yamamoto, G., Fukunaga, H., and Hashida, T. (2008c). The electrical properties of polymer nanocomposites with carbon nanotube fillers. Nanotechnology *19*, 215701–215710.

Hwang, E.-S., Kim, Y.-J., and Ju, B.-K. (2004). Flexible polysilicon sensor array modules using "etch-release" packaging scheme. Sensors and Actuators A: Physical *111*, 135–141.

Iijima, S. (1991). Helical microtubules of graphitic carbon. Nature *354*, 56–58.

Kanda, Y. (1982). A graphical representation of the piezoresistance coefficients in silicon. IEEE Transactions on Electron Devices *29*, 64–70.

Kang, I., Schulz, M. J., Kim, J. H., Shanov, V., and Shi, D. (2006). A carbon nanotube strain sensor for structural health monitoring. Smart Materials and Structures *15*, 737-748.

Kang, J. H., Park, C., Scholl, J. A., Brazin, A. M. Y. H., Holloway, N. M., High, J. W., Lowther, S. E., and Harrison, J. S. (2009). Piezoresistive Characteristics of Single Wall Carbon Nanotube / Polyimide Nanocomposites. Journal of Polymer Science: Part B: Polymer Physics, *47*, 994–1003.

Karube, Y., and Fukunaga, H. (2011). A carbon nanotube/polymer strain sensor with linear and anti-symmetric piezoresistivity. Journal of Composite Materials *45*, 1315–1323.

Kilbride, B. E., Coleman, J. N., Fraysse, J., Fournet, P., Cadek, M., Drury, a., Hutzler, S., Roth, S., and Blau, W. J. (2002). Experimental observation of scaling laws for alternating current and direct current conductivity in polymer-carbon nanotube composite thin films. Journal of Applied Physics *92*, 4024–4030.

Kirkpatrick, S. (1973). Percolation and Conduction. Reviews of Modern Physics *45*, 574–588.

Kovacs, J. Z., Velagala, B. S., Schulte, K., and Bauhofer, W. (2007). Two percolation thresholds in carbon nanotube epoxy composites. Composites Science and Technology *67*, 922–928.

Kymakis, E., and Amaratunga, G. a. J. (2006). Electrical properties of single-wall carbon nanotube-polymer composite films. Journal of Applied Physics *99*, 084302–084308.

Li, C., Thostenson, E. T., and Chou, T.-W. (2007). Dominant role of tunneling resistance in the electrical conductivity of carbon nanotube–based composites. Applied Physics Letters *91*, 223114–223116.

Li, C., Thostenson, E. T., and Chou, T.-W. (2008a). Effect of nanotube waviness on the electrical conductivity of carbon nanotube-based composites. Composites Science and Technology *68*, 1445–1452.

Li, C., Thostenson, E. T., and Chou, T.-W. (2008b). Sensors and actuators based on carbon nanotubes and their composites: A review. Composites Science and Technology *68*, 1227–1249.

Li, Z., Dharap, P., Nagarajaiah, S., Barrera, E. V., and Kim, J. D. (2004). Carbon Nanotube Film Sensors. Advanced Materials *16*, 640–643.

Liu, Y., and Chen, X. (2003). Evaluations of the e ective material properties of carbon nanotube-based composites using nanoscale representative volume element. Mechanics of Materials *35*, 69–81.

Mahar, B., Laslau, C., Member, S., Yip, R., and Sun, Y. (2007). Development of Carbon Nanotube-Based Sensors — A Review *7*, 266–284.

Marques, M. a. L., Troiani, H. E., Miki-Yoshida, M., Jose-Yacaman, M., and Rubio, a. (2004). On the Breaking of Carbon Nanotubes under Tension. Nano Letters *4*, 811–815.

Martin, C. A., Sandler, J. K. W., Shaffer, M. S. P., Schwarz, M.-K., Bauhofer, W., Schulte, K., and Windle, A. H. (2004). Formation of percolating networks in multi-wall carbon-nanotube–epoxy composites. Composites Science and Technology *64*, 2309–2316.

McLachlan, D. S., Chiteme, C., Park, C., Wise, K. E., Lowther, S. E., Lillehei, P. T., Siochi, E. J., and Harrison, J. S. (2005). AC and DC percolative conductivity of single wall carbon nanotube polymer composites. Journal of Polymer Science Part B: Polymer Physics *43*, 3273–3287.

Minot, E., Yaish, Y., Sazonova, V., Park, J.-Y., Brink, M., and McEuen, P. (2003). Tuning Carbon Nanotube Band Gaps with Strain. Physical Review Letters *90*, 1–4.

Nan, C.-W., Shen, Y., and Ma, J. (2010). Physical Properties of Composites Near Percolation. Annual Review of Materials Research *40*, 131–151.

Natsuki, T., Endo, M., and Takahashi, T. (2005). Percolation study of orientated short-fiber composites by a continuum model. Physica A: Statistical Mechanics and its Applications *352*, 498–508.

Odom, T. W., and Huang, J. (1998). Atomic structure and electronic properties of single-walled carbon nanotubes. Nature *391*, 1997–1999.

Park, M., Kim, H., and Youngblood, J. P. (2008). Strain-dependent electrical resistance of multi-walled carbon nanotube/polymer composite films. Nanotechnology *19*, 55705–55711.

Prylutskyy, Y. I., Durov, S. S., Ogloblya, O. V., Buzaneva, E. V., and Scharff, P. (2000). Molecular dynamics simulation of mechanical, vibrational and electronic properties of carbon nanotubes. Computational Materials Science *17*, 352–355.

Ramaratnam, a. (2006). Reinforcement of Piezoelectric Polymers with Carbon Nanotubes: Pathway to Next-generation Sensors. Journal of Intelligent Material Systems and Structures *17*, 199–208.

Reilly, C. J., and Sanchez, J. E. (1999). The piezoresistance of aluminum alloy interconnect structures. Journal of Applied Physics *85*, 1943–1948.

Ren, X., and Seidel, G. D. (2012). Computational micromechanics modeling of piezoresistivity of carbon nanotube polymer nanocomposites. *8342*, 83421F–83421F–15.

Ruschau, G. R., Yoshikawa, S., and Newnham, R. E. (1992). Resistivities of conductive composites. Journal of Applied Physics *72*, 953–959.

Safadi, B., Andrews, R., and Grulke, E. a. (2002). Multiwalled carbon nanotube polymer composites: Synthesis and characterization of thin films. Journal of Applied Polymer Science *84*, 2660–2669.

Saito, R., Dresselhaus, G., Dresselhaus, M. S. (1998). Physical Properties of Carbon Nanotubes (London: Imperial College Press).

Salvato, M., Cirillo, M., Lucci, M., Orlanducci, S., Ottaviani, I., Terranova, M. L., and Toschi, F. (2012). Macroscopic effects of tunnelling barriers in aggregates of carbon nanotube bundles. Journal of Physics D: Applied Physics *45*, 105306–105311.

Sandler, J. K. W., Kirk, J. E., Kinloch, I. A., Shaffer, M. S. P., and Windle, A. H. (2003). Ultra-low electrical percolation threshold in carbon-nanotube-epoxy composites. Polymer *44*, 5893–5899.

Simmons, J. G. (1963). Generalized Formula for the Electric Tunnel Effect between Similar Electrodes Separated by a Thin Insulating Film. Journal of Applied Physics *34*, 1793–1803.

Smith, C. S. (1954). Piezoresistance Effect in Germanium and Silicon. Physical Review *94*, 42–49. Available at: http://link.aps.org/doi/10.1103/PhysRev.94.42.

Stampfer, C., Jungen, a, Linderman, R., Obergfell, D., Roth, S., and Hierold, C. (2006). Nano-electromechanical displacement sensing based on single-walled carbon nanotubes. Nano letters *6*, 1449–1453.

Stauffer D. and Aharony A. (1994). Introduction to Percolation Theory (London: Taloy & Francis).

Suhr, J., Koratkar, N., Keblinski, P., and Ajayan, P. (2005). Viscoelasticity in carbon nanotube composites. Nat Mater *4*, 134–137.

Theodosiou, T. C., and Saravanos, D. A. (2010). Numerical investigation of mechanisms affecting the piezoresistive properties of CNT-doped polymers using multi-scale models. Composites Science and Technology *70*, 1312–1320.

Thostenson, E. T., and Chou, T.-W. (2007). Multifunctional composites with self-sensing capabilities: carbon nanotube-based networks. Proceedings of SPIE *6526*, 65261X.

Thostenson, E. T., Li, W. Z., Wang, D. Z., Ren, Z. F., Chou, T. W., and Introduction, I. (2002). Carbon nanotube/carbon fiber hybrid multiscale composites. Journal of Applied Physics *91*, 6034.

Tombler, T., Zhou, C., Alexseyev, L., Kong, J., Dai, H., Liu, L., Jayanthi, C., Tang, M., and Wu, S. (2000). Reversible electromechanical characteristics of carbon nanotubes under local-probe manipulation. Nature *405*, 769–772.

Tserpes, K. I., Papanikos, P., Labeas, G., and Pantelakis, S. G. (2008). Multi-scale modeling of tensile behavior of carbon nanotube-reinforced composites. Theoretical and Applied Fracture Mechanics *49*, 51–60.

Veedu, V. P., Cao, A., Li, X., Ma, K., Soldano, C., Kar, S., Ajayan, P. M., and Ghasemi-Nejhad, M. N. (2006). Multifunctional composites using reinforced laminae with carbon-nanotube forests. Nat Mater *5*, 457–462.

Wang, D., Song, P., Liu, C., Wu, W., and Fan, S. (2008). Highly oriented carbon nanotube papers made of aligned carbon nanotubes. Nanotechnology *19*, 75609.

Xu, Siqi;Rezvanian, Omid; Peters, Kara; Zikry, A. M. (2012). The Viability and Limits of Percolation Theory in Modeling the Electrical Behavior of Carbon Nanotube Polymer Composites. Nanotechnology, submitted.

Xu, Siqi;Rezvanian, Omid; Zikry, A. M. (2012). Electro-Thermo-Mechanical Modeling and Analyses of Carbon Nanotube Polymer Composites. Journal of Engineering Materials and Technology, submitted.

Yang, L., and Han, J. (2000). Electronic Structure of Deformed Carbon Nanotubes. Physical Review Letters *85*, 154–157.

Yap, H. W., Lakes, R. S., and Carpick, R. W. (2007). Mechanical instabilities of individual multiwalled carbon nanotubes under cyclic axial compression. Nano letters *7*, 1149–1154.

Yasuoka, T., Shimamura, Y., and Todoroki, A. (2010). Electrical Resistance Change under Strain of CNF/Flexible-Epoxy Composite. Advanced Composite Materials *19*, 123–138.

Yu, A., Itkis, M. E., Bekyarova, E., and Haddon, R. C. (2006). Effect of single-walled carbon nanotube purity on the thermal conductivity of carbon nanotube-based composites. Applied Physics Letters *89*, 133102–133104.

Yu, C., Kim, Y. S., Kim, D., and Grunlan, J. C. (2008). Thermoelectric behavior of segregated-network polymer nanocomposites. Nano letters *8*, 4428–4432.

Yu, Y., Song, G., and Sun, L. (2010). Determinant role of tunneling resistance in electrical conductivity of polymer composites reinforced by well dispersed carbon nanotubes. Journal of Applied Physics *108*, 084319–084313.

Zhang, W., Suhr, J., and Koratkar, N. (2006). Carbon Nanotube/Polycarbonate Composites as Multifunctional Strain Sensors. Journal of Nanoscience and Nanotechnology *6*, 960–964.

Zhao, Q., Wood, J. R., and Wagner, H. D. (2001). Stress fields around defects and fibers in a polymer using carbon nanotubes as sensors. Applied Physics Letters *78*, 1748–1750.

APPENDIX

APPENDIX

As a supplement for Chapter 4, some results of different CNTs arrangements and tunneling distances for the three loading conditions are presented in this section. The contours are as below.

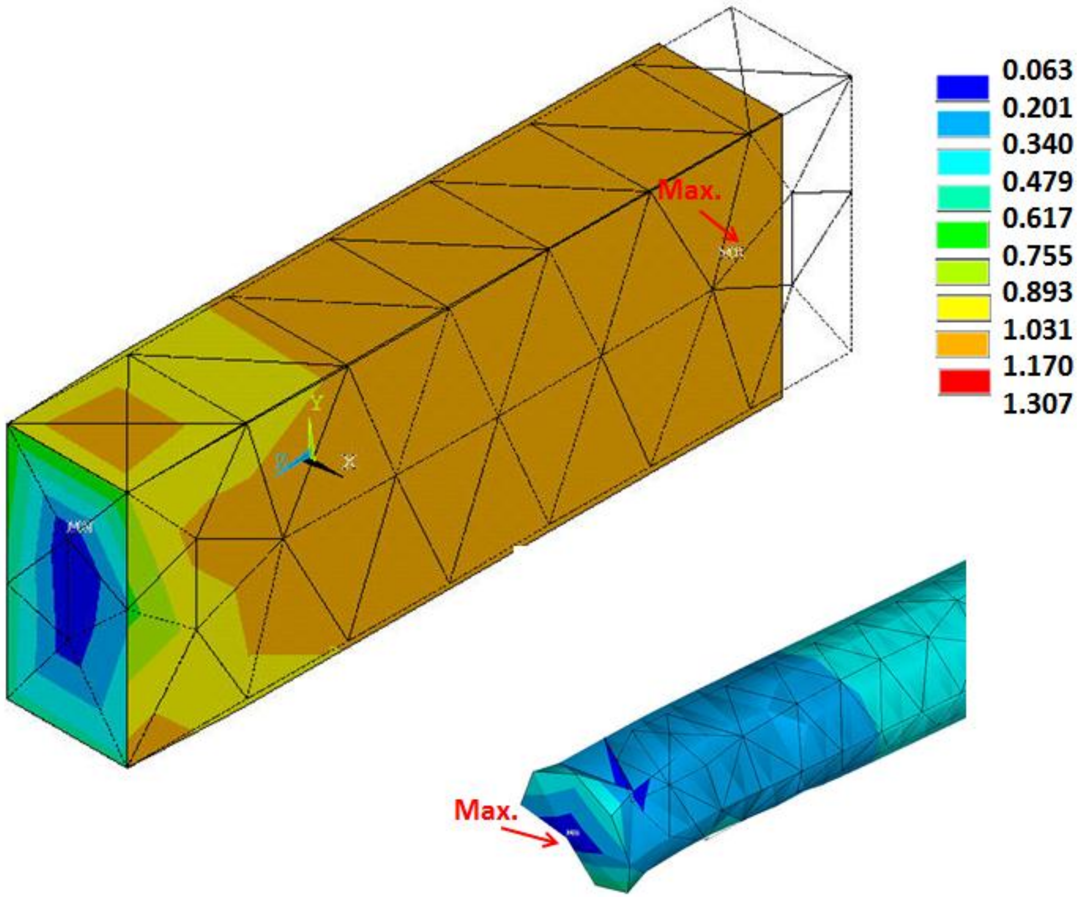

Figure A1 von Mises stress for three aligned CNTs in the polymer matrix under compression (tunnel distance 1 nm, applied strain 1%).

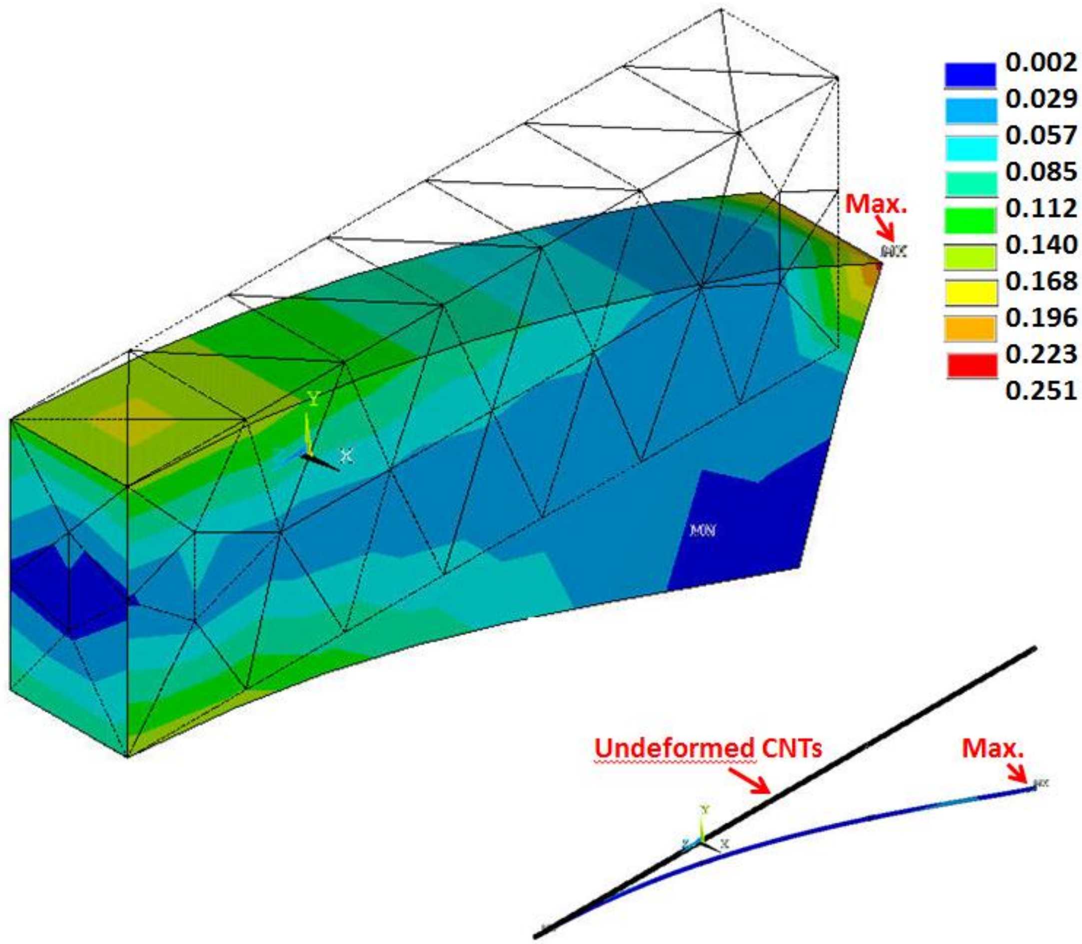

Figure A2 von Mises stress for three aligned CNTs in the polymer matrix under bending (tunnel distance 1 nm, applied strain 1%).

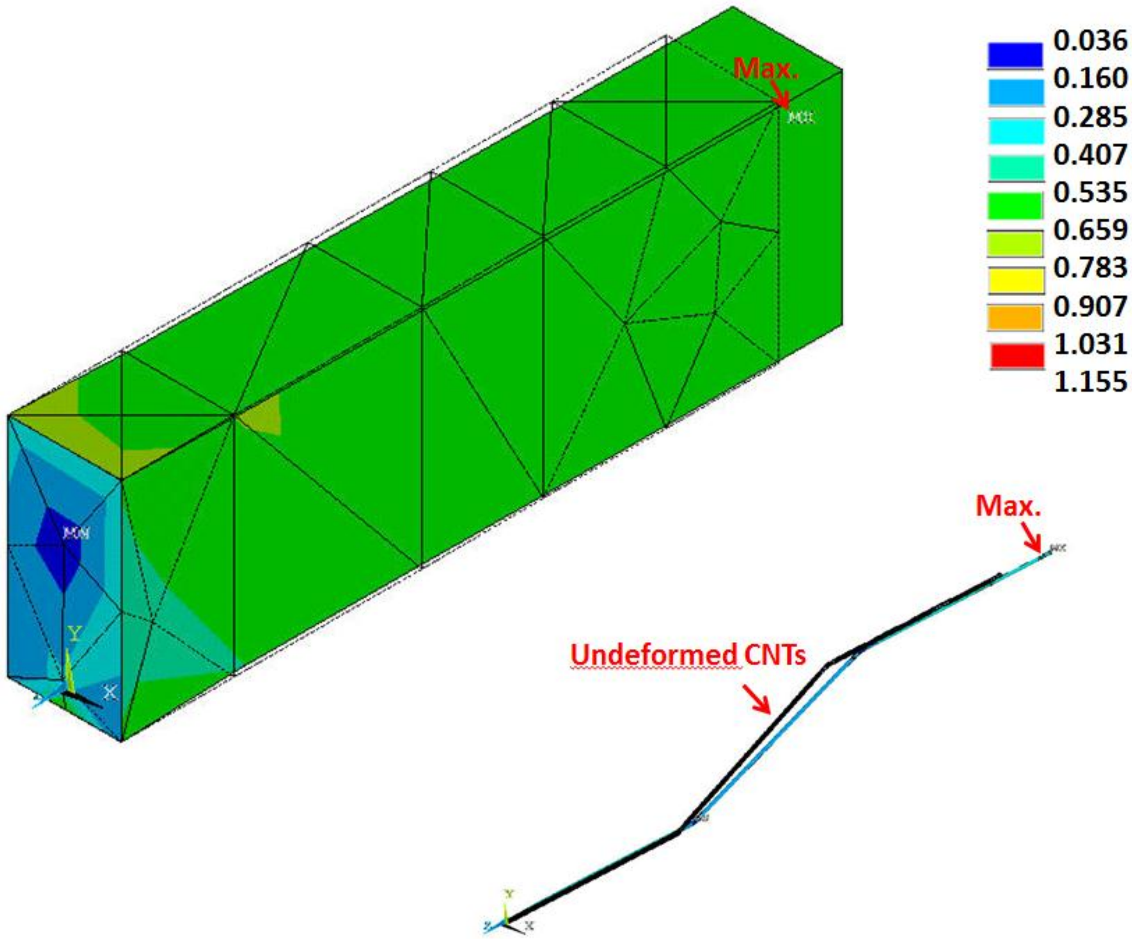

Figure A3 von Mises stress for the percolated path in the polymer matrix under tension (tunnel distance 1 nm, applied strain 1%).

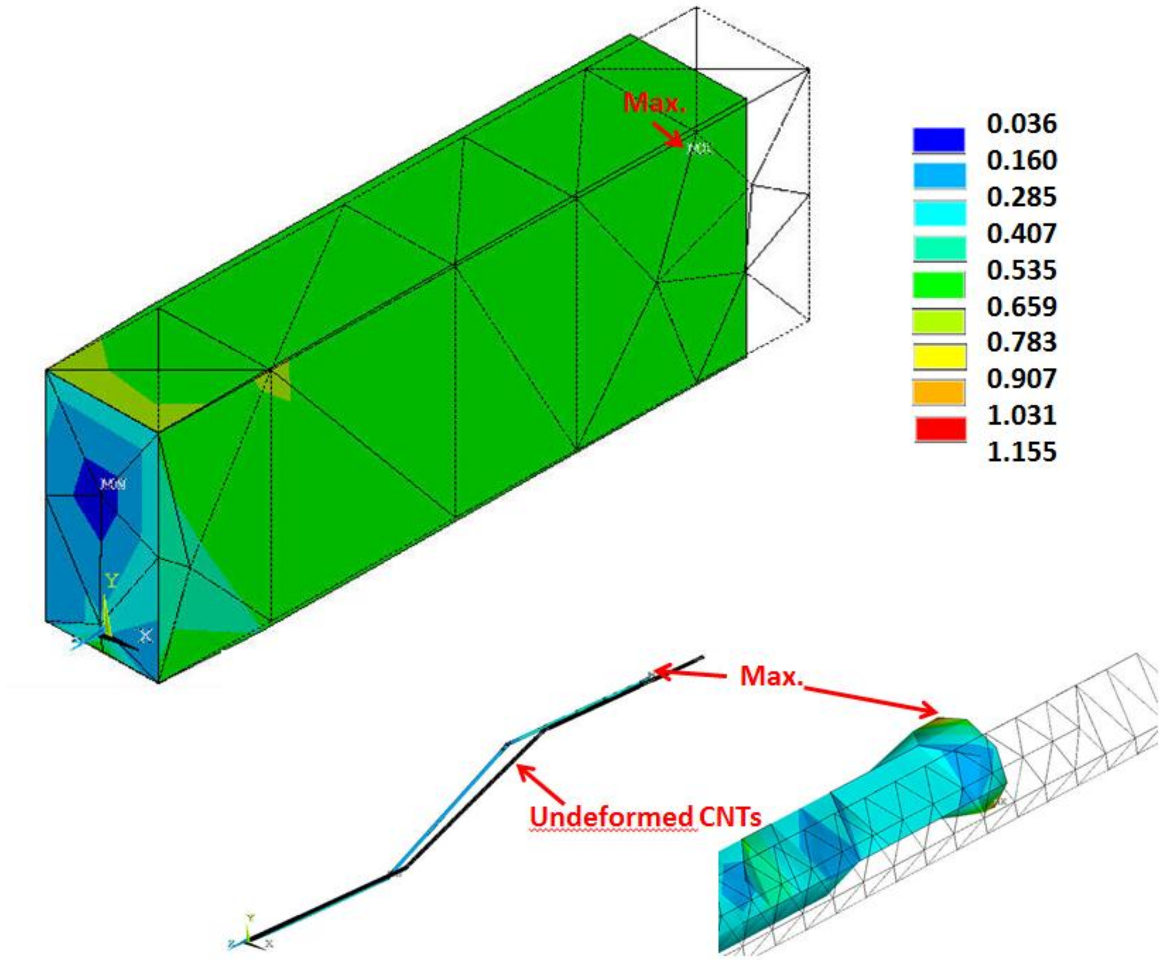

Figure A4 von Mises stress for the percolated path in the polymer matrix under compression (tunnel distance 1nm, applied strain 1%).

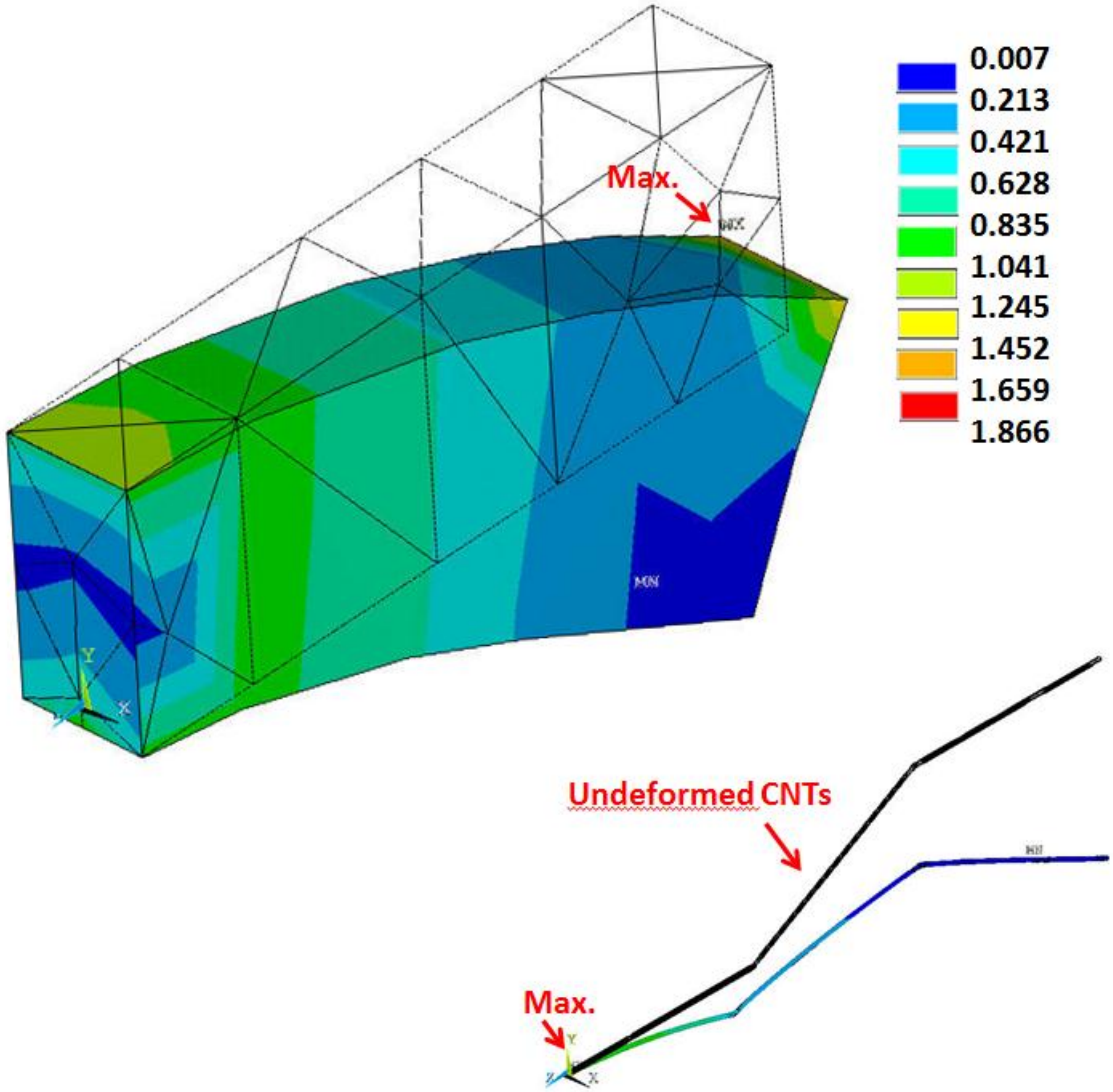

Figure A5 von Mises stress for the percolated path in the polymer matrix under bending (tunnel distance 1 nm, applied strain 1%).

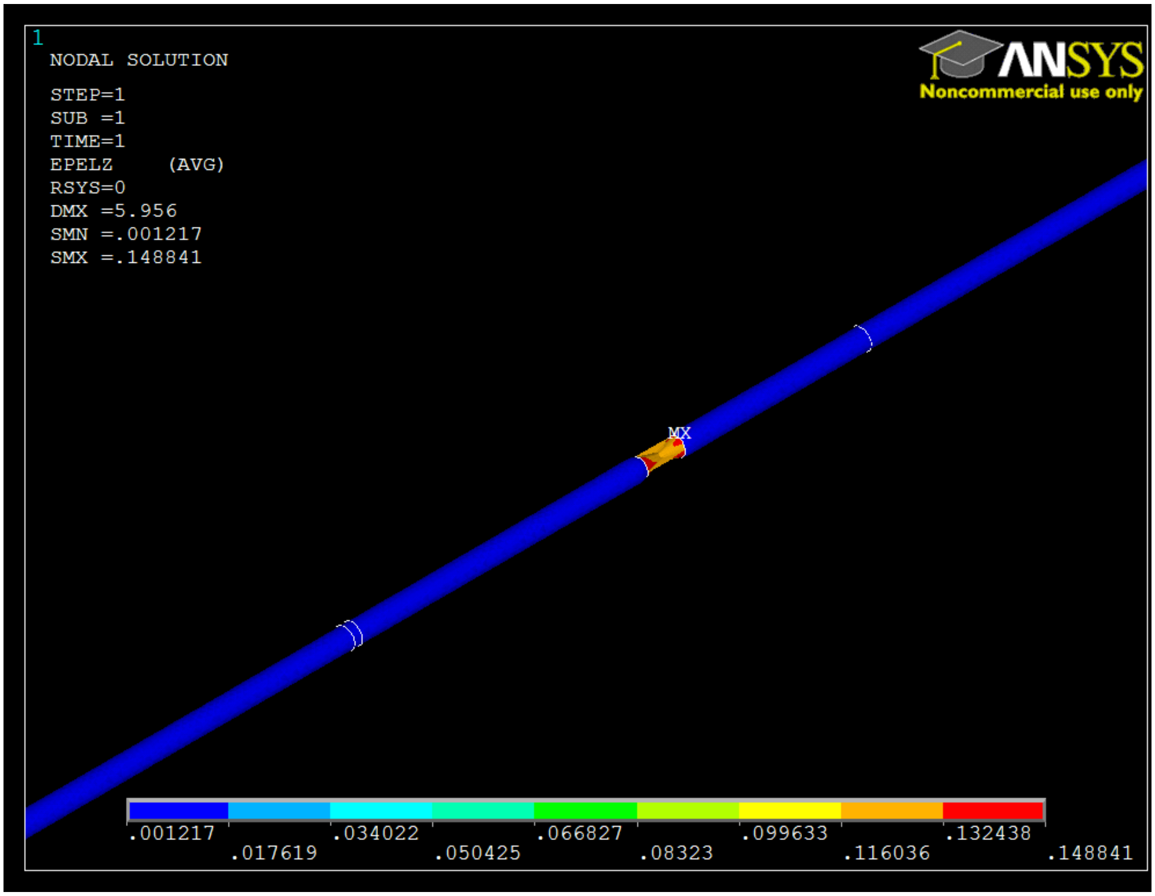

Figure A6 Strain in the z direction for three aligned CNTs in the polymer matrix under bendign (tunnel distance 3 nm, applied strain 1%).

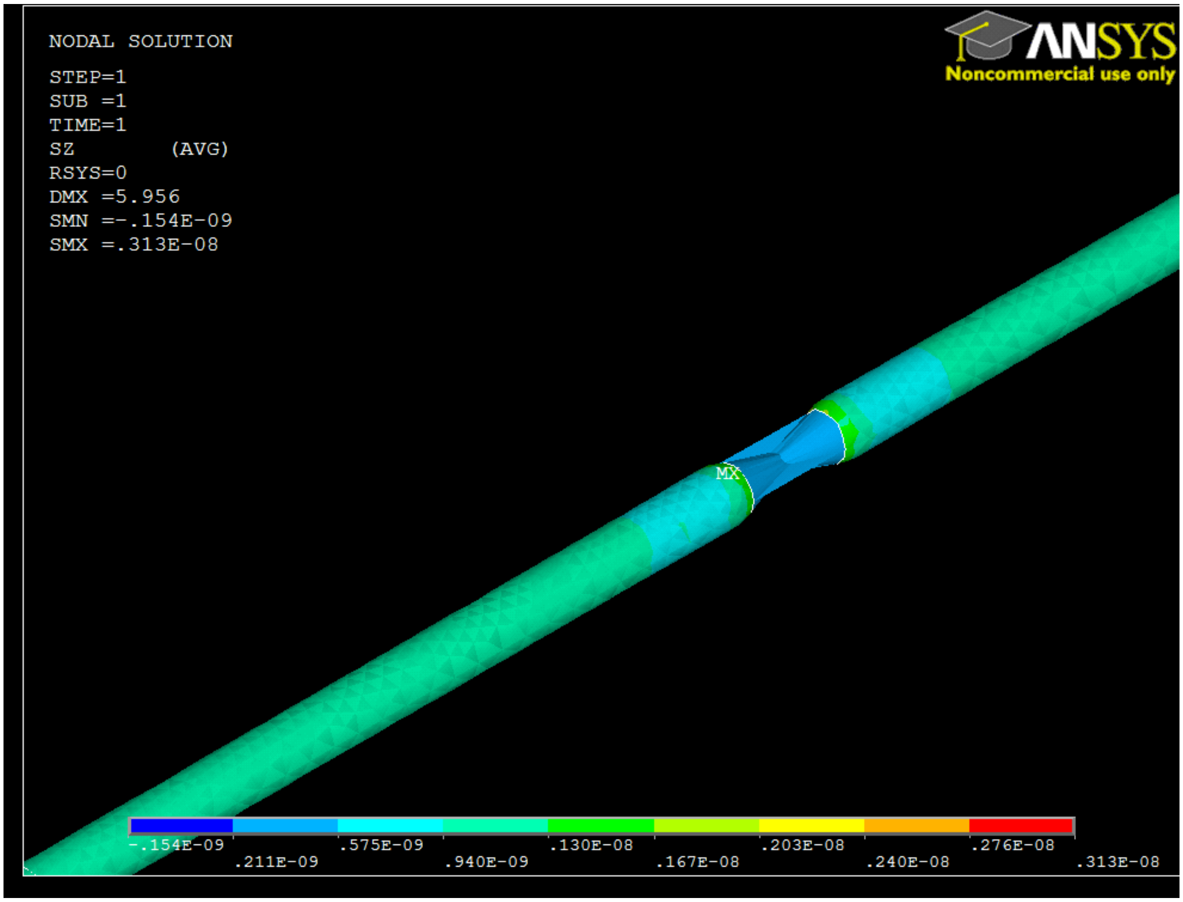

Figure A7 Stress in the z direction for three aligned CNTs in the polymer matrix under bendign (tunnel distance 3 nm, applied strain 1%).

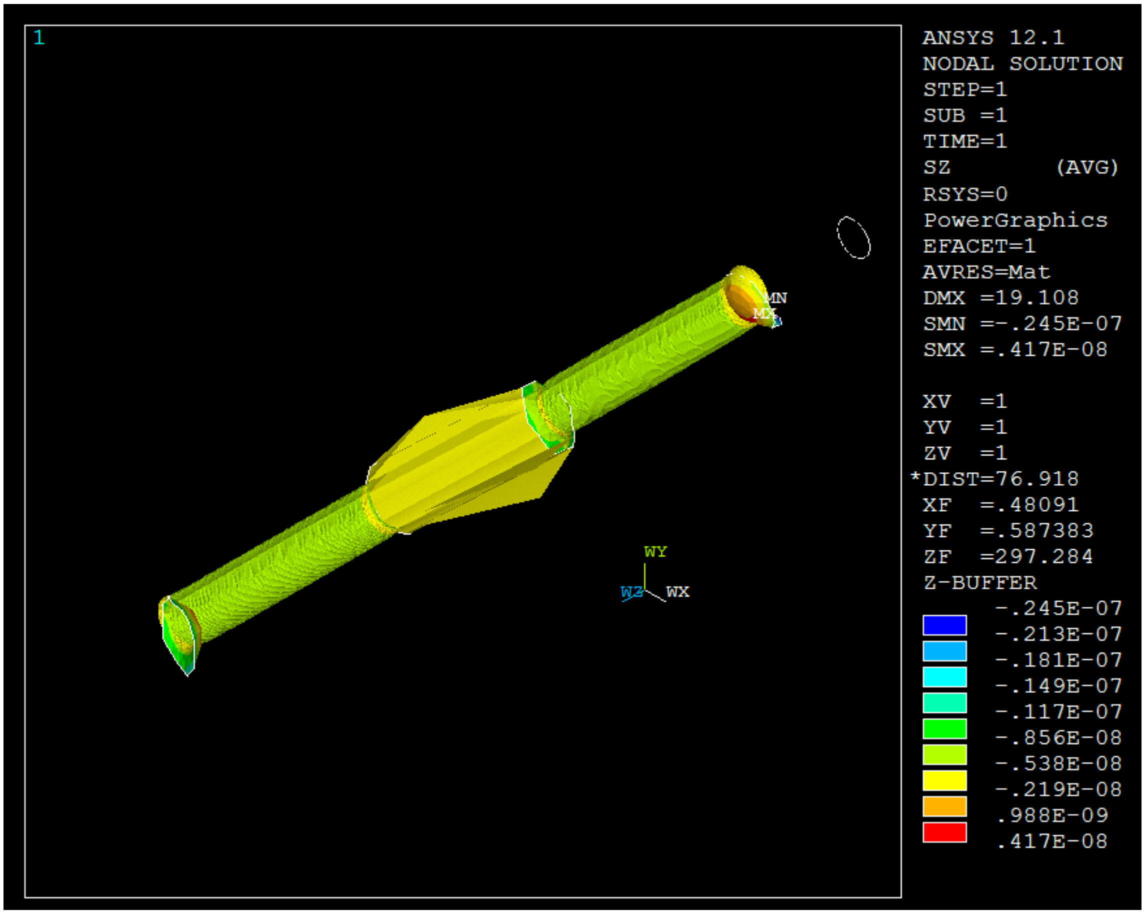

Figure A8 Stress in the z direction for two aligned CNTs in the polymer matrix under compression (tunnel distance 1 nm, applied strain 5%).